8-3-2007

White Dwarfs in the Solar Neighborhood

John P. Subasavage, Jr.

WHITE DWARFS IN THE SOLAR NEIGHBORHOOD

by

JOHN P. SUBASAVAGE, JR.

Under the Direction of Todd J. Henry

ABSTRACT

The study of white dwarfs (WDs) provides insight into understanding WD formation rates, evolution, and space density. Individually, nearby WDs are excellent candidates for astrometric planetary searches because the astrometric signature is greater than for an identical, more distant WD system. As a population, a complete volume-limited sample is necessary to provide unbiased statistics; however, their intrinsic faintness has allowed some to escape detection.

The aim of this dissertation is to identify nearby WDs, accurately characterize them, and target a subset of potentially interesting WDs for follow-up analyses. The most unambiguous method of identifying new WDs is by their proper motions. After evaluating all previous southern hemisphere proper motion catalogs and selecting viable candidates, we embarked on our own southern hemisphere proper motion survey, the SuperCOSMOS-RECONS (SCR) survey. A number of interesting objects were discovered during the survey, including the 24th nearest star system – an M dwarf

with a brown dwarf companion. After a series of spectroscopic observations, a total of 56 new WD systems was identified (18 from the SCR survey and 38 from other proper motion surveys).

CCD photometry was obtained for most of the 56 new systems in an effort to model the physical parameters and obtain distance estimates via spectral energy distribution fitting. An independent distance estimate was also obtained by deriving a color-M_V relation for several colors based on WDs with known distances. Any object whose distance estimate was within 25 pc was targeted for a trigonometric parallax via our parallax program, CTIOPI.

Currently, there are 62 WD systems on CTIOPI. A subset of 53 systems has enough data for at least a preliminary parallax (24 are definitive). Of those 53 systems, nine are previously known WDs within 10 pc that we are monitoring for perturbations from unseen companions, and an additional 29 have distances within 25 pc. Previously, there were 109 known WDs with parallaxes placing them within 25 pc; therefore, our effort has already increased the nearby sample by 27%. In addition, at least two objects show hints of perturbations from unseen companions and need follow-up analyses.

INDEX WORDS: white dwarfs, nearby stars, proper motion, trigonometric parallax, Sirius, Procyon, 40 Eridani, spectroscopy, photometry, astrometry, stellar structure, double degenerate

WHITE DWARFS IN THE SOLAR NEIGHBORHOOD

by

JOHN P. SUBASAVAGE, JR.

A Dissertation Presented in Partial Fulfillment of Requirements for the Degree of

Doctor of Philosophy

in the College of Arts and Sciences

Georgia State University

2007

WHITE DWARFS IN THE SOLAR NEIGHBORHOOD

by

JOHN P. SUBASAVAGE, JR.

Major Professor:	Todd J. Henry
Committee:	Pierre Bergeron
	Douglas R. Gies
	Philip A. Ianna
	Harold A. McAlister
	William H. Nelson

Electronic Version Approved:

Office of Graduate Studies
College of Arts & Sciences
Georgia State University
August 2007

DEDICATION

To my family, my mother, Dorothy; my father, John Sr.; my brother, Robbie; and my sister, Jenny. My parents have been instrumental in all aspects of personal development throughout my life and are largely responsible for who I am today (for better or worse). My siblings have always been there for me, through good times and bad. To the love of my life, Jennifer, whose assured love and support has gotten me through the daily ups and downs of life during graduate school. I can only hope that she will grant me an extension of her love and support throughout my tenure on this pale blue dot. Lastly, to my two beloved puppies, Kelu and Sophie, who always make me smile and keep me in shape with two-mile walks everyday.

Acknowledgments

The science presented in a dissertation is achieved by nothing short of a monumental effort, virtually impossible for one individual to accomplish alone. I must say that this dissertation marks the most substantial accomplishment thus far in my life. There are a multitude of individuals who had a hand in helping me achieve this milestone. With any luck, I hope to give credit to everyone to whom credit is due.

First and foremost, my advisor, Dr. Todd Henry, is an amazing person, both professionally and personally. I feel I have adopted (perhaps inadvertently) many of his principles pertaining to the pursuit of science. Attention to detail as well as the careful scruntiny he employs when reviewing others' data and conclusions preserves the quality of his research. No doubt, I have learned from Dr. Henry how to be thorough and meticulous in my scientific endeavors. Perhaps one of the most difficult aspects of research for me initially was scientific writing. Working with Dr. Henry, an expert (in my opinion) in writing clearly and concisely, has honed my writing skills immeasurably (though I need more work because he still returns draft manuscripts covered in red ink). On the personal side, after I finished my undergraduate studies at the University of Virginia six years ago, Dr. Henry offered me a job and even offered me lodging at his home until I got settled here in Atlanta. Having met him only once prior to that, Dr. Henry took an extreme leap of faith that undoubtedly set the stage for my acceptance into and progression through graduate school to the point of

writing this dissertation. I am deeply indebted to my advisor and friend, Dr. Todd Henry.

I also want to thank Dr. Phil Ianna, my advisor at the University of Virginia who introduced me to the real-life aspects of astronomy research. He, like Dr. Henry, played a pivotal role in my choice of profession. I attribute the moment at which I decided I wanted to be an astronomer to my first observing run in Chile in August 2000 that was arranged by Dr. Ianna. He managed to look past a level of immaturity on my part (I missed several days of work after I was set on fire by an act of sheer stupidity), introduced me to Dr. Henry, and must have put in a good word for me because I was offered a job in Atlanta. Also, I thank Dr. Ianna for opting to be a member of my committee.

There have been several undergraduates, graduates, and postdoctoral researchers that have aided my research along the way, either intellectually or physically (i.e., data reduction). Most notably, I would like to thank Dr. Wei-Chun Jao, whose parallax and photometry reduction pipelines made the bulk of this research possible. I also like to thank other RECONS team members at Georgia State University, Dr. Hektor Monteiro, Thom Beaulieu, Misty Brown, Jennifer Winters, Charlie Finch, and Justin Cantrell. No less notable, Dr. John McFarland and Rajesh Deo were extremely helpful in meeting all of my computer systems/software needs. Dr. Verandra (Alvin) Das provided to the astronomy graduate students a latex dissertation package that proved immensely helpful in compiling this dissertation. I also thank all of the graduate

students in the astronomy program here at Georgia State University. Graduate school is very arduous for everyone and I think we help each other make it through.

The success of the research presented in this dissertation relied heavily on collaborations with those far more knowledgeable than myself in their respective areas of expertise. In particular, I want to thank three collaborators that have helped realize the full potential of the data we have acquired. Dr. Pierre Bergeron of the Université de Montréal has aided in the modeling and interpretation of our white dwarf data. He has also graciously opted to travel to Georgia and sit on my committee. A former student of Dr. Bergeron, Dr. Patrick Dufour, now a postdoctoral researcher at the University of Arizona, has also contributed to the modeling of our white dwarf data. Last but not least, Dr. Nigel Hambly of the University of Edinburgh Royal Observatory has compiled a wealth of photographic plate data that was used in our proper motion survey.

I am indebted to the remainder of my committee members, Dr. Doug Gies, Dr. Hal McAlister, and Dr. William Nelson, for agreeing to sit on my committee, read my dissertation, and identify flaws (there are certainly going to be a few). I must thank the Georgia State astronomy faculty for all of the knowledge they have imparted to me either through classes or one-on-one discussions. I know I have much to learn but the foundation has been laid.

TABLE OF CONTENTS

Tables

FIGURES

Abbreviations

2MASS .... Two Micron All Sky Survey
ACS .... Advanced Camera for Surveys
AOC .... Adaptive Optics Coronagraph
APM .... Automatic Plate Measuring Machine
ASPENS .... Astrometric Search for Planets Encircling Nearby Stars
CCD .... Charge-Coupled Device
CIA .... Collision-Induced Absorption
CNS .... Catalog of Nearby Stars
CTIO .... Cerro Tololo Inter-American Observatory
CTIOPI .... Cerro Tololo Inter-American Observatory Parallax Investigation
DCR .... Differential Color Refraction
DECL .... Declination
DSS .... Digitized Sky Survey
EC .... Edinburgh-Cape Survey
ESA .... European Space Agency
ESO .... European Southern Observatory
FGS .... Fine Guidance Sensors
FHWM .... Full Width at Half Maximum
GAC .... Galactic Anticenter
GC .... Galactic Center
H-R .... Hertzsprung-Russell Diagram
HA .... Hour Angle
HPM .... High Proper Motion
HeAr .... Helium-Argon Lamp
HST .... *Hubble Space Telescope*
IRAF .... Image Reduction and Analysis Facility
LEHPM .... Liverpool-Edinburgh High Proper Motion Survey
LHS .... Luyten Half-Second Catalog
LMC .... Large Magellanic Cloud

LSPM .... Lépine-Shara Proper Motion Survey
MACHO .... Massive Compact Halo Object
NGP .... North Galactic Pole
NLTT .... New Luyten Two-Tenths Catalog
NOAO .... National Optical Astronomy Observatory
PG .... Palomar-Green Survey
POSS-I .... The National Geographic Society, Palomar Observatory Sky Atlas
QSO .... Quasi-Stellar Object
RA .... Right Ascension
RECONS .... Research Consortium on Nearby Stars
RPM .... Reduced Proper Motion
S/N .... Signal to Noise Ratio
SCR .... SuperCOSMOS-RECONS Proper Motion Survey
SCR1845 .... SCR 1845−6357
SDSS .... Sloan Digital Sky Survey
SED .... Spectral Energy Distribution
SGP .... South Galactic Pole
SIPS .... Southern Infrared Proper Motion Survey
SMARTS .... Small and Moderate Aperture Research Telescopes System
SMC .... Small Magellanic Cloud
SPY .... SN Ia Progenitor Survey
SSS .... SuperCOSMOS Sky Survey
STScI .... Space Telescope Science Institute
USNO .... United States Naval Observatory
WD .... White Dwarf
WFPC2 .... Wide Field Planetary Camera 2
WTC .... Wroblewski-Torres-Costa Proper Motion Survey
YPC .... Yale Parallax Catalog

Chapter 1

Introduction

All stars less massive than ~ 8 $M_\odot$ will become white dwarfs (WDs), such that they will eventually be one of the most populous classes of objects in the Universe. WDs are nothing more than burning embers that were once the cores of thriving stars. The Sun, for instance, will live out its main-sequence lifetime (~ 10 billion years in total), spend an additional ~ 1 billion years as an evolving red giant, and finally blow off its outer layers into the void of space as a planetary nebula. While these outer layers dissipate into darkness, what remains is the electron degenerate central core and a residual atmosphere with a surface temperature of $\sim 60,000$ K. Over a relatively short time, astronomically speaking, radiation pressure from the core pushes off most of the residual atmosphere leaving the exposed core with a surface temperature greater than $\sim 100,000$ K. The surrounding nebula fades to black and the core, roughly the size of the Earth, begins to cool, and is formally considered to be a WD. Because there are no significant fueling/heating mechanisms in WDs, they continue to cool uninterrupted for billions of years until they, too, become too faint to see.

1.1 In the Beginning

Fortunately, the Universe is not old enough for even the oldest WDs to disappear completely; however, they have proven to be elusive because of their faintness. The very existence of WDs escaped detection observationally until the mid-19th century.

A firm theoretical understanding of these objects was realized in the early 20th century, only after quantum mechanics was sufficiently honed and the theory of general relativity was available.

1.1.1 Sirius B

The first WD (although the namesake was coined nearly a century later) was discovered as a close companion to the brightest star in the night sky, the Dog Star, Sirius. The existence of the companion was first inferred astrometrically as a perturbation on the position of Sirius in 1834 by Friedrich Wilhelm Bessel who predicted that the likely cause of the perturbation was a faint companion with a $\sim$50 year period (Bessel 1844). This companion was first seen directly in 1862 near apastron by the son of lensmaker Alvan Clark, who was testing the new 18-inch refractor, the largest of the day, purchased by Dearborn Observatory at Northwestern University. Although this faint companion was now visible, its true nature was a complete mystery because of Sirius' overwhelming glow, $\sim$10,000 times brighter than the faint companion. Observations continued for decades (when the companion was far enough from Sirius to be seen) to better map out the orbit. As the orbital parameters became better constrained, Arthur Auwers (1864) estimated that the mass of the companion necessary to produce the perturbation seen on Sirius would have to be roughly half that of Sirius. If both components had the same physical makeup, the diameter of the companion would be $\sim$80% of the diameter of Sirius (Struve 1866); the vast brightness difference prohibited such a scenario.

Roughly 50 years after the first observation, again at apastron, the companion was separated from Sirius by ∼10″. Telescopes and instrumentation were available to not only resolve the companion but to obtain a spectrum of it. After making attempts for two years, Adams (1915) finally managed to obtain a spectrum using the 60-inch reflector at Mt. Wilson Observatory under superb seeing conditions. The companion spectrum was clearly demarcated on the photographic plate from the spectrum produced by the overall glow of Sirius. The determination was spectral type A0, identical to that of Sirius. One could easily argue that this was an indication of contamination from the much brighter Sirius, so the mystery of the Dog Star's companion would continue to linger.

1.1.2 Procyon B

In 1840, Bessel noticed a significant discrepancy between the predicted and true positions of another bright star near the Sun, Procyon. Ironically, this discrepancy was also likely indicative of an unseen companion with a ∼50 year orbit (Bessel 1844). Procyon was observed for decades in hopes of resolving a companion whose mass was expected to be "not less than three-quarters of the mass of the Sun" (Auwers 1862).

In 1873, famed double star observer Otto Wilhelm von Struve detected a faint object 11.7″ from the primary (Struve 1873). After comparing the separation and position angle with those predicted by the theoretical orbit calculated by Arthur Auwers, he was convinced this object was the infamous perturber on Procyon. Furthermore,

Struve's distinguished status as a double star expert eliminated any skepticism of these results, causing Dr. Auwers to revise his orbit based on these observations (although Dr. Auwers states that if these observations are correct, Procyon A would be the most massive star known at ~ 80 M$_\odot$ and the companion would be ~ 7 M$_\odot$) (Auwers 1873). Other researchers tried desperately to resolve Struve's companion but none did. After careful reconsideration, Struve became convinced that the companion he saw was merely an optical illusion. The cause of this illusion was unknown but it seemed to occur when observing bright stars. As a test, he observed three bright stars, Regulus, Capella, and Arcturus, and found a faint source $\sim 10''$ nearly horizontal from the primary in all three cases (Anonymous 1877). Thus, the perturbing companion to Procyon remained undetected.

Nearly two decades later, the mystery was resolved when Schaeberle (1896) witnessed a faint companion separated by $4.6''$ from Procyon. He used Lick Observatory's relatively new 36-inch refractor, which held optics developed by the great Alvan Clark. Within a year of steady monitoring, Schaeberle was convinced that the faint companion was indeed responsible for the perturbation of Procyon. Eventually, Procyon B was considered an object similar to Sirius B even though a spectrum was impossible to obtain. In fact, the first reliable spectrum of the companion had to await the arrival of *Hubble Space Telescope* (*HST*) a century later (Provencal et al. 2002).

1.1.3 40 Eridani B

Another star near the Sun, a K dwarf named 40 Eridani (σ^2 Eridani), was found to be a wide binary in 1783 by Sir William Friedrich Wilhelm Herschel. The primary, 40 Eridani A, is separated by more than $1'$ from the fainter companion. In 1851, Otto Wilhelm von Struve discovered that the fainter companion was actually a double star with a separation $\sim6''$. The brighter component of the double star, the WD, was labeled 40 Eridani B while the fainter, an M dwarf, was labeled 40 Eridani C. Observers continually monitored the double star, realizing that the period was long and the orbit was significantly elliptical. After 40 years, the M dwarf had passed through nearly a $60°$ arc allowing Burnham (1893) to estimate a period of ~180 years (the currently accepted value is ~250 years).

For a decade before the turn of the 20th century and several decades after, Harvard College Observatory cataloged spectral types for literally hundreds of thousands of stars, now known as the Henry Draper Catalog. A prominent astronomer of the time, Henry Norris Russell, was a friend and colleague of E. C. Pickering, then director of Harvard Observatory. Around 1910, Russell thought it would be a good idea to obtain spectra of certain parallax stars; he suggested 40 Eridani B as a start. Pickering promptly telephoned Mrs. Williamina Fleming, then the curator of astronomical photographs at Harvard Observatory. Indeed, a spectrum of this object had been taken, yet not classified. Within half an hour, she retrieved the spectrum and stated,

unquestionably, that it was of spectral type A. Pickering looked to Russell and said, "I wouldn't worry. It's just these things which we can't explain that lead to advances in our knowledge." Russell later stated of that moment, "I knew enough, even then, to know what it meant. I was flabbergasted. I was really baffled trying to make out what it meant. Well, at that moment, Pickering, Mrs. Fleming and I were the only people in the world who knew of the existence of white dwarfs." Pickering and Russell exchanged letters from December 1910 and June 1911 addressing the anomaly of 40 Eridani B's luminosity and spectrum although nothing was published (Philip et al. 1977).

In May of 1914, Russell published a benchmark paper describing the first Russell diagram [now known as the Hertzsprung-Russell (H-R) Diagram]. This diagram was first seen by the astronomical community at the 1913 American Astronomical Society meeting in Atlanta, GA. On this diagram lies a single point notably below and to the left of the main-sequence (see Figure 1.1). Russell states, "The single apparent exception is the faint double companion to σ^2 Eridani, concerning the parallax and brightness of which there can be no doubt, but the spectrum of which, though apparently of Class A, is rendered very difficult of observation by the proximity of its far brighter primary." hinting at his reluctancy to trust the spectrum (Russell 1914). A few months later, in October of 1914, Walter Adams (who, the following year, also published the first spectral type of Sirius B as discussed above) published a single paragraph article stating that "the spectrum of [40 Eridani B] is A0" (Adams 1914).

Figure. 1.1: First published Russell Diagram (now known as the Hertzsprung-Russell Diagram). 40 Eridani B is the isolated point below and to the left of the main-sequence. The Y-axis is absolute magnitude. Reproduced from Russell (1914).

Nearly a decade later, Willem Luyten (1922) coined the term "white dwarf". Prominent theoretician Arthur Eddington (1924) adopted this terminology and referred to these three objects as such. In that work, Eddington points out that the densities implied in these WDs ($\sim$53,000 times that of water for Sirius B) "is not absurd, and we should accept it without demur if the evidence were sufficient". He goes on to point out that at these densities, Einstein's recently formulated theory of relativity predicts a gravitational redshift of $\sim$20 km s^{-1}, a quantity capable of direct measurement. Shortly thereafter, Adams (1925) made careful measurements of the spectra of Sirius A and B and found a relative difference (after inclusion of the differences due to orbital motion) of 21 km s^{-1}. Adams concludes "the results may be considered, therefore, as affording direct evidence from stellar spectra for the validity of the third test of the theory of general relativity, and for the remarkable densities predicted by Eddington for the dwarf stars of early type of spectrum". While both the predicted gravitational redshift (based on using the mean molecular mass of hydrogen) and the observed gravitational redshift (based on spectra that were highly contaminated by the spectral features of Sirius A) were too small by a factor of four with respect to the modern value ($+89 \pm 16$ km s^{-1}, Greenstein et al. 1971), these results provided momentum to achieve a deeper theoretical understanding of WDs.

1.2 The Theory behind White Dwarfs

Not surprisingly, Arthur Eddington was one of the first to evaluate the theory of WDs. He was able to show that at these extreme densities and energies, electrons flowed freely within the matter, energetic enough to escape any nearby nuclei. A paradox arose from this analysis – if one assumes there is a correlation between energy and temperature (entirely valid based on observations of the era), then one expects a star's internal temperature to be higher than at the surface to drive the radiation (hence energy) out. Presumably, radiation will continue to be emitted as long as the star contains matter at a high temperature. According to Eddington, eventually the star will have radiated so much energy that it will have less energy than normal matter in a low density environment and at zero temperature (Eddington 1926). Of course, this is not possible and arose because of some simplifying assumptions. The most exact statistical mechanics would be necessary to resolve this paradox.

1.2.1 A Sequential Progression of our Understanding

Quantum Mechanics was born near the turn of the 20th century. During its first few decades, physicists worked to refine the theory and exploit its many implications. By the mid 1920s, it was generally agreed that an electron in an atom could be characterized by four quantities, the principal quantum number, the orbital angular momentum quantum number, the magnetic quantum number, and the intrinsic

angular momentum quantum number (although this quantity was not predicted by current theory of that time but was necessary based on experiment). In 1925, Wolfgang Pauli showed that no two electrons could occupy the same quantum mechanical state (i.e., containing all four identical quantum numbers), a "rule" now known as the Pauli exclusion principle. The following year, Enrico Fermi announced a statistical approach to describe atoms that incorporated the exclusion principle, now known as Fermi-Dirac statistics.

Later that year, physicist Ralph Fowler utilized these latest tools to solve Eddington's paradox (Fowler 1926). He demonstrated that individual electrons in such a dense environment must be degenerate in that all possible low energy quantum mechanical states are occupied. At absolute zero, the electrons still have a kinetic energy equivalent to the thermal energy of normal particles in a low density environment up to millions of degrees. In addition, he showed that the pressure, P, of the WD gas is unaffected by its temperature and is only affected by its mass density, ρ, being related as $P \propto \rho^{5/3}$ (Lang & Gingerich 1979). This result further paved the road for a deeper theoretical understanding of the internal makeup of WDs by subsequent researchers.

In 1927, Werner Heisenberg presented an essay describing a fundamental limitation dictated by quantum mechanics now known as Heisenberg's uncertainty principle. It states that the precision to which one can simultaneously know both the position and the momentum of a particle can be no better than $\hbar/2$ ($\hbar = h/2\pi$), where h is Planck's constant. This, coupled with the Pauli exclusion principle, provides two key-

stones to the theoretical framework describing degeneracy pressure, to be discussed further in the next section.

In 1929, Wilhelm Anderson demonstrated that the electrons within a degenerate gas begin to reach velocities approaching a sizable fraction of the speed of light. He utilized the equations of special relativity to show that for a relativistic degenerate electron gas, the relation between pressure and mass density is $P \propto \rho^{4/3}$. He and Edmund C. Stoner quickly realized that this degenerate gas can only be stable up to a finite mass (for WD masses larger than ~ 1 $M_\odot$), above which there are no equilibrium WD configurations; however, no detailed calculations were performed.

In 1931, Subrahmanyan Chandrasekhar derived the equation of state of a degenerate gas in the extreme relativistic limit and found a uniquely determined WD mass. Above this limit, the instability produces a catastrophic explosion, obliterating the WD, which we now know as a Type Ia supernova. The canonical maximum mass is ~ 1.4 $M_\odot$ and is known as the Chandrasekhar limit (even though Anderson and Stoner recognized this effect first) because of the detailed derivations he completed. This calculation marked a significant advancement in our understanding of the nature of WDs – almost two decades after the first WDs were fairly well characterized observationally.

1.2.2 The Physics of Electron Degeneracy Pressure

Electrons are fermions and as such, they obey the Pauli exclusion principle; therefore, no two electrons can have the same quantum mechanical state. All particles, including electrons, obey the Heisenberg uncertainty principle, which limits the accuracy to which one can know a particle's position and momentum simultaneously. This can be expressed as

$$\Delta x \Delta p_x > \frac{\hbar}{2} \tag{1.1}$$

where Δx and Δp_x are the uncertainties in position and momentum respectively and $\hbar$ is Planck's constant, h, divided by 2π. One can approximate the electron degeneracy pressure using a straightforward approach and a few assumptions. We start with the pressure integral expression as follows

$$P = \frac{1}{3} \int_0^\infty n_p p v \ dp, \tag{1.2}$$

where p and v are the particle's initial momentum and velocity respectively, while n_p is the number density of particles having momenta between p and $p + dp$. If we assume (rather unrealistically) that all of the electrons have the same momentum p then this integral reduces to

$$P \approx \frac{1}{3} n_e p v, \tag{1.3}$$

with n_e representing the total electron number density. We need to find expressions for each variable in our simplified pressure equation.

Step 1: Because WDs have overall charge neutrality, we expect that the number density of ions (n_+) of atomic number Z will equal the number density of electrons (i.e., $Zn_+ = n_e$). Additionally, because nucleons are significantly more massive than electrons, we can neglect the electron mass in the determination of the mass density ρ (i.e., $\rho = A m_p n_+ + m_e n_e \simeq A m_p n_+$, where A is the atomic mass, m_p is the rest mass of the proton, and m_e is the rest mass of the electron). Coupled together, these two relations give an expression for the electron number density

$$n_e = \left(\frac{\# \text{ electrons}}{\text{nucleon}} \right) \left(\frac{\# \text{ nucleons}}{\text{volume}} \right) = \left(\frac{Z}{A} \right) \frac{\rho}{m_p}. \tag{1.4}$$

Step 2: Because of the Pauli exclusion principle, electrons have to be separated by at least the amount of their physical size. If we evaluate this limit, we find that the separation between neighboring electrons $\Delta x \approx n_e^{-1/3}$. Substituting this into Heisenberg's uncertainty relation gives us an estimate of the momentum of the electron,

$$p \approx \Delta p \approx \frac{\hbar}{\Delta x} \approx \hbar n_e^{1/3} \tag{1.5}$$

$$p \approx \hbar \left[\left(\frac{Z}{A} \right) \frac{\rho}{m_p} \right]^{1/3},$$ (1.6)

ignoring the factor of two that arises because electrons can have anti-parallel spins.

Step 3: Perhaps the most trivial expression is that for the velocity; nonrelativistic electrons have velocity

$$v = \frac{p}{m_e}$$ (1.7)

$$v \approx \frac{\hbar}{m_e} \left[\left(\frac{Z}{A} \right) \frac{\rho}{m_p} \right]^{1/3}.$$ (1.8)

Incorporating Eqs. (1.4), (1.6), and (1.8) into Eq. (1.3), we find that the electron degeneracy pressure is

$$P \approx \frac{\hbar^2}{3m_e} \left[\left(\frac{Z}{A} \right) \frac{\rho}{m_p} \right]^{5/3}.$$ (1.9)

This expression is a fairly close approximation (within roughly a factor of five) to the more precise expression given as

$$P = \frac{(3\pi^2)^{2/3}}{5} \frac{\hbar^2}{m_e} \left[\left(\frac{Z}{A} \right) \frac{\rho}{m_p} \right]^{5/3}.$$ (1.10)

While this result describes the electron degeneracy pressure that is the stabilizing mechanism preventing WD collapse, the details are not quite right. For instance, we have neglected relativistic effects that would be present because the electrons are mov-

ing a significant fraction of the speed of light in a WD. Subrahmanyan Chandrasekhar evaluated the degenerate pressure in the limit that $v = c$ and obtained

$$P = \frac{(3\pi^2)^{1/3}}{4}\hbar c \left[\left(\frac{Z}{A}\right)\frac{\rho}{m_p}\right]^{4/3}, \qquad (1.11)$$

which corresponds to a dynamically unstable situation. Any deviation from equilibrium will cause electron degeneracy to fail and the WD will collapse. This situation arises at a maximum mass for the WD, the Chandrasekhar limit, and the implications are vital to our current understanding of cosmology as discussed next.

1.3 Why are White Dwarfs Useful?

The very nature of WDs, in that their physics is moderately well understood, allows us to use their predictable attributes as constraints for a broad range of astrophysically interesting problems. Here I outline only a few and begin with the largest scale applications and end with those closest to home (the focus of my research).

1.3.1 Indicators of the Age of the Universe

We have long sought an answer to the question, how old is the universe? Early estimates using approximate ages of the oldest stars in the Galaxy yielded an age of $\sim$15 billion years. However, early estimates based on the Hubble constant (i.e., the expansion of the universe) yielded an age of $\sim$9 billion years. The discrepancy could be explained if the Hubble constant is not constant. A particular type of WD, a Type

Ia supernova, has been used to probe deeper into this conundrum. These supernovae erupt because a close companion dumps matter onto a WD, pushing it beyond the critical Chandrasekhar limit. In theory, all Type Ia supernovae will have the same luminosities because the masses and physical processes involved are the same. Thus, they can be used as standard candles to infer the universe's expansion rate because a measure of the apparent brightness provides a constraint on the distance. After observing 50 Type Ia supernovae (36 "nearby" and 14 with redshifts from 0.16 to 0.62), Riess et al. (1998) have concluded that the farthest supernovae are fainter than expected. These results imply that the universe is expanding at an accelerating rate (hence the Hubble constant is not constant) and was awarded the "Breakthrough of the Year" in 1998 by Science Magazine. Accounting for this effect, the cosmological models predict a more consistent age of $\sim$14 billion years.

Because WDs do not have significant energy generation mechanisms, they merely cool as they radiate the thermal energy left over from when they were "alive". This property enables us to infer a WD's age from its temperature (i.e., the oldest WDs are the coolest). As a completely independent check on the universe's age, Richer et al. (2002) have used the Wide Field Planetary Camera 2 (WFPC2) on *HST* to image the faintest WDs in the nearest globular cluster, M4. They find that the coolest WDs in this cluster are between 12 and 13 billion years old. Including the relatively short amount of time it took for the cluster to form after the Big Bang, this age is entirely consistent with the Type Ia supernovae conclusions. The second nearest globular

cluster, NGC 6397, has undergone similar intense observations using *HST*, except the Advanced Camera for Surveys (ACS) was used instead of the WFPC2 (ACS has a resolution superior to WFPC2). Hansen et al. (2007) measured the most precise age determination of NGC 6397 to date, 11.47 ± 0.47 billion years, by observing and modeling the entire WD cooling sequence. This slightly younger age implies that NGC 6397 was formed at a redshift $\sim$3, an era in which star formation was at a peak, as measured by deep cosmological surveys (Madau et al. 1996; Thompson et al. 2006).

1.3.2 Proxies for Galactic Components and Dark Matter

By the very same process, WD cooling ages can constrain ages of Galactic components, thin disk, thick disk, and halo. Several researchers have attempted to tackle this problem by generating a WD luminosity function. In general, a luminosity function is derived using a complete volume limited sample by counting the number of objects within various luminosity bins. The point at which the luminosity function "turns over" and the number of WDs falls off quickly gives an indication of the age of the oldest members in that sample. It has been pointed out that thick disk WDs dominate the luminosity function at low luminosities, so the age derived would pertain to the thick disk rather than the thin disk. The results seem to indicate that the Galactic thick disk is no older than 10 billion years, while the thin disk's major star formation was 7 to 8 billion years ago (see Reid 2005, and references therein). Unfortunately, the halo WD population is, at present, not well defined.

One would expect halo WDs to be $\sim$14 billion years old – nearly as old as the Galaxy. This is used as a constraint for halo WD members rather than using WDs to constrain the age of the halo. The reason for this is that halo WDs have been suggested to explain at least some of the dark matter in the Galaxy. By observing microlensing events in the direction of the Large Magellanic Cloud (LMC), Alcock et al. (2000) find that $\sim$20% of the halo is made up of massive compact halo objects (MACHOs) with masses from 0.1 $M_\odot$ to 1 $M_\odot$, with a peak at 0.5 $M_\odot$. Because the local WD mass distribution peaks at $\sim$0.6 $M_\odot$ (Liebert et al. 2003), it has been suggested that MACHOs are actually old, faint WDs. Attempts to detect these faint, compact objects have led to significant controversy. Oppenheimer et al. (2001b) claim to have directly detected halo dark matter by discovering 38 cool WDs with space motions indicative of halo-type kinematics. More recently, Bergeron et al. (2005) have shown that many (or perhaps all, depending on whether they are hydrogen or helium WDs) of these objects are likely too warm (hence too young) to be halo WDs, although precise trigonometric parallaxes are necessary to constrain the modeling.

A large scale effort called SPY (SN Ia Progenitor surveY) is currently underway to identify progenitors to Type Ia supernovae. With fairly high resolution spectra, this team has determined the kinematics of 398 hydrogen WDs, which they claim is the "largest homogeneous sample of [WDs] for which 3D space motions have been determined" (Pauli et al. 2006). Again, based on kinematics, they find seven halo candidates, indicating that 2% of their magnitude limited sample belongs to the halo.

If we assume these 398 WDs are representative of all WDs, then these results indicate that WDs do not make up a sizeable fraction of the dark matter in the halo, much less a sizeable fraction of the MACHOs. Our understanding of objects in the halo is rather neophytic, thus, the possibility remains that halo WDs do contribute significantly to the dark matter in the Galaxy.

1.3.3 Surrogates for Planetary Evolution

Unlike the previous two sections that describe useful applications for WDs that have been tested and sometimes confirmed, this application has yet to be witnessed observationally. Currently known are two exoplanet systems that contain WDs (GJ 86 and HD 147513); however, the planets orbit distant main-sequence companions to the WDs rather than the WDs themselves (Raghavan et al. 2006). Theory dictates that the Sun will lose more than half of its mass and become a WD. When it does, the outer planets will remain in orbit (albeit with transformations of their own). Presumably, this has already occurred in the Milky Way and systems such as these merely await detection. If found, we could probe these systems to better understand what impact stellar evolution has on planetary evolution, both individually (i.e., atmospheric changes) and as a system (i.e., orbit migrations).

Because of the faintness and spectral signatures of WDs (i.e., few, if any, broad absorption lines), current radial velocity techniques are inadequate for planet detection, leaving astrometric techniques as the only viable option. For a given system, the

astrometric signature is inversely related to distance. Hence, nearby WDs are excellent candidates for astrometric planetary searches because the astrometric signature is greater than for an identical WD system more distant. As a population, a complete volume limited WD sample is necessary to provide unbiased statistics; however, their intrinsic faintness has allowed many to escape detection.

One main focus of my dissertation research is to significantly improve the WD sample within 25 pc, as well as to monitor WDs within 10 pc to detect astrometric perturbations caused by unseen companions. Also, I intend to thoroughly characterize nearby WDs using many aspects of observational astronomy including photometry, spectroscopy, and astrometry. With this wealth of data, unusual objects are sure to present themselves (as you will soon see). In particular, I hope to identify potential double degenerates (binary WDs). Once identified, I will utilize additional high resolution observational techniques, i.e., speckle, adaptive optics, high resolution spectroscopy, and interferometry via *HST*'s Fine Guidance Sensors (FGS), in hopes of resolving the pair and constraining dynamical masses for the components. These results will lead to a better understanding of binary evolution and will test the reliability of the theoretical WD mass-radius and initial-to-final-mass relationships.

Chapter 2

Known Nearby WD Statistics

As of August 2006, there are 5557 WD systems catalogued in the McCook and Sion online WD database[1] (McCook & Sion 1999), the most comprehensive WD database available. More than half of these systems have been catalogued in recent years by the Sloan Digital Sky Survey (SDSS). Yet, only 318 systems have trigonometric parallaxes, and of those, only 109 systems have trigonometric parallaxes placing them within 25 pc (the horizon of the Catalog of Nearby Stars (CNS, Gliese & Jahreiß 1991) and the NStars database (Henry et al. 2003)). If we constrict the volume to encompass only those WDs within 10 pc (the RECONS horizon), we find a mere 18 systems each containing only one WD. While this may seem small compared to the 230 main-sequence systems within 10 pc (as of January 1, 2007), this sample of WDs is thought to be largely complete; e.g., Holberg et al. (2002) predict that all WDs out to 13 pc have been found. We need to evaluate these assertions by taking a closer look at the 10 pc WD sample.

2.1 WDs within 10 pc (the RECONS Horizon)

Is the 10 pc WD sample complete? If it is, then there are interesting "curiosities" about the WDs' proper motions and sky distribution. Note that the characteristics presented here are probably not statistically significant because we are evaluating a very small sample of objects (18); hence they are addressed as "curiosities".

---

[1]See http://heasarc.gsfc.nasa.gov/W3Browse/star-catalog/mcksion.html

2.1.1 Proper Motion Distribution

Table 2.1 is a compilation of the astrometric data for the WD 10 pc sample prior to the results contained in this dissertation. The first curiosity occurs if we look at the proper motions (column 4). With one exception, all 10 pc WDs have proper motions greater than $1.0''$ yr^{-1} (94%). By comparison, of the 230 main-sequence systems within 10 pc, only 114 have proper motions greater than $1.0''$ yr^{-1} (50%). There exists the possibility that selection effects, which arise from several WD discovery methods to be discussed in Chapter 3, are to blame. It is necessary to first address a few other possibilities for this discrepancy.

Table. 2.1: Astrometric Data for Known White Dwarfs within 10 pc.

WD Name	R.A.	Decl.	μ	θ	Ref.	Parallax	Ref.	$V_{\tan}$	Notes
	(J2000)		($''$ yr^{-1})	(deg)		(mas)		(km s^{-1})	
(1)	(2)	(3)	(4)	(5)	(6)	(7)	(8)	(9)	(10)
2359−434......	00 02 10.73	−43 09 55.6	1.020	139.7	S	127.40± 6.80	Y	37.9	
0038−226......	00 41 26.03	−22 21 02.3	0.604	230.5	S	101.20±10.40	Y	28.3	
0046+051......	00 49 09.91	+05 23 19.1	2.978	152.9	H	231.88± 1.79	Y,H	60.9	1
0413−077......	04 15 21.80	−07 39 29.3	4.088	213.2	H	199.00± 0.77	Y,H	97.4	1
0426+588......	04 31 11.48	+58 58 37.6	2.427	147.6	H	180.63± 0.78	Y,H	63.7	1,2
0435−088......	04 37 47.41	−08 49 10.6	1.573	171.9	S	105.20± 2.60	Y	70.9	
0552−041......	05 55 09.53	−04 10 07.1	2.377	167.0	L	155.00± 2.10	Y	72.7	
0553+053......	05 56 25.47	+05 21 48.4	1.026	205.1	Le	125.00± 3.60	Y	38.9	
0642−166......	06 45 08.92	−16 42 58.0	1.339	204.1	H	380.02± 1.28	Y,H	16.7	1,2
0736+053......	07 39 18.12	+05 13 30.0	1.259	214.7	H	286.05± 0.81	Y,H	20.9	1,2
0738−172......	07 40 20.78	−17 24 49.2	1.252	116.0	L	112.40± 2.70	Y	52.8	
0752−676......	07 53 08.16	−67 47 31.5	2.128	135.8	S	141.20± 8.40	Y	71.4	
0839−327......	08 41 32.43	−32 56 32.9	1.745	322.0	S	112.70± 9.70	Y	73.4	
1132−325......	11 34 29.49	−32 49 52.8	1.063	320.8	H	104.84± 0.81	Y,H	46.1	1,2
1142−645......	11 45 42.93	−64 50 29.7	2.688	97.4	H	216.57± 2.01	Y,H	58.8	1
1334+039......	13 36 31.85	+03 40 46.1	3.880	252.8	Le	121.40± 3.40	Y	151.5	
1748+708......	17 48 08.02	+70 52 36.0	1.685	311.6	Le	164.70± 2.40	Y	48.5	
2251−070......	22 53 53.35	−06 46 54.5	2.586	105.2	S	123.70± 4.30	Y	99.1	

NOTES.—Units of right ascension are hours, minutes, and seconds, and units of declination are degrees, arcminutes, and arcseconds.

(1) Parallax is a weighted mean of the independent measurements of the *Hipparcos* and the Yale Parallax catalogs.

(2) Coordinates, proper motion, and parallax are for the primary component. These quantities are not determined directly for the WD secondary because the angular separation is small.

REFERENCES.—(H) Perryman et al. 1997; (L) Luyten 1979a; (Le) Lépine & Shara 2005; (S) SCR, this work; (Y) van Altena et al. 1995

The first possible explanation is that WDs, in general, are old objects that have completed numerous orbits around the Galaxy over their lifetimes. Thus, they have had plenty of time to undergo close encounters with giant molecular clouds, which cause perturbations that change their velocity vectors and may give them abnormally large transverse velocities relative to our lines of sight. If this is the case with the 10 pc WD sample, we should see similar characteristics in another aging population, the M dwarfs. Reid et al. (2002) conducted simulations that predict the average age of an M dwarf to be 4.5 Gyr, assuming a disk age of 10 Gyr and a uniform birth rate. In addition, M dwarfs are significantly less massive so perturbations will be amplified. Therefore, we should expect to see a similar proper motion distribution in the nearby M dwarf population. Of the 230 main-sequence systems within 10 pc, 179 have M dwarf primaries. This subset of 179 systems has only 86 (48%) with proper motions greater than $1.0''$ yr^{-1}. Figure 2.1 illustrates this discrepancy. Therefore, disk heating of WDs is probably not a significant factor to explain the WD proper motion distribution.

A second possible explanation for only high μ WDs nearby is that high velocity (i.e., tangential velocities > 100 km s^{-1}) WDs are the donor remnants of Type Ia supernovae events. In this scenario, a WD component of a binary system accretes material from its companion. The accretion must be large enough to facilitate steady burning; otherwise, nova eruptions will occur and relieve the WD of its accreted mass. Conversely, the accretion must be small enough to prevent a swelling of the accretion

Figure. 2.1: Histogram plot of the proper motion distributions for the 10 pc WDs (blue) and the 10 pc red dwarfs (red). Proper motions are binned by 0.5″.

disk to the point that it swallows the donor and produces a common envelope phase (Hansen 2003). When the accretion pushes the WD beyond the Chandrasekhar limit, it will go supernova and the donor companion will retain its presupernova orbital velocity. The donor companion will then, over time, evolve into a WD. This scenario will inevitably produce a population of high velocity WDs. While this scenario might sound like a rarity, Hansen (2003) suggests that the local density could be as high as 2×10^{-4} pc^{-3}. Thus, we would expect to find only one within 10 pc. As predicted,

the tangential velocities for all but one[2] of the 10 pc WD sample (column 9 of Table 2.1) are less than 100 km s^{-1}. WD 1334+039, with a tangential velocity of 151.5 km s^{-1}, might very well represent an example of the donor remnant scenario. To date, no mention is made in the published literature of this possibility. Nonetheless, we can reasonably conclude that the donor remnant scenario cannot explain the proper motion distribution of the 10 pc WD sample because the majority of the sample does not have velocities that are high enough.

There seems, as yet, to be no solid explanation for the fact that all but one of the known WDs within 10 pc have rather large proper motions other than the obvious – the sample is incomplete and is biased against slower proper motions. We will return to this discussion in § 2.3 and evaluate whether the evidence supports the hypothesis that all WDs within 10 pc are known. First, we will examine another type of distribution for the 10 pc WD sample in hopes of unraveling this mystery – the sky distribution.

2.1.2 Sky Distribution

With the knowledge that many different types of stars of different masses, ages, and chemical compositions become WDs, we would expect to find WDs homogeneously within the Galactic disk at least on 10 pc or 25 pc scales. We can assume, at least

---

[2]A revised parallax for WD 2251−070, discussed in § 8.3, refines the tangential velocity to a value of 105.6 km s^{-1}.

Figure. 2.2: Sky distribution plot for the 10 pc WD sample (18 systems represented by stars). The filled arrows represent the proper motion vectors for each WD. The overplotted light curves are Galactic coordinate gridlines in increments of 10° with the north and south Galactic poles labeled as "NGP" and "SGP", respectively. The heavy curve is the Galactic plane with the Galactic center and the Galactic anticenter labeled as "GC" and "GAC", respectively. The encircled dot is the direction of the apex of solar motion and the encircled cross is the direction of the antapex of solar motion.

as a first guess, that a volume limited WD sample (providing it is a large enough sample) should be evenly distributed across the sky. It can easily be argued that the 10 pc WD sample (18 objects) is not nearly large enough to expect a homogeneous distribution. What is interesting, nonetheless, is the actual distribution of this sample (plotted in Figure 2.2).

On this plot, the 18 WDs are labeled with filled stars. Attached to each star is a filled arrow that represents the proper motion vector of each WD. The light curves represent Galactic coordinate gridlines incremented by $10°$, with the north and south Galactic poles labeled as "NGP" and "SGP", respectively. The Galactic plane is represented with a heavy curve and the Galactic center as well as the Galactic anticenter are labeled "GC" and "GAC", respectively. The encircled dot and cross represent the direction of the apex and antapex of solar motion, respectively, as defined by Mihalas & Binney (1981). In general, we expect to find relatively few high proper motion objects in the directions of the apex and antapex of solar motion because any object rotating in the Galactic disk with the Sun will have little or no tangential motion (just as it is hard to estimate the speed of an oncoming vehicle when you are in the middle of the road, while it is easier and safer to estimate the speed when standing off to the side of the road and watch the vehicle go by). One exception would be if a star was not rotating with the Galactic disk but rather is passing through the disk much like a halo object would. Yet, when we look at Figure 2.2, we see the majority of 10 pc WD systems clustered rather close to the antapex of solar motion (encircled cross). Interestingly enough, the majority of these have proper motion vectors pointing south and four have position angles within $\sim 10°$ of one another and of these, three have proper motions within $0.3'' \, \text{yr}^{-1}$ of one another (see Table 2.1). One possible explanation is that these are members of a moving group although further analysis is necessary to make a reliable assertion to this effect.

Given that all but one of these systems has a proper motion greater than $1.0'' \text{ yr}^{-1}$, we might assume that these WDs are not rotating in the disk. Thus, they likely belong to another Galactic population such as the halo or the thick disk. We can rule out the notion that any of these are halo objects simply because they are too young, including their main-sequence lifetimes, which are estimated from the masses of the WDs and subsequent inferences about the masses of the progenitors. Perhaps a few may belong to the thick disk but many are still too young for even that population.

Another interesting "curiosity" is the number of 10 pc WD systems in the northern hemisphere vs. the southern hemisphere. Historically, the northern hemisphere has been better sampled because deep all sky surveys began earlier. Only within the past several decades has the southern hemisphere been similarly observed. However, if we were to draw a line at Declination $= 0°$ in Figure 2.2 and count the number of systems above and below it, we would find that 12 of 18 systems (two-thirds) lie in the southern hemisphere – in complete contrast to expectations – and only two lie north of declination $= +10°$!

Given the evidence presented here, we could arrive at one of two conclusions, (1) that the 10 pc WD sample is complete and these curiosities are not statistically significant because of the sample size or, (2) that the 10 pc WD sample is incomplete with a significant bias against lower proper motions. I, for one, am in favor of the second option and hope to fill in some of the potentially missing WDs.

2.2 WDs within 25 pc (the NStars Horizon)

The advantage of extending the sample out to 25 pc is that we begin to reach a statistically significant sample. In total, there are 109 WD systems that have trigonometric parallaxes placing them within 25 pc. By evaluating this sample in a similar manner as that of the 10 pc sample, we will see that at least a few WDs are still missing within 25 pc.

2.2.1 Proper Motion Distribution

To avoid a lengthy table of astrometric data for the 109 WD systems within 25 pc in this section, I have included a table of relevant data for this sample in Appendices A and B. Rather than comparing this WD sample to the sample of red dwarfs within 25 pc, which number in the thousands, I have compared them to the sample of A and F main-sequence stars within 25 pc. This sample was compiled by sifting the *Hipparcos* catalog for objects within 25 pc that have M_V between 0.6 (A0 = 0.6, Binney & Merrifield 1998) and 4.3 (G0 = 4.4, Binney & Merrifield 1998). A further constraint, a color boundary, was added to remove any evolved stars (at least highly evolved stars). If the star's $(B - V)$ was less than the value defined by the line

$$(B - V) = \frac{M_V + 0.02}{6.2},$$

(2.1)

Figure. 2.3: H-R Diagram for *Hipparcos* stars within 25 pc. The A and F main-sequence stars selected by color are inclosed in the shaded parallelogram defined by limits discussed in the text.

then it was included in the sample. In total, 138 A and F stars make up this sample

and are inclosed in the shaded region of Figure 2.3. We can be highly confident that

the A and F stars represent a complete sample (except for any that were removed be-

cause of bad color or no color information) because the *Hipparcos* catalog is complete

to a V of 7.3. At this magnitude, even a late F star ($M_V = 4.3$) would be detected

out to $\sim$40 pc. The main-sequence sample was selected for comparison because it is

these stellar types that were the progenitors of most of the WDs in the 25 pc sample.

A comparison might hint at the incompleteness of the WD sample and may shed light

on what effect stellar evolution has on the kinematics of an object.

Figure. 2.4: Histogram plot of the proper motion distributions for the 25 pc WDs (blue) and the 25 pc A and F main-sequence stars (green). The bin height of WD systems at lower proper motion bins is indicated by a solid line through the taller bin height of the main-sequence systems. Proper motions are binned by 0.25″.

We see from Figure 2.4 that the proper motions of the two samples are not consistent. The main-sequence sample is skewed to lower proper motions. The dearth of WDs at lower proper motions relative to the main-sequence sample might indicate that the WD sample is incomplete in this proper motion regime. What is clear from Figure 2.4, with the confidence we have in the completeness of the main-sequence sample, is that these two samples are fundamentally different in terms of proper motion. We can be reasonably confident that the number of WD systems moving faster

than $1.0'' \, \mathrm{yr}^{-1}$ is complete (except for perhaps a few very cool and faint WDs). Thus, the discrepancy at larger proper motions is likely a real effect. A number of scenarios might provide an explanation. The most likely are (1) age effects mentioned in § 2.1.1, (2) population membership (i.e., thin disk vs. thick disk) and, (3) a velocity kick during the later stages of evolution.

The above comparison may indicate that we should expect WDs to have larger proper motions than their main-sequence progenitors. In light of this, it may be no surprise that the 10 pc WD sample analyzed in § 2.1 is heavily skewed to larger proper motions. After a brief assessment of the sky distribution for the 25 pc WD sample, we'll compile all the analyses to determine if we are missing nearby WDs.

2.2.2 Sky Distribution

Not so surprising because of the greater numbers, the 25 pc WD sample is far more homogeneously distributed across the sky than the 10 pc WD sample as shown in Figure 2.5. Again, proper motion vectors are represented by arrows. Perhaps worthy of note, most of the highest proper motion WDs (longest arrows) are found in the half of the sky between right ascensions 0 hours and 12 hours. When we divide up the sky by equal area bins, we see subtle inhomogeneities in the number densities.

As is evident in Table 2.2, there appears to be a paucity of systems in the southern hemisphere but particularly in the quarter of sky below declination $= -30°$ (where telescopes in the United States cannot reach). As mentioned previously, the sampling
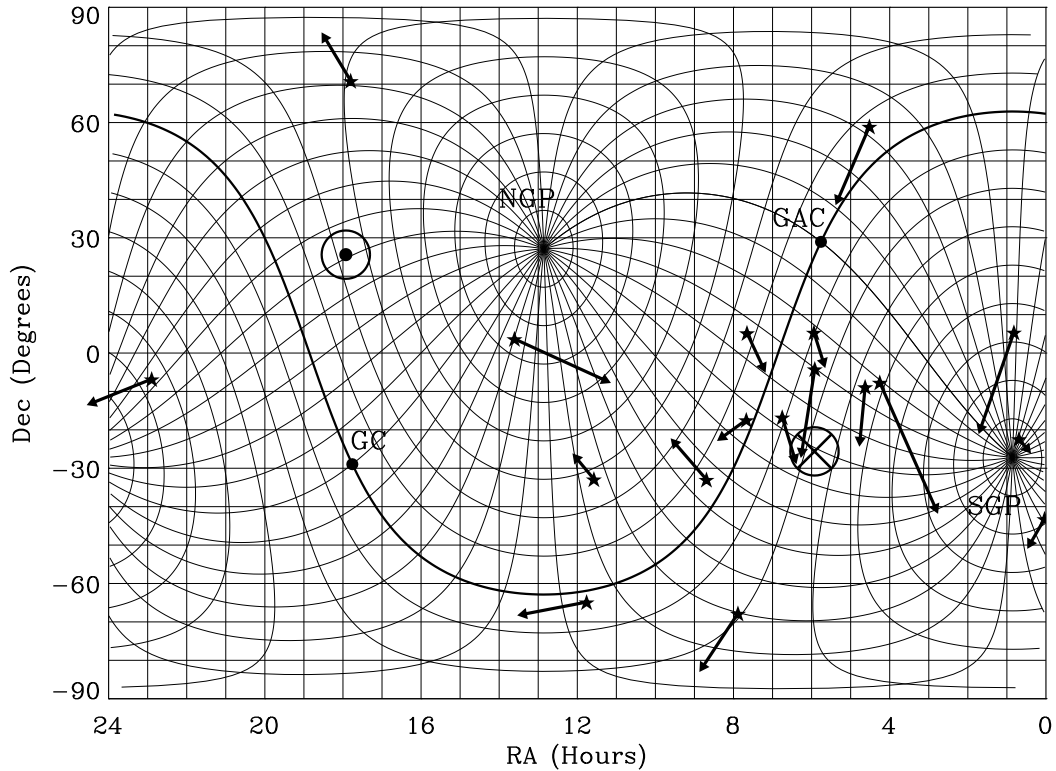
Figure. 2.5: Sky distribution plot for the 25 pc WD sample (109 systems represented by filled stars). The filled arrows represent the proper motion vectors for each WD. The overplotted light curves are Galactic coordinate gridlines in increments of 10° with the north and south Galactic poles labeled as "NGP" and "SGP" respectively. The heavy curve is the Galactic plane with the Galactic center and the Galactic anticenter labeled as "GC" and "GAC", respectively. The encircled dot is the direction of the apex of solar motion and the encircled cross is the direction of the antapex of solar motion.

Table. 2.2: 25 pc WD Sky Distribution

Declination Range	# of Systems
+90 to +30..........	32
+30 to +00..........	37
−00 to −30..........	25
−30 to −90..........	15

of the two hemispheres is not equal. It seems we now have a good indication that there are nearby WDs that we do not yet know about. The next aim is to quantify how many systems are missing.

2.3 Missing WDs

Thus far, the analyses aimed at identifying incompleteness in the WD sample are rather ambiguous. It seems the nearby WD sample has larger proper motions than both a young A and F dwarf sample and an older M dwarf sample (for the 10 pc sample). This effect may be a natural consequence of stellar evolution or it may be a selection effect that is biased against slower proper motion. As an independent approach, we will evaluate incompleteness by setting a distance limit within which we believe the sample is complete and then extrapolate to a further distance assuming a constant density.

If we make two assumptions, (1) that all WDs out to 10 pc are known and (2) that the WD local density is constant out to 25 pc, we can estimate the number of missing WDs out to 25 pc. We have already assessed that the first assumption may be problematic. The second assumption is likely valid because we are concerned with a rather small volume compared to the ∼300 pc scale height derived for main-sequence objects with $M_V \geq 3$ within 1 kpc of the Galactic disk (Gilmore & Reid 1983). The equation for density as a function of height above/below the disk is:

$$D(z) = D(0)e^{-|z|/\beta}, \tag{2.2}$$

where $D(0)$ is the density in the plane, and β is the scale height (300 pc in this case). If we set $D(0) = 1$, we can evaluate the percentage of the decline in density as we climb out of the plane to $z = 50$ pc. In doing so, we find that at 50 pc, the density will be $\sim$79% that of the density at the plane (assuming the Sun is at a z of 20 pc). In addition, WDs as a population tend to be older than many main-sequence stars and certainly make up a portion of the thick disk, which has a larger scale height ($\sim$1350 pc, Gilmore & Reid 1983). We can reasonably assume that the WD scale height is larger than the 300 pc assumed for this calculation, so that the $\sim$79% is a lower limit. Thus, we expect there to be no significant density gradient over the 50 pc diameter "bubble" we are evaluating.

Figure 2.6 shows that if these two assumptions hold true, we are missing 64% of the WDs that are between 10 pc and 25 pc. Also indicated is the tick mark at 13 pc, the distance assumed to be complete by Holberg et al. (2002). What is evident from this analysis is that the 13 pc WD sample is not likely complete and that the number of WDs out to 10 pc follows the constant density curve rather well, hinting that perhaps this sample is complete. If it is not complete, the number missing out to 25 pc increases (i.e., the constant density curve climbs vertically) such that the percentage missing of 64% is only a lower limit.

Figure. 2.6: A plot of the number of missing WDs assuming that all WDs out to 10 pc are known and that the local WD density is constant out to 25 pc. The red curve is the constant density curve and the blue filled circles are the WDs with trigonometric parallaxes within 25 pc. There is a tick mark at 10 pc noting the limit of completeness assumed. There is another tick mark at 13 pc noting the limit of completeness assumed by other authors (e.g. Holberg et al. 2002).

Some of these missing WDs are not actually missing; they are known but do not yet have trigonometric parallax determinations. Parallaxes are required for inclusion in the sample because we see, all too often, distance estimates that are erroneous. Many authors include WDs with estimated distances weighted equally with distances determined via trigonometric parallax. This is, in fact, the reason Holberg et al. (2002) believe the nearby WD population to be complete to 13 pc. The main contaminant that leads to erroneous distance estimates is unresolved multiplicity. If a WD is presumed to be nearby but is actually an unresolved pair of equal magnitude WDs, the distance will be underestimated by $\sim$40%. Another contaminant is misclassification. Cool WDs show little or no absorption lines and if a noisy spectrum is obtained and no prominent lines are seen, the object is classified as a WD (because no other astronomical object that we know of has a featureless spectrum). Often times, with a higher signal to noise (S/N) spectrum, these objects are reclassified as more luminous and distant subdwarfs with a few narrow absorption lines that blended with the noise in the poorer spectrum. Even if all the known WDs presumed to be within 25 pc are actually that near, we are still missing $\sim$53% using the constant density analysis. While I have targeted the known WDs estimated to be within 25 pc for trigonometric parallax determinations, I also wanted to seek out and identify new WDs that could be nearby (especially within 10 pc).

Chapter 3

How do We Detect WDs?

For the past several decades that WDs have been hunted, there have been three primary approaches that led to successful WD detections. Here I discuss each, and provide example applications.

3.1 Color Selection

By taking images of the sky through different filters, we can determine the approximate colors of objects. If we know what color a specific type of object should be, we can single out objects of that color for follow-up spectroscopy. For instance, most WDs are relatively hot and will appear blue. In practice, there is usually considerable contamination from other types of objects that have similar colors such as distant A and F dwarfs. One survey that employed this method found considerable contamination, mainly from distant hot sdO and sdB "subdwarfs". The Palomar-Green (PG) survey used two photographic plates of different colors to select ultraviolet excess (i.e., blue) objects for a quarter of the entire sky (Green 1976). These objects were then followed up spectroscopically to discern their true identities. Of the 1715 stellar-like objects with ultraviolet excesses, the majority were hot sdO and sdB objects (53%), while 448 were WDs (26%) (Green et al. 1986). The nature of the selection criteria implies that these WDs will be hot, thus luminous and distant (a hundred pc or more).

More recently, this approach has been used by the SDSS, which uses colors from five CCD photometric bands (Harris et al. 2003). Using combinations of colors, the hot WDs ($T_{\text{eff}} \geq 20{,}000$ K) are fully distinguished from QSOs. The only contaminant is that of the hot subdwarfs, sdO and sdB, which have evolved past their planetary nebula phase and are on their way to becoming WDs. At moderate temperatures, T_{eff} $\sim$7,000 K to 12,000 K, low-redshift QSOs and emission line galaxies become contaminants. Below $T_{\text{eff}} \sim$7,000 K, main-sequence stars become dominant contaminants so that follow-up spectroscopy for all candidates is not feasible. Despite this, the SDSS is responsible for doubling the number of known WDs in just a few years. The downside is that the survey is covering much of the same area as that of the PG survey, near the galactic cap, so that 75% of the sky remains neglected. Also, the coolest (i.e., oldest) WDs are largely being missed because of main-sequence contamination. It is these cool WDs that have a greater probability of being nearby because they are the least luminous and, given a magnitude limited survey, can only be detected if they are relatively close. A different approach is necessary to better target nearby WDs.

3.2 Proximity to Known Nearby Stars

A straightforward approach to finding nearby WDs is to look in the vicinity of nearby main-sequence stars. We have already seen in Chapter 1 that the first three WDs discovered are companions to bright, nearby stars. A fortunate property of most

of the nearby stars is that they exhibit significant proper motion across the sky. If one compares the star field around a nearby star at two epochs separated by at least a few years, one would see the position of the nearby star shift relative to background stars. If this star had a widely separated (and bright enough to appear on the images) companion, it would exhibit the same proper motion as the primary. Gould & Chanamé (2004) used this technique to evaluate stars that have measured parallaxes via the *Hipparcos* space astrometry mission (Perryman et al. 1997). They found 424 faint companions that exhibited the same proper motions as the primaries, and of those 20 are WDs. All but one of these WDs have parallaxes within 100 pc, but only six are within 25 pc.

Another application of the same approach was used by Oppenheimer et al. (2001a), in which they observed all the stars within 8 pc and north of declination $= -35°$. They used the newly designed adaptive optics coronagraph (AOC) fit to the 60 inch telescope on Mt. Palomar. After imaging 107 systems at two different epochs with this instrument, they found seven new companions. Curiously enough, none of these new companions were WDs. It seems all four WD companions to stars within 8 pc were discovered prior to 1930, the three mentioned previously (Sirius B, Procyon B, 40 Eridani B) and Stein 2051 B discovered by Stein (1930). Even more interesting, two of these (Sirius B and Procyon B) were discovered astrometrically, decades before they were actually seen.

3.3 Proper Motion Selection

The third approach is, by far and away, the most effective method of identifying nearby WDs. Because WDs are generally blue and faint, they can easily be confused with main-sequence stars of similar temperatures that are much farther away. One way to minimize this confusion is to select objects that have sizeable proper motions (i.e., $\mu > 0.2''$ yr^{-1}). The assumption here is that if distant blue main-sequence objects have sizeable proper motions, their space motions would be large enough that they would no longer be bound to the Galaxy and should have left long ago. Presumably, if any remain today, these types of objects are rare and contribute negliglibly to surveys. Thus, we conclude that detected objects must be much less luminous, less distant, WDs. Of course, a more quantitative approach is necessary for this method to be useful.

Dating back to the early 20th century, before WDs were well understood, Ejnar Hertzsprung (1922) used a method now known as reduced proper motion (RPM) to separate dwarfs from giants. It basically serves to correlate proper motion with proximity. Though not entirely valid, it acts as a powerful diagnostic for assigning rough luminosity classes. At the time, its applicability to WDs was not yet conceived. The modern form of the equation is nearly identical to the absolute magnitude equation with μ replacing distance.

$$H = m + 5 + 5\log\mu, \tag{3.1}$$

where m is the apparent magnitude of the object and μ is its proper motion in units of arcsec yr^{-1}. This equation effectively relates two observable quantities, apparent magnitude and proper motion, to a combination of two intrinsic properties, luminosity (absolute magnitude) and tangential velocity. We know that transverse velocity is related to distance by

$$V_T = 4.74\mu d \tag{3.2}$$

$$d = \frac{V_T}{4.74\mu}, \tag{3.3}$$

where V_T is an object's transverse velocity in units of km sec^{-1} and d is its distance in pc. We can then incorporate this into the absolute magnitude equation,

$$m = M + 5\log d - 5, \tag{3.4}$$

where M is absolute magnitude. Finally, we correlate RPM with tangential velocity as follows,

$$H = M + 5\log V_T - 3.38. \tag{3.5}$$

As a result, the RPM diagram is also efficient at separating high velocity objects such as halo/thick disk subdwarfs. Note, the term "subdwarf" as used here is very different than the hot sdO and sdB type subdwarfs mentioned in § 3.1 (see Jao et al. 2007, in preparation for a full discussion). Here, subdwarf refers to the old metal-poor stars likely not formed in the thin disk (luminosity class VI).

The most comprehensive proper motion catalog ever compiled for the northern hemisphere was done by Lépine & Shara (2005), called the LSPM-North catalog (to be discussed further in § 4.3). In it are 61,977 stars that have proper motions greater than $0.15''$ yr^{-1}. Prior to this work, the proper motion catalog standard for 25 years was the NLTT Catalogue (discussed in § 4.1). Also included is the best available magnitude and color information for each star, primarily from photographic plates. With these two pieces of information, the authors created a RPM diagram, shown in Figure 3.1. The WD region is clearly delineated from the halo/thick disk subdwarf region. There is significant contamination between the halo subdwarfs and the disk dwarfs. While no single object's luminosity class is confirmed without follow-up spectroscopy, it is clear that this approach provides a vetted sample of promising WD candidates.

In an effort to identify new nearby WDs in the southern hemisphere, I used the RPM diagram as well. To date, no similar comprehensive proper motion catalog to the LSPM-North catalog has been compiled in the southern hemisphere. Therefore, I will briefly outline the various proper motion studies conducted in the south, as

Figure. 3.1: Reduced proper motion diagram for the 61,977 stars in the LSPM-North catalog. Clearly delineated are the WDs from the halo subdwarfs, which are much less delineated from the dwarfs. Reproduced from Lépine & Shara (2005).

well as give a detailed description of the proper motion survey we conducted, called the SuperCOSMOS-RECONS proper motion survey. I will then discuss my WD discoveries from the RPM diagram once these surveys have been addressed.

Chapter 4

Proper Motion Surveys

Stars have been known to exhibit proper motions for centuries. A small sample of stars have rather large proper motions. This quantity for a given star is usually the first measurement indicating that the star is nearby. This reasoning follows the analogy of a passenger riding in a car and looking out the window. The nearby light posts along the road pass very quickly, while the distant mountains in the background seem to move very slowly. Similarly, if a star has a very large proper motion, it seems to speed by while the background stars stay put. The difference in the analogy is that neither the light posts nor the mountains have any intrinsic motion; all of the perceived motion is because of the moving car. In contrast, not only is the Sun (our celestial car) moving, but also every other star in the Galaxy. Thus, proper motion is a convolution of our motion and the star's intrinsic motion, which is why proper motion and distance are not perfectly correlated. Nonetheless, the compilations of proper motions have proved vital for detecting nearby stars.

Proper motion objects are primarily discovered by imaging the same piece of sky at least twice separated by several years in time. This technique of imaging for the sake of detecting proper motion stars first began near the turn of the 20th century (e.g., Kretz 1900). By blinking the two photographic plates, the high proper motion (HPM) objects were easily noticed because their positions change relative to the background stars. Because the motion is relative to the background stars, it is known

as relative proper motion. Another older technique used to discover HPM objects is with meridian circle observations (e.g. Tucker 1905). This technique uses a telescope that only observes the meridian and measures the precise time that a star crosses the meridian. The change in this measurement over time for a given object reflects the star's proper motion. Because this measurement does not depend on background stars, it is considered an absolute measurement. The correction from relative to absolute depends on the average proper motion of the background stars and is on order of a few milliarcseconds (mas).

4.1 The LHS and NLTT Surveys

The first catalog of stars with proper motions greater than $0.5''$ yr^{-1} was compiled by van Maanen (1915) and contained 533 entries. Over time, measurement precision improved and more objects were found. Arguably the most famous compilation of stars with proper motions greater than $0.5''$ yr^{-1} was that of Luyten (1979a). Willem Luyten was a prominent astronomer throughout much of the 20th century, remembered for coining the term "white dwarf" in 1922 and the publication of his proper motion catalogs in 1979. The Luyten Half-Second (LHS) catalogue contains 3602 objects with proper motions greater than $0.5''$ yr^{-1} (Luyten 1979a). The majority of the objects in this compilation were discovered via the Palomar Survey and the Bruce Proper Motion Survey. The Palomar Survey covered declinations north of $-33°$ and reached magnitude limits of m_{pg} $\sim$21.1 and m_R $\sim$19.4. The Bruce Survey covered

the remainder of the southern hemisphere but only reached a magnitude limit of m_{pg} ~ 16.0.

As a continuation of this effort, Luyten compiled the New Luyten Two-Tenths (NLTT) catalogue, which consisted of 58,845 objects with proper motions greater than $0.18''$ yr^{-1} (Luyten 1979b). With a sample size this large, it is informative to plot the sky distribution of these objects to see if there are any undersampled regions.

Figure. 4.1: Plot of the sky distribution of the 58,845 objects in the NLTT catalogue. The heavy line represents the Galactic plane. Coordinates are epoch J2000.

As is evident in Figure 4.1, the southern hemisphere is grossly undersampled, especially at declinations below $-33°$. Also evident is the region $\sim 10°$ above and

below the Galactic plane, which is depleted of points. As Luyten pointed out, these are "high density fields in low galactic latitude which cannot now be handled". While it will take a more careful analysis to deal with these high density fields, the region south of declination $= -33°$ remained a happy hunting ground for new proper motion objects.

4.2 The Lowell Proper Motion Survey

Lowell Observatory was founded in 1894 by Percival Lowell, who is widely known as the proponent for intelligently designed canals on Mars (i.e., martian man-made). Lowell also calculated the position of the planet that caused Neptune's erroneous orbital perturbation. This effort led to the serendipitous discovery of the now re-categorized planet Pluto in 1930 by Clyde Tombaugh. In order to be certain there were no other distant planets brighter than the search limits, the survey continued until 1945. At its termination, the survey covered the entire northern hemisphere and one-quarter of the southern hemisphere. In 1955, Henry Giclas, a prominent astronomer who has spent his entire career at Lowell Observatory, proposed to take second epoch images and compare them to the "Pluto Search" data taken 25 years earlier (Putnam 1994). The project was started in 1957 and continued for nearly 20 years. The result was a proper motion catalogue published in installments in the Lowell Observatory Bulletins between 1958 and 1978. The northern survey contained 8,991 objects fainter than 8th magnitude that had proper motions greater than $0.26''$

yr^{-1} (Giclas et al. 1971). The southern survey contained 2,758 objects with proper

motions greater than $0.20''$ yr^{-1} (Giclas et al. 1978). The limiting magnitude for both

surveys is $m_{pg} \sim 16.5$.

Figure. 4.2: Plot of the sky distribution of the 11,749 objects in the Lowell proper motion catalog. The heavy line represents the Galactic plane. Coordinates are epoch J2000.

The sky distribution, shown in Figure 4.2, is fairly homogeneous in the northern

hemisphere with only a few patches of the southern hemisphere surveyed. Note that

many of these objects were included in Luyten's NLTT catalogue so the two catalogs

do not necessarily contain unique objects.

4.3 The Lépine-Shara North Proper Motion Survey

By far the most comprehensive proper motion survey in the northern hemisphere, the Lépine-Shara proper motion survey (LSPM), contains 61,977 objects that have proper motions greater than $0.15''$ yr^{-1} (Lépine & Shara 2005). The limiting magnitude is $V \sim 21$ and the completeness is estimated to be better than 99% at high Galactic latitudes ($|b| > 15°$) and better than 90% at low Galactic latitudes ($|b| \leq 15°$). This catalog has now rendered the LHS and NLTT catalogues obsolete for northern hemisphere objects. The technique used in this survey is known as SUPERBLINK, which is software that processes the scans of the photographic plates so that both epochs of the same piece of sky overlay nearly perfectly. One is then subtracted from the other so that any object that has moved will appear as a pair of objects. A significant benefit of this software is that it is successful at detecting HPM objects in high density fields. In fact, Lépine et al. (2002a,b, 2003a,b,c, 2004) found a total of 201 new objects with proper motions greater than the LHS limit of $0.5''$ yr^{-1} in the northern hemisphere. Nearly all of these new detections were in the crowded fields near the Galactic plane.

The completeness of this catalog suggests that the nonuniform distribution shown in Figure 4.3 is perhaps real. Lépine argues that proper motion selected samples are intrinsically nonuniform because proper motion surveys are more sensitive to thick disk and halo objects at high Galactic latitudes due to asymmetric drift. Lépine and

Figure. 4.3: Plot of the sky distribution of the 61,977 objects in the Lépine-Shara North proper motion catalog. The heavy line represents the Galactic plane. Coordinates are epoch J2000.

collaborators are nearing completion of a similar catalog for the southern hemisphere (Lépine, private communication) at the time of the writing of this thesis.

4.4 Southern Hemisphere Proper Motion Surveys

A quick glance at the sky coverage plots of the three previously discussed proper motion surveys should lead the reader to the conclusion that the southern hemisphere is severely undersampled for proper motion objects. First epoch observations began for both the northern and southern hemispheres at roughly the same time;

however, the southern hemisphere plates taken by the Bruce refracting telescope in Peru had a much brighter limiting magnitude ($m_{pg} \sim 16$). It was not until the mid-1970s that deep all southern sky observations began, using the European Southern Observatory's (ESO) Schmidt telescope in Chile and the British-Australian Schmidt telescope in Australia. These observations were completed in the early 1980s and almost immediately, the second epoch observations began and continued until 2002. As such, there have been several post-2000 proper motion surveys in the southern hemisphere, many of which focus on small patches rather than the entire southern sky.

4.4.1 The Wroblewski-Torres-Costa Proper Motion Survey

One of the first proper motion surveys that focused on the southern hemisphere was the Wroblewski-Torres-Costa (WTC) survey (Wroblewski & Torres 1989, 1991, 1994, 1996, 1997; Wroblewski & Costa 1999, 2001). This survey utilized plates taken using the Maksutov Astrograph operated by the University of Chile. First epoch plates were taken for 164 5°×5° fields in 1969 and 1970 with a magnitude limit $m_{pg} \sim 20$. These fields were selected because they have enough galaxies to be used as local reference frames. Second epoch observations with a similar limiting magnitude began in 1985 in an effort to identify HPM objects ($\mu > 0.15''$ yr^{-1}). In addition to recovering 1,262 objects from the NLTT catalogue, they discovered 2,495 new HPM objects. These new HPM objects are plotted in Figure 4.4a.

Figure. 4.4: (*a*) Sky distribution for the 2,495 new HPM objects discovered by the Wroblewski-Torres-Costa proper motion survey. (*b*) Sky distribution for the 1,082 new and known objects detected by the Calan-ESO proper motion survey (*points*) and for the 227 new and known detections by Scholz and collaborators (*open triangles*). (*c*) Sky distribution for the 11,289 new and known objects in the Liverpool-Edinburgh proper motion catalog. (*d*) Sky distribution of the 7,047 new and known objects detected by the Southern Infrared proper motion survey. Heavy lines in each plot represent the Galactic plane. All coordinates are epoch J2000.

4.4.2 The Calan-ESO Proper Motion Survey

This survey utilized the plates taken during the ESO survey conducted at La Silla using the ESO Schmidt telescope. ESO areas were chosen at random with the exception that all fields avoid regions near the Galactic plane because of overcrowding,

which resulted in the selection of 17 total areas (three in Ruiz et al. 1993 and 14 in Ruiz et al. 2001). In addition, three more HPM objects (ER 2, ER 6, and ER 8) were serendipitously discovered while conducting a search for supernovae, although one object (ER 6) is unrecoverable because coordinates are not given (Ruiz & Maza 1987). For the 1993 and 2001 publications respectively, the limiting magnitudes for the ESO m_R plates are quoted as $\sim$20.5 and $\sim$19.5, and the proper motion limits are $\mu > 0.10''$ yr^{-1} and $\mu > 0.20''$ yr^{-1}. A total of 1083 objects were detected, of those, 883 were not in the NLTT catalogue (although many had proper motions below the NLTT cutoff of $\mu \geq 0.18''$ yr^{-1}). Both new and known objects are plotted in Figure 4.4b (less the one object for which coordinates were unavailable).

4.4.3 The Proper Motion Survey of Scholz and Collaborators

Scholz and collaborators conducted a proper motion survey in the southern hemisphere in the region between 0^h and 7^h in right ascension and $-63°$ and $-32°$ in declination (Scholz et al. 2000). They utilized survey plates taken at the UK Schmidt telescope that had been scanned using the automatic plate measuring (APM) machine. In total, 40 fields that cover $6°\times6°$ each were selected based on image quality and the epoch spread between them. For each field, the B_J plate (limiting magnitude of $\sim$22.5) and the R_{59F} plate (limiting magnitude of $\sim$21) were digitally blinked to detect HPM objects with proper motions between 0.3 and 1.0$''$ yr^{-1}. In total, 204 objects were detected and of those, 101 were new detections. This collaboration

continued the survey to other regions of the southern sky (and with different proper motion constraints) and published several papers addressing the most interesting objects rather than compiling a catalog. Three new HPM objects were discovered by Lodieu et al. (2002), nine were discovered by Scholz et al. (2002a), two were discovered by Scholz et al. (2002b), one each was discovered by Hambaryan et al. (2004), Scholz & Meusinger (2002), and Scholz et al. (2004b), and six were discovered by Scholz et al. (2004a). The combined number of published detections from this collaboration is 227 (plotted in Figure 4.4b), with 124 of these being new detections.

4.4.4 The Liverpool-Edinburgh High Proper Motion Survey

The Liverpool-Edinburgh high proper motion survey (LEHPM) utilized the digitized scans from the SuperCOSMOS Sky Survey (SSS) to detect HPM objects (Pokorny et al. 2004). The SSS is a database of plate scans from both the ESO and UK Schmidt surveys in the R-band (R_{ESO} and R_{59F}, respectively) as well as the UK Schmidt B_J and I_{IVN} that cover the entire southern hemisphere. In this survey, only the two R-bands were used for detections and they have similar limiting magnitudes of $\sim$19.5. This survey covers south of declination $-20°$, including nearly 7000 square degrees around the south Galactic cap, avoiding the Galactic plane by $20°$ in either direction. Fields near the Magellanic Clouds or for which the two R-band plates had less than a three year spread in epochs were discarded. The final survey contained 11,289 objects with proper motions greater than $0.18''$ yr^{-1}. No cross-referencing was done by the

authors so it is unclear (without a monumental amount of effort) what percentage of the objects are new detections. Nonetheless, the LEHPM survey was perhaps the most comprehensive survey in the southern hemisphere upon its publication. Figure 4.4c shows the sky distribution of the HPM detections.

4.4.5 The Southern Infrared Proper Motion Survey

Another survey to utilize digitized scans from the SSS, the Southern Infrared Proper motion Survey (SIPS) targeted very red objects (Deacon et al. 2005a, hereafter SIPS 1; Deacon & Hambly 2007, hereafter SIPS 2). Because of overcrowding, this survey avoids the Galactic plane by $15°$ in either direction. As an initial sift, the Two Micron All Sky Survey (2MASS) database was used to identify all objects in the search area with infrared colors indicative of mid-M to late-T type dwarfs (see Figure 1 of Deacon et al. 2005a) that were brighter than $J = 16$. The remaining candidates were then compared to the SSS I_{IVN} plate for counterparts. Any counterpart that did not display at least the minimum proper motion cutoff ($0.4''$ yr^{-1} in SIPS 1 and $0.1''$ yr^{-1} in SIPS 2) was discarded. The remaining detections were checked by eye to ensure there were no spurious detections. The resulting effort from SIPS 1 produced 143 objects, of which 68 were new detections, with proper motions greater than $0.5''$ yr^{-1}. From SIPS 2, a total of 6,904 objects were detected, of which 5,583[1] were new detections. Both new and known detections are plotted in Figure 4.4d.

---

[1]A concurrent proper motion survey by Finch et al. (2007), discussed in Section 5.5, detected many overlapping objects and it is unclear which publication will appear first (i.e., who will be the original discoverer).

It is clear that at least most of the southern hemisphere is becoming better sampled, though not nearly as well as the northern hemisphere via Lépine & Shara (2005). Many of the southern surveys are patchy, evaluating small regions for which enough data were available. This fact prompted us to team up with Nigel Hambly, the curator of the SSS at the University of Edinburgh Royal Observatory, to conduct an all southern sky sift for HPM objects – the topic of the next chapter.

Chapter 5

The SuperCOSMOS-RECONS Proper Motion Survey

The deep all southern sky survey conducted using the UK Schmidt telescope located at Siding Springs Observatory in Australia ended in 2002, after nearly 30 years of data acquisition. With the entire southern sky covered in each of three wavebands (B_J, R_{59F}, and I_{IVN}), there existed the possibility of combining all of the data to obtain multi-epoch information. First, it was necessary to scan the plates and generate digitized images. This was done at the University of Edinburgh Royal Observatory using the SuperCOSMOS machine. This fast, high-precision plate scanning instrument produced scans with $0.67''$ pixels. For comparison, the Digitized Sky Survey (DSS) scans, used for the monumental proper motion effort of Lépine & Shara (2005) in the northern hemisphere, had $1.6''$ pixels and $1.0''$ pixels for epochs one and two, respectively. Two additional surveys were also scanned using the SuperCOSMOS machine, the ESO R band and the first Palomar Observatory Sky Survey (POSS-I) E band (equivalent to R). The five surveys which make up the digitized SSS are listed in Table 5.1.

Table. 5.1: SSS Plate Information

Filter	Time Span	Decl. Range	Mag. Limit	$\Delta\lambda$[a]
B_J...............	1974 - 1994	$-90° \leq \delta \leq \ 0°$	B $\sim$ 23	3950 - 5400 Å
R_{59F}.............	1984 - 2001	$-90° \leq \delta \leq \ 0°$	R $\sim$ 22	5900 - 6900 Å
I_{IVN}.............	1978 - 2002	$-90° \leq \delta \leq \ 0°$	I $\sim$ 19	7150 - 9000 Å
R_{ESO}............	1978 - 1990	$-90° \leq \delta \leq -20°$	R $\sim$ 22	6300 - 6900 Å
E_{POSS-I}.........	1949 - 1958	$-18° \leq \delta \leq \ 0°$	R $\sim$ 20	6200 - 6700 Å

[a] Filter wavelength coverage reproduced from Morgan (1995).

One can imagine that the scanning process alone for this amount of data is a long term project. Once all the data are digitized, rigorous calibration procedures must be applied to the data so that this inhomogeneous dataset can be combined into one homogeneous catalog. Calibrations, both astrometric and photometric, were carried out and presented by Hambly et al. (2001a,b,c) and the accuracies they derived are shown in Table 5.2.

Table. 5.2: Global Properties of the SSS Catalog Data

Astrometric properties:	Absolute accuracy	Units
α, δ ($B_J < 19$)	0.1	arcsec
α, δ (faint images)	0.3	arcsec
$\mu_{\alpha,\delta}$ ($R < 17$)	10.0	mas yr^{-1}
$\mu_{\alpha,\delta}$ (faint images)	50.0	mas yr^{-1}
zeropoint error $\mu_{\alpha,\delta}$ ($R < 17$)...	<10.0	mas yr^{-1}
zeropoint error $\mu_{\alpha,\delta}$ ($R > 17$)...	$\leq$1.0	mas yr^{-1}

Photometric properties:	Accuracy absolute	relative	Units
$\sigma_{B,R,I}$ ($< 19, 18, 17$)	0.3	0.05	mag
$\sigma_{B,R,I}$ (faint images)............	0.3	0.3	mag
$\sigma_{(B-R)}$ ($B_J < 17$)	0.07	0.07	mag
$\sigma_{(B-R)}$ (faint images)...........	0.16	0.16	mag

Image detection/ completeness	external completeness	external reliability
$B_J < 19.5$	$\sim$100%	$\sim$100%
$B_J \sim 21$, R ~ 19	$\sim$75%	$\sim$90%

NOTE.—Table reproduced from Table 4 of Hambly et al. (2001c).

What is important to note is that while plate magnitudes are inherently unreliable because of the non-linearity of photographic emulsions, the color information is significantly more accurate in the SSS catalog. In particular, moderately bright objects (i.e., $B_J < 17$) have colors accurate to better than 0.1 mag (except perhaps for

the brightest objects that are completely saturated on the plate). Also, the proper motions (μ in Table 5.2) for the moderately bright objects are determined to $\sim$10 mas yr^{-1} and are defined by the extragalactic reference frame. Once each epoch's plate is mapped to a common coordinate system, the mean stellar displacement is zero (because stars dominate the number density in each image) but the galaxies are non-zero. The zeropoint error in proper motion (see "Astrometric properties" in Table 5.2) is the global offset that sets the mean galactic displacement to zero. With the wealth of good quality data for the undersampled southern hemisphere, we embarked on our own proper motion survey known as the SuperCOSMOS-RECONS (SCR) proper motion survey.

The SCR survey was published in four works. Hambly et al. (2004) outline the search method and present the five systems with $\mu \geq 1.0''$ yr^{-1} south of $\delta = -47°$. Henry et al. (2004) present four additional systems that contain stars of spectral types M6.0 V or later. The complete sample of new discoveries was published in two installments – between declinations $-90°$ and $-47°$ (Subasavage et al. 2005a), and between declinations $-47°$ and $0°$ (Subasavage et al. 2005b). Finder charts are given in Appendix E for all of the new systems reported here, as well as for the seven new wide companions.

5.1 Search Methodology

In an effort to find new HPM objects, primarily to identify new nearby stars, we employed constraints to our sift of the SSS database. We wanted to target relatively bright objects that are more likely to be nearby. Also, as noted in Table 5.2, proper motions are better determined for objects brighter than $R_{59F} = 17.0$ so we chose our faint limit to be $R_{59F} = 16.5$. In addition, we targeted objects with $10.0'' \text{ yr}^{-1} \geq \mu \geq 0.4'' \text{ yr}^{-1}$. The fast limit was determined based on the highest proper motion star known, Barnard's Star with $\mu = 10.369'' \text{ yr}^{-1}$. The slow limit was determined so that we would be consistent with the LHS survey of objects with $\mu \geq 0.5'' \text{ yr}^{-1}$ (Luyten 1979a) for comparison purposes. Our extension of the cutoff to $\mu \geq 0.4''$ yr^{-1} in this survey is to ensure that no known LHS stars were missed due to proper motion measurement errors for objects very near the $0.5'' \text{ yr}^{-1}$ limit.

Software, developed and run by Nigel Hambly, trawled the SSS database with these constraints in place. Four photographic plate sets (B_J, R_{59F}, R_{ESO}, and I_{IVN}) are positionally error mapped to a common coordinate system using the Evans & Irwin (1995) error mapping algorithm. The software then pairs all images that appear on all four plates and excludes those that did not move at least the amount corresponding to our slow proper motion limit. Any remaining unpairings or inconsistencies are then processed individually, searching all possible combinations out to a radius defined by the fast proper motion limit. For example, the position of an un-

paired object is compared to positions of other unpaired objects out to the distance corresponding to a $\mu = 10.0'' \text{ yr}^{-1}$ and over 360°. Thus, it is possible for a single unpairing to have multiple hits that may not correspond to proper motion. This "brute force" method will undoubtedly produce many spurious detections, especially at larger proper motions because the area searched increases as the square of the radius, but we wanted to maximize completeness within our parameter space.

Spurious detections are usually the result of plate defects. Scratches and dust specks are the most likely culprits although the halos that surround bright stars on the plates are also common contaminants, especially because the radius changes from one plate to the next (depending on color). Blending of an object on one plate but not all plates also produced spurious detections. It is possible for objects of extreme colors (i.e., very red) to be detected and associated with a moving object when in fact the object was not detected on a plate (i.e., the B_J plate for red objects) because of its color. This particular scenario was negligible for this phase of the survey given the relatively bright magnitude limit constraint (i.e., the object would need to have a $B_J - R_{59\text{F}} > 6.5$ to not be detected on the B_J plate with a magnitude limit of ∼23). Another rare source of contamination occurred when there was actually a common proper motion pair at a relatively close separation. This would produce four unpaired objects, all within the radius defined by the fast proper motion limit, in the initial trawl. Two pairings would be of the same object with a true proper motion and two pairings would associate the first epoch of one object with the second epoch of the

other object. While this is perhaps not a true contaminant because there are actually proper motion objects involved, the detections by the software had to be labeled as spurious for two of the pairings.

Needless to say, removing spurious detections and ensuring only real detections remained was a daunting task. Visual inspection is time consuming and not feasible for a large number of detections. Instead, the available information was examined using various "acceptability constraints". The software output contains the positions, proper motions, and plate magnitudes of the detections. Additionally, it contains several parameters pertaining to the detection. For instance, there is an ellipticity associated with each image detected on each plate as well as a goodness-of-fit parameter associated with the fit of the proper motion using all available plates. Our testbed region was the sky between declinations $-90°$ and $-80°$ (a relatively small piece of sky including 1.5% of the southern sky). This sift produced 99 detections so a visual inspection of each one was performed. By evaluating the real and spurious detections in this sample, we were able to employ additional constraints for the rest of the southern sky that eliminate many of the spurious detections before the visual inspection was performed. First, the plate magnitudes were checked for consistency between the two R plates (R_{59F} and R_{ESO}) and that the colors matched those of a real object, i.e., $B_J - R_{59F}$ and $B_J - I_{IVN}$ are both positive or negative. There exists a small possibility that a magnitude is corrupt because the object was blended with a background source during that epoch of observation. Thus, it is possible (albeit un-

likely) for a real HPM object to fail the two color checks. To eliminate the rejection of real objects because of this effect, if a detection failed the color checks, the ellipticities of the detection were checked. If two or more ellipticities for a given detection were larger than 0.2, the object was labeled as spurious without a visual inspection. An automatic sift of the visually inspected 99 detections found between declinations -90° and 0° demonstrated that no real objects were rejected in this sample.

For detections not initially labeled as spurious, the coordinates were cross-checked with the NLTT Catalogue, the SIMBAD database, and recent HPM publications (i.e., the southern hemisphere surveys discussed in Section 4.4). If the coordinates agreed to within a few arcminutes and the magnitudes and proper motions were consistent, the detection was considered previously known. In a few cases, the coordinates and proper motions agreed well but the magnitudes did not. These objects were revealed to be new wide common proper motion companions to previously known HPM stars. Detections not listed in previous proper motion surveys were flagged for visual inspection as potentially new HPM objects.

In total, 5303 detections were found having $10.0'' \text{ yr}^{-1} > \mu \geq 0.4'' \text{ yr}^{-1}$ brighter than $R_{59\text{F}} = 16.5$ between declinations -90° and 0°. This survey includes 46% of the entire sky and 92% of the southern sky. Figure 5.1 is a map of the 894 plate fields in the southern sky. Of those, 71 fields have not been searched because of crowding near the Galactic plane and Magellanic Clouds or because of a limited spread in epochs for available plates. The hit rate for real HPM objects decreases with increasing proper

Figure. 5.1: Plate coverage for the SCR survey. Plates colored in white were excluded from the search, primarily because of source crowding (Galactic plane, LMC, and SMC) or a limited time span between plates.

motion, because reliable source association between different epochs is more difficult for fast-moving sources. For objects with $10.0'' \, \text{yr}^{-1} > \mu \geq 1.0'' \, \text{yr}^{-1}$, only 10% are to be real, whereas 87% of objects detected with $1.0'' \, \text{yr}^{-1} > \mu \geq 0.4'' \, \text{yr}^{-1}$ are real.

The final count of real, distinct, new systems with $10.0'' \, \text{yr}^{-1} > \mu \geq 0.4'' \, \text{yr}^{-1}$ and brighter than $R_{59\text{F}} = 16.5$ is 299. In addition, seven new common proper motion companions to previously known HPM stars have been discovered but not included in the count of new systems because at least one member of the system was known. Of the 299 new systems, 148 have $\mu \geq 0.5'' \, \text{yr}^{-1}$ that are additions to the classic LHS sample. These constitute an 8% increase in the sample of all stellar systems with $\mu \geq 0.5'' \, \text{yr}^{-1}$ in the southern sky. Table 5.3 lists all of the new systems and new companions to known systems. The Table is divided into two proper motion bins, $\mu \geq 0.5'' \, \text{yr}^{-1}$ (for comparison with the LHS sample), and $0.5'' \, \text{yr}^{-1} > \mu \geq 0.4'' \, \text{yr}^{-1}$.

Coordinates, proper motions, and plate magnitudes have been extracted from the SSS. Coordinates are for epoch and equinox J2000. Errors in the coordinates are typically $\pm 0.3''$ and internal errors in the proper motions are given in column 5. Internal errors in the position angles are usually $\pm 0.1°$. As an external check, we compared the SCR proper motions and position angles of LHS recoveries with the values in the original LHS Catalog. Figure 5.2 shows this comparison. In general, the two astrometric surveys agree quite well. The two extreme discrepancies, LHS 2627 and LHS 5208, occur in the position angle plot on the right. In both cases, the position

Figure. 5.2: Comparison of LHS astrometry with new data from the SCR search. The solid line represents the equal value line in each plot. The two extreme outliers in the position angle plot are discussed in the text.

angles derived by Bakos et al. (2002) are in agreement with the SCR determinations. Thus, the LHS Catalogue determinations are likely in error. Omitting these two erroneous values, the average difference in proper motions and position angles between the LHS catalog and the SCR survey is 0.022 $''$ yr^{-1} and 2.0°, respectively.

Photometric magnitudes are given for three sets of plates: B_J, R_{59F}, and I_{IVN} (columns 7, 8, and 9, respectively). The R_{ESO} magnitude is not listed because it was not used in the analyses; R_{59F} is more consistently determined over the entire southern sky. Magnitude errors are ∼0.3 mag or better for $m > 15$ and actually get larger at brighter magnitudes due to systematic errors (Hambly et al. 2001c). A few plate magnitude values are missing because of blending problems that preclude accurate magnitude determinations.

Infrared photometry has been used to extend the color baseline, which allows more accurate photometric distance estimates for red dwarfs and permits a reliable separation of the white and red dwarfs. The infrared JHK_S photometry (columns 10, 11, and 12, respectively) has been extracted from 2MASS via Aladin. Each SCR object has been identified by eye to ensure that no extracted magnitudes are in error. In nearly every case, the errors are smaller than 0.03 mag. Exceptions include objects with $J > 15$, $H > 14.5$, and $K_S > 14$, for which the errors are 0.05 mag or greater. In two cases, SCR 1246−1236 and SCR 2012−5956, the error is null for K_S, and the value is therefore unreliable. Distance estimates determined empirically and discussed in § 5.3.1 are given in column 14.

5.2 Comparison to Previous Proper Motion Surveys

A primary goal of the SCR effort is to further complete the LHS Catalogue for stars with $\mu \geq 0.5''$ yr^{-1}. There are 1462 LHS stars in the LHS Catalogue brighter than photographic R magnitude (R_{pg}) of 16.5 in the southern sky. Of the 1152 known LHS stars in the southern sky with $10.0 < R_{pg} \leq 16.5$, we recover 1032 (90%). We recover only 234 of 310 (75%) LHS stars brighter than $R = 10.0$, because the search is less sensitive to bright objects that are saturated in the photographic emulsions. This recovery rate is somewhat less successful for stars moving faster than $1.0''$ yr^{-1} (199 of 251, 79%) than for stars with $1.0''$ yr$^{-1} > \mu \geq 0.5''$ yr^{-1} (1067 of 1211, 88%). This effect is likely tied to the lower recovery rate for bright objects because many of the fastest movers are very nearby and very bright (e.g., Sirius, Procyon).

Table 5.3: Proper Motions and Photographic and Infrared Photometry for the SCR Sample

Name (1)	R.A. (J2000) (2)	Decl. (J2000) (3)	μ (arcsec) (4)	σ_μ (arcsec) (5)	θ (deg) (6)	B_J (7)	R_{59F} (8)	I_{IVN} (9)	J (10)	H (11)	K_S (12)	$R_{59F} - J$ (13)	Est. Distance (pc) (14)	Notes (15)
					SuperCOSMOS−RECONS sample with $\mu \geq 0.5''$ yr^{-1}									
SCR 0005−6103........	00 05 56.49	−61 03 55.2	0.504	0.009	84.3	18.19	16.02	13.37	12.04	11.43	11.18	3.98	43.2 ± 13.7	a
SCR 0006−6617........	00 06 33.73	−66 17 30.8	0.559	0.011	161.7	16.94	15.11	13.18	12.01	11.36	11.11	3.10	63.2 ± 18.6	
SCR 0038−5038........	00 38 48.00	−50 38 22.3	0.726	0.010	115.1	16.77	14.92	12.76	11.43	10.94	10.66	3.49	44.9 ± 13.1	
SCR 0051−8441........	00 51 16.42	−84 41 59.0	0.502	0.007	77.2	18.22	16.20	14.57	13.26	12.71	12.50	2.94	128.6 ± 41.6	
SCR 0111−4908........	01 11 47.51	−49 08 09.0	0.542	0.008	213.1	18.93	16.50	13.01	11.54	11.00	10.61	4.96	23.6 ± 10.8	
SCR 0125−4545........	01 25 18.04	−45 45 31.2	0.759	0.007	137.8	17.04	16.13	15.80	15.11	14.84	14.91	1.02	[515.7 ± 140.7]	
SCR 0130−0532........	01 30 43.82	−05 32 22.1	0.552	0.006	118.2	...	16.05	13.63	12.06	11.48	11.19	3.99	42.4 ± 11.7	b,c
SCR 0138−6029........	01 38 01.13	−60 29 56.0	0.580	0.009	83.3	17.46	15.17	12.44	11.19	10.66	10.29	3.98	28.7 ± 10.2	
SCR 0142−3133........	01 42 20.39	−31 33 35.9	0.749	0.012	155.1	18.21	16.11	13.81	12.15	11.65	11.36	3.96	47.2 ± 14.0	
SCR 0210−6622........	02 10 45.17	−66 22 26.6	0.769	0.020	56.3	16.86	14.60	12.15	10.97	10.43	10.09	3.63	30.0 ± 9.5	
SCR 0223−0558........	02 23 26.64	−05 58 47.4	0.530	0.006	84.5	17.70	15.47	13.49	12.36	11.79	11.56	3.11	73.4 ± 19.8	
SCR 0234−8204........	02 34 44.28	−82 04 25.3	0.618	0.017	333.3	20.29	14.13	12.81	11.11	10.51	10.25	3.03	28.5 ± 18.7	
SCR 0247−6627........	02 47 05.35	−66 27 14.3	0.711	0.016	53.4	15.94	13.79	12.15	10.63	10.10	9.78	3.16	31.3 ± 10.3	
SCR 0252−7038........	02 52 32.02	−70 38 22.3	0.767	0.013	201.0	13.56	11.66	10.86	10.73	10.23	10.04	0.92	69.1 ± 20.0	
SCR 0300−4653........	03 00 45.22	−46 53 50.1	0.779	0.008	68.7	17.62	15.40	12.80	11.79	11.31	11.02	3.61	49.5 ± 18.2	c
SCR 0308−8212........	03 08 54.56	−82 12 30.6	0.507	0.009	27.3	17.80	15.62	13.09	11.70	11.15	10.89	3.92	38.9 ± 11.7	
SCR 0342−6407........	03 42 57.44	−64 07 56.4	1.071	0.023	141.2	17.17	15.13	12.34	11.32	10.89	10.58	3.81	39.3 ± 15.5	
SCR 0406−6735........	04 06 06.79	−67 35 28.9	0.608	0.007	150.2	17.29	14.98	13.99	13.53	13.06	12.80	1.45	[239.4 ± 66.1]	
SCR 0411−8654........	04 11 38.07	−86 54 09.8	0.557	0.006	46.5	17.83	15.79	13.39	12.06	11.53	11.26	3.73	51.3 ± 14.9	
SCR 0420−7005........	04 20 12.54	−70 05 58.8	0.670	0.007	21.2	18.18	15.68	12.58	11.19	10.59	10.25	4.49	22.5 ± 9.2	
SCR 0424−7243........	04 24 33.63	−72 43 04.8	0.563	0.006	33.5	16.43	15.03	12.67	11.21	10.67	10.40	3.82	38.0 ± 13.6	
SCR 0433−7740........	04 33 26.62	−77 40 09.7	0.514	0.006	49.6	17.92	15.86	14.76	14.05	13.49	13.36	1.81	[291.4 ± 83.1]	
SCR 0452−7321........	04 52 06.87	−73 21 56.7	0.554	0.008	53.6	17.98	16.29	13.83	11.98	11.44	11.12	4.31	39.1 ± 14.3	
SCR 0623−6701........	06 23 09.04	−67 01 18.9	0.514	0.007	27.9	...	16.15	13.64	12.58	12.09	11.81	3.57	76.3 ± 27.0	
SCR 0631−8811........	06 31 31.28	−88 11 36.8	0.516	0.006	349.9	16.96	14.67	11.46	10.04	9.46	9.07	4.63	12.8 ± 5.1	
SCR 0634−5403........	06 34 36.88	−54 03 12.7	0.524	0.006	176.6	17.18	14.89	12.29	11.07	10.44	10.13	3.82	27.6 ± 9.1	
SCR 0640−0552........	06 40 13.97	−05 52 23.5	0.592	0.008	170.5	11.23	8.79	7.59	6.84	6.21	5.96	1.95	8.5 ± 2.3	
SCR 0642−6707........	06 42 27.15	−67 07 19.9	0.811	0.008	120.4	17.00	14.69	11.60	10.61	10.15	9.81	4.08	24.1 ± 10.2	
SCR 0658−0655........	06 58 14.14	−06 55 35.4	0.574	0.003	130.6	16.73	14.68	12.93	12.33	11.76	11.53	2.35	[104.9 ± 28.5]	
SCR 0701−0655........	07 01 17.79	−06 55 49.4	0.582	0.003	183.8	17.68	15.75	14.57	13.73	13.19	13.00	2.02	[234.3 ± 69.0]	
SCR 0702−6102........	07 02 50.33	−61 02 47.6	0.786	0.006	41.4	17.50	15.10	11.73	10.36	9.85	9.52	4.75	15.9 ± 7.6	
SCR 0717−0501........	07 17 17.10	−05 01 04.0	0.580	0.004	133.6	13.86	11.34	8.83	8.87	8.35	8.05	2.47	15.9 ± 5.8	
SCR 0723−8015........	07 23 59.65	−80 15 17.8	0.828	0.006	330.4	18.68	16.44	13.27	11.30	10.82	10.44	5.14	19.3 ± 5.6	
SCR 0725−8530........	07 25 22.19	−85 30 58.3	0.612	0.011	192.5	15.40	13.39	11.47	10.53	10.02	9.70	2.86	36.8 ± 10.0	
SCR 0730−5707........	07 30 11.11	−57 07 42.4	0.505	0.007	82.7	15.08	13.03	11.23	10.23	9.73	9.47	2.80	33.8 ± 9.1	c
SCR 0730−7527........	07 30 15.98	−75 27 29.4	0.569	0.009	0.5	14.47	12.46	11.44	11.52	11.03	10.85	0.94	99.5 ± 25.9	
SCR 0740−4257........	07 40 11.80	−42 57 40.1	0.714	0.013	318.1	14.52	12.37	9.99	8.68	8.09	7.77	3.69	10.0 ± 2.9	
SCR 0758−2235........	07 58 53.17	−22 35 52.8	0.547	0.012	153.8	14.87	12.72	10.81	10.71	10.19	9.98	2.01	56.1 ± 17.1	
SCR 0802−2002........	08 02 37.92	−20 02 26.4	0.670	0.008	139.9	15.81	13.29	10.61	10.43	9.80	9.57	2.86	32.3 ± 14.6	c
SCR 0805−5912........	08 05 46.18	−59 12 50.6	0.637	0.007	155.0	15.76	13.76	11.33	10.07	9.52	9.22	3.69	20.4 ± 6.0	
SCR 0813−2926........	08 13 07.54	−29 26 06.9	0.521	0.006	252.6	16.62	14.62	11.82	11.48	10.98	10.73	3.14	56.4 ± 23.8	
SCR 0815−3600........	08 15 15.98	−36 00 58.9	0.612	0.010	350.6	16.29	13.80	11.29	10.74	10.17	9.88	3.06	34.6 ± 14.4	c
SCR 0816−7727........	08 16 35.70	−77 27 12.0	0.676	0.006	325.4	16.41	14.43	13.58	12.62	12.07	11.87	1.81	[145.7 ± 47.3]	
SCR 0818−3110........	08 18 40.27	−31 10 20.4	0.842	0.008	162.6	15.74	14.80	14.52	14.92	14.73	14.83	−0.12	...	b,c,d
SCR 0821−6703........	08 21 26.67	−67 03 20.4	0.758	0.005	327.6	16.44	15.08	14.61	13.79	13.57	13.34	1.28	[267.6 ± 83.4]	b
SCR 0827−3002........	08 27 40.82	−30 02 60.0	0.621	0.010	330.3	16.08	13.14	11.30	10.67	10.17	9.92	2.47	41.1 ± 14.4	c
SCR 0829−2951........	08 29 09.73	−29 51 39.2	0.570	0.010	158.3	15.99	13.44	11.54	11.04	10.56	10.32	2.40	54.8 ± 17.0	
SCR 0829−6203........	08 29 24.67	−62 03 23.2	0.585	0.005	299.2	17.78	15.72	13.42	11.69	11.21	10.92	4.02	37.9 ± 11.6	
SCR 0838−8148........	08 38 20.47	−81 48 46.1	0.625	0.005	9.4	17.50	15.37	13.55	12.32	11.82	11.57	3.06	77.9 ± 21.3	
SCR 0843−2937........	08 43 09.45	−29 37 30.9	0.514	0.007	145.1	16.13	13.94	11.68	10.53	10.01	9.72	3.41	28.3 ± 8.3	c
SCR 0845−3051........	08 45 51.93	−30 51 31.4	0.563	0.008	257.2	16.41	14.22	12.00	10.82	10.30	10.04	3.40	32.9 ± 9.4	c
SCR 0847−3046........	08 47 09.79	−30 46 12.7	0.590	0.007	170.7	15.40	13.46	11.10	10.39	9.91	9.60	3.07	33.8 ± 11.0	c

Table. 5.3: continued

Name (1)	R.A. (J2000) (2)	Decl. (3)	μ (arcsec) (4)	σ_μ (arcsec) (5)	θ (deg) (6)	B_J (7)	R_{59F} (8)	I_{IVN} (9)	J (10)	H (11)	K_S (12)	$R_{59F} - J$ (13)	Est. Distance (pc) (14)	Notes (15)
						SuperCOSMOS−RECONS sample with $\mu \geq 0.5''$ yr^{-1}								
SCR 0852−6608.........	08 52 49.99	−66 08 46.9	0.508	0.006	333.7	17.81	15.49	12.88	11.34	10.73	10.39	4.16	26.3 ± 7.7	
SCR 0853−6123.........	08 53 03.11	−61 23 48.4	0.587	0.006	145.7	17.93	15.73	12.96	11.82	11.27	10.91	3.91	40.3 ± 15.0	
SCR 0904−3804.........	09 04 46.52	−38 04 07.5	0.643	0.007	145.0	16.88	14.93	13.16	12.03	11.57	11.36	2.90	80.2 ± 22.5	c
SCR 0912−8311.........	09 12 59.55	−83 11 51.6	0.812	0.006	331.8	17.99	15.74	13.19	11.56	10.98	10.69	4.17	30.4 ± 8.8	
SCR 0913−1049.........	09 13 54.20	−10 49 33.2	0.670	0.004	219.9	...	15.19	14.08	13.38	12.86	12.67	1.81	[200.4 ± 56.5]	
SCR 0914−4134.........	09 14 17.43	−41 34 38.9	0.749	0.008	312.5	16.33	13.69	10.98	9.98	9.42	9.12	3.71	18.2 ± 8.0	
SCR 0927−4137.........	09 27 07.25	−41 37 12.5	0.511	0.016	120.5	11.93	10.65	10.01	10.32	9.89	9.80	0.33	...	c,d
SCR 0942−6428.........	09 42 17.90	−64 28 43.5	0.531	0.011	307.3	14.76	12.59	12.04	11.96	11.33	11.18	0.63	111.3 ± 31.5	c
SCR 0956−4234.........	09 56 37.01	−42 34 27.5	0.620	0.005	146.8	17.00	14.67	11.82	10.99	10.47	10.21	3.68	33.3 ± 15.3	c
SCR 1005−4322.........	10 05 03.16	−43 22 28.4	0.653	0.014	292.5	14.76	12.51	10.14	9.85	9.32	9.06	2.66	29.2 ± 10.4	c
SCR 1053−3858.........	10 53 49.42	−38 58 58.7	0.622	0.006	320.1	15.85	13.79	11.81	10.91	10.43	10.13	2.88	44.7 ± 12.2	c
SCR 1057−5103.........	10 57 02.98	−51 03 35.0	0.622	0.009	277.2	15.96	13.85	12.20	11.15	10.64	10.43	2.70	54.1 ± 14.6	
SCR 1058−3854.........	10 58 47.18	−38 54 15.2	0.565	0.006	284.1	15.65	14.60	12.19	11.01	10.52	10.21	3.59	42.9 ± 16.9	c
SCR 1107−4135.........	11 07 55.93	−41 35 52.8	1.189	0.006	282.8	16.66	14.72	13.65	12.19	11.69	11.47	2.53	[95.4 ± 36.3]	
SCR 1110−3608.........	11 10 29.03	−36 08 24.7	0.527	0.007	268.5	17.20	15.07	12.72	10.93	10.34	10.00	4.14	22.3 ± 7.1	c
SCR 1125−3834.........	11 25 37.28	−38 34 43.2	0.586	0.006	252.1	16.04	13.80	11.66	10.09	9.51	9.19	3.71	18.1 ± 5.4	c
SCR 1132−8446.........	11 32 21.98	−84 46 28.4	0.650	0.006	279.9	17.64	15.87	13.94	12.22	11.76	11.51	3.65	62.7 ± 23.4	c
SCR 1132−4039.........	11 32 57.92	−40 39 21.4	0.725	0.008	296.8	15.26	13.38	11.22	10.38	9.89	9.65	3.00	35.9 ± 10.6	c
SCR 1138−7721.........	11 38 16.82	−77 21 48.0	2.141	0.007	286.7	16.45	14.12	11.45	9.40	8.89	8.52	5.60	8.8 ± 2.7	
SCR 1149−4248.........	11 49 31.61	−42 48 10.2	0.951	0.007	259.9	15.43	13.09	12.41	11.67	11.11	10.90	1.42	[99.4 ± 30.6]	c
SCR 1151−4142.........	11 51 07.83	−41 42 17.5	0.713	0.010	247.5	...	15.65	13.03	11.51	10.99	10.68	4.14	33.2 ± 9.9	c
SCR 1158−5103.........	11 58 38.90	−51 03 31.8	0.521	0.005	294.2	18.27	16.16	14.11	13.17	12.68	12.44	2.98	123.6 ± 34.5	
SCR 1159−4256.........	11 59 37.69	−42 56 39.3	0.610	0.007	219.0	14.20	11.96	10.35	9.54	8.98	8.72	2.42	26.7 ± 7.0	c
SCR 1204−4037.........	12 04 15.54	−40 37 52.6	0.695	0.013	150.0	14.70	12.61	10.72	9.57	9.02	8.75	3.04	21.2 ± 5.7	c
SCR 1214−4603.........	12 14 40.01	−46 03 14.4	0.750	0.005	250.8	16.80	14.53	11.60	10.32	9.75	9.44	4.21	18.0 ± 6.9	c
SCR 1220−4546.........	12 20 07.98	−45 46 18.2	0.758	0.005	286.3	16.53	14.59	13.35	12.70	12.16	11.95	1.89	[150.8 ± 42.6]	c
SCR 1227−4541.........	12 27 46.82	−45 41 16.7	1.304	0.011	282.0	16.40	14.19	13.31	12.75	12.40	12.27	1.44	[188.2 ± 53.0]	c
SCR 1230−3411.........	12 30 01.76	−34 11 24.2	0.527	0.007	234.9	15.29	13.18	10.92	9.34	8.77	8.44	3.84	12.6 ± 3.7	c
SCR 1247−0525.........	12 47 14.74	−05 25 13.5	0.722	0.007	319.8	15.90	13.38	10.92	10.13	9.62	9.29	3.25	24.2 ± 9.6	c
SCR 1321−3629.........	13 21 14.84	−36 29 18.3	0.554	0.009	247.8	18.61	16.32	13.84	12.14	11.57	11.24	4.18	38.4 ± 11.2	c
SCR 1322−7254.........	13 22 27.37	−72 54 36.6	0.572	0.009	270.7	16.24	14.12	12.25	11.14	10.55	10.31	2.97	44.1 ± 11.8	
SCR 1327−3551.........	13 27 39.52	−35 51 01.5	0.535	0.007	236.0	17.01	14.69	12.57	11.13	10.60	10.33	3.56	33.3 ± 9.4	c
SCR 1328−7253.........	13 28 42.10	−72 53 47.4	0.789	0.005	247.2	17.91	15.97	13.77	12.47	12.00	11.69	3.50	71.2 ± 20.3	
SCR 1338−5622.........	13 38 48.13	−56 22 20.6	0.547	0.010	260.6	15.46	14.90	13.06	13.14	12.57	12.34	1.75	[170.7 ± 56.7]	
SCR 1345−5101.........	13 45 41.48	−51 01 01.5	0.527	0.006	168.4	16.61	14.51	12.17	10.91	10.39	10.12	3.60	31.9 ± 9.2	
SCR 1400−3935.........	14 00 32.30	−39 35 29.4	0.507	0.006	255.7	17.45	15.44	14.20	13.47	12.90	12.66	1.97	[199.7 ± 56.4]	c
SCR 1412−3941.........	14 12 21.14	−39 41 33.8	0.636	0.006	240.2	16.24	14.22	12.44	10.99	10.43	10.18	3.23	37.6 ± 11.8	c
SCR 1429−4808.........	14 29 41.38	−48 08 31.2	0.791	0.006	351.4	17.11	15.48	12.52	11.25	10.78	10.45	4.24	32.8 ± 11.8	
SCR 1437−4002.........	14 37 21.41	−40 02 50.9	0.525	0.012	230.1	16.18	13.87	12.36	10.79	10.21	9.90	3.08	32.3 ± 11.5	c
SCR 1442−4810.........	14 42 16.59	−48 10 50.8	0.507	0.008	248.0	16.92	14.33	14.13	12.98	12.47	12.29	1.35	[173.8 ± 61.9]	
SCR 1455−3914.........	14 55 51.60	−39 14 33.2	0.798	0.012	266.4	16.61	14.52	13.57	12.50	11.98	11.79	2.02	[130.8 ± 42.0]	c
SCR 1457−4705.........	14 57 05.34	−47 05 26.4	0.517	0.008	226.4	16.93	15.23	14.48	13.53	12.96	12.82	1.70	[215.1 ± 75.8]	c
SCR 1505−4620.........	15 05 27.33	−46 20 16.2	0.517	0.011	239.8	15.80	13.74	12.02	11.07	10.51	10.28	2.67	51.2 ± 13.7	c
SCR 1511−3403.........	15 11 38.62	−34 03 16.6	0.561	0.006	202.9	16.04	14.05	12.09	10.05	9.42	9.13	4.00	16.1 ± 7.4	c
SCR 1533−3634.........	15 33 27.70	−36 34 02.6	0.555	0.006	237.2	16.08	14.62	13.37	11.54	10.99	10.76	3.08	58.9 ± 29.2	c
SCR 1601−3421.........	16 01 55.72	−34 21 57.0	0.683	0.012	118.2	17.05	15.75	12.94	10.96	10.33	9.98	4.79	20.2 ± 11.9	c
SCR 1608−4442.........	16 08 43.92	−44 42 28.8	0.628	0.012	193.1	16.59	14.95	12.94	10.88	10.35	10.10	4.07	27.5 ± 13.2	c
SCR 1608−2913AB.....	16 08 45.49	−29 13 06.6	0.540	0.016	231.0	13.61	11.65	9.91	9.68	9.15	8.51	1.97	28.9 ± 8.4	e
SCR 1613−3040.........	16 13 53.57	−30 40 59.0	0.522	0.009	216.7	16.68	15.41	14.32	13.15	12.58	12.38	2.26	[143.0 ± 48.7]	c
SCR 1637−3203.........	16 37 50.55	−32 03 11.5	0.587	0.007	221.6	18.42	15.76	13.74	11.70	11.10	10.82	4.06	30.3 ± 11.9	c
SCR 1637−4703.........	16 37 56.52	−47 03 45.5	0.503	0.007	215.4	16.17	13.49	14.16	10.60	10.04	9.70	2.89	20.8 ± 13.7	c
SCR 1648−2049.........	16 48 23.38	−20 49 35.4	0.679	0.008	245.8	15.71	14.00	13.25	11.56	10.99	10.77	2.44	68.6 ± 32.8	c

Table 5.3: continued

Name (1)	R.A. (J2000) (2)	Decl. (J2000) (3)	μ (arcsec) (4)	σ_μ (arcsec) (5)	θ (deg) (6)	B_J (7)	R_{59F} (8)	I_{IVN} (9)	J (10)	H (11)	K_S (12)	$R_{59F}-J$ (13)	Est. Distance (pc) (14)	Notes (15)
					SuperCOSMOS−RECONS sample with $\mu \geq 0.5''$ yr^{-1}									
SCR 1659−6958.........	16 59 27.99	−69 58 18.7	0.749	0.007	216.3	15.77	14.19	12.02	10.53	9.99	9.70	3.65	27.9 ± 9.6	
SCR 1726−8433.........	17 26 23.04	−84 33 08.4	0.518	0.008	134.8	15.42	13.31	11.16	9.87	9.33	9.02	3.44	20.1 ± 5.5	
SCR 1735−7020.........	17 35 40.71	−70 20 21.6	0.963	0.005	190.1	18.19	16.14	14.04	12.82	12.31	12.10	3.32	[90.9 ± 25.2]	
SCR 1738−1057.........	17 38 35.48	−10 57 25.3	0.510	0.004	178.3	17.24	15.80	14.12	11.64	11.11	10.90	4.16	41.0 ± 26.9	
SCR 1756−5927.........	17 56 27.94	−59 27 18.0	0.537	0.006	210.0	18.02	15.73	14.68	13.44	12.89	12.69	2.29	[170.6 ± 56.3]	
SCR 1805−4326.........	18 05 12.34	−43 26 06.1	0.781	0.006	160.3	17.52	15.13	12.69	11.83	11.37	11.09	3.30	56.6 ± 21.0	
SCR 1808−8120.........	18 08 00.06	−81 20 48.8	0.680	0.009	200.0	17.32	15.45	13.19	11.36	10.79	10.52	4.09	31.0 ± 11.2	
SCR 1811−4239.........	18 11 17.20	−42 39 02.5	0.732	0.010	180.9	13.68	12.13	11.21	11.38	10.82	10.65	0.75	...	
SCR 1817−5318.........	18 17 06.43	−53 18 04.8	0.617	0.009	209.9	14.69	13.27	12.46	11.93	11.43	11.23	1.34	[114.6 ± 33.6]	f
SCR 1822−0928.........	18 22 44.35	−09 28 20.0	0.523	0.003	196.4	17.56	15.92	13.85	11.52	10.98	10.60	4.40	29.8 ± 17.0	
SCR 1835−8754.........	18 35 14.60	−87 54 08.9	0.639	0.006	199.5	18.18	16.02	15.10	14.11	13.56	13.29	1.92	[264.2 ± 83.5]	
SCR 1841−4347.........	18 41 09.79	−43 47 32.6	0.790	0.007	264.2	17.65	15.19	12.32	10.48	9.94	9.60	4.71	14.6 ± 2.0	
SCR 1843−7849.........	18 43 35.71	−78 49 02.6	0.745	0.008	194.9	17.57	15.70	14.65	13.27	12.74	12.59	2.43	[168.4 ± 62.5]	
SCR 1845−6357.........	18 45 05.09	−63 57 47.7	2.558	0.012	74.8	...	16.33	12.53	9.54	8.97	8.51	6.78	3.5 ± 1.2	
SCR 1847−1922.........	18 47 16.69	−19 22 20.8	0.626	0.011	230.7	15.36	13.08	10.94	9.91	9.38	9.09	3.17	23.0 ± 6.6	
SCR 1848−6855.........	18 48 21.14	−68 55 34.5	1.287	0.013	194.3	...	16.07	13.97	11.89	11.40	11.10	4.97	34.8 ± 13.4	
SCR 1855−6914.........	18 55 47.87	−69 14 14.8	0.832	0.011	145.3	18.01	15.63	12.20	10.47	9.88	9.51	5.16	12.5 ± 4.5	
SCR 1902−5044.........	19 02 47.53	−50 44 00.6	0.510	0.009	150.2	16.54	14.52	12.98	11.99	11.48	11.26	2.53	86.7 ± 23.9	
SCR 1913−1001.........	19 13 24.60	−10 01 46.6	0.576	0.004	211.8	16.64	14.81	13.88	12.71	12.16	11.93	2.10	[138.9 ± 49.1]	
SCR 1916−3638.........	19 16 46.56	−36 38 05.9	1.303	0.007	184.1	18.20	15.88	14.78	13.66	13.12	12.95	2.22	[199.2 ± 60.9]	c
SCR 1918−4554.........	19 18 29.45	−45 54 31.0	0.700	0.012	220.4	17.89	15.29	12.66	11.21	10.65	10.30	4.08	25.5 ± 8.5	c
SCR 1924−3356.........	19 24 48.30	−33 56 10.3	0.549	0.013	146.2	15.48	13.77	12.71	12.45	11.99	11.77	1.32	[149.8 ± 40.9]	c
SCR 1931−0306.........	19 31 04.70	−03 06 18.6	0.578	0.004	31.0	17.87	16.06	...	11.15	10.56	10.23	4.91	18.0 ± 4.8	
SCR 1940−3944.........	19 40 21.31	−39 44 10.7	0.525	0.009	167.5	15.19	13.22	11.17	10.38	9.84	9.57	2.84	35.6 ± 10.1	
SCR 1946−4945.........	19 46 02.47	−49 45 49.0	0.585	0.006	210.2	17.34	15.39	14.53	13.51	12.95	12.78	1.88	[218.5 ± 72.4]	c
SCR 1954−7356.........	19 54 06.43	−73 56 50.8	0.535	0.008	148.6	16.85	14.89	12.96	11.81	11.31	11.08	3.08	64.3 ± 17.8	
SCR 2001−4239.........	20 01 16.47	−42 39 37.1	0.594	0.008	165.5	17.08	14.90	13.25	11.84	11.34	11.09	3.06	60.7 ± 18.2	
SCR 2007−1915.........	20 07 45.91	−19 15 53.7	0.629	0.011	186.3	16.00	13.79	11.77	10.88	10.38	10.14	2.91	43.2 ± 12.1	
SCR 2012−5956.........	20 12 31.79	−59 56 51.6	1.440	0.011	165.6	16.66	15.63	15.13	14.93	15.23	15.41	0.70	...	b,f,k
SCR 2035−6505.........	20 35 05.60	−65 05 26.1	0.785	0.011	166.0	17.22	15.07	13.18	12.23	11.73	11.51	2.85	84.3 ± 22.7	
SCR 2040−5501.........	20 40 12.40	−55 01 25.7	0.514	0.013	125.4	16.56	14.26	12.16	10.56	10.02	9.69	3.70	22.9 ± 6.9	
SCR 2043−6501.........	20 43 10.43	−65 01 17.6	0.533	0.013	170.0	16.18	14.04	12.04	11.25	10.76	10.52	2.79	55.3 ± 15.6	
SCR 2051−1329.........	20 51 13.57	−13 29 16.2	0.694	0.005	103.7	17.51	15.32	13.05	11.42	10.92	10.61	3.90	33.6 ± 9.8	
SCR 2101−5437.........	21 01 45.76	−54 37 31.7	0.667	0.011	241.5	16.90	14.59	13.46	12.79	12.26	12.08	1.80	[157.0 ± 43.1]	
SCR 2109−5226.........	21 09 02.56	−52 26 18.1	0.791	0.012	176.5	18.00	15.97	14.93	13.76	13.29	13.05	2.21	[221.8 ± 72.9]	
SCR 2128−5532.........	21 28 41.23	−55 32 32.1	0.699	0.010	123.3	16.37	14.23	12.04	10.70	10.06	9.78	3.53	26.4 ± 7.4	
SCR 2130−7710.........	21 30 07.07	−77 10 37.5	0.589	0.007	118.0	18.28	15.93	13.44	11.29	10.67	10.36	4.64	20.6 ± 7.3	
SCR 2132−3922.........	21 32 29.69	−39 22 50.3	0.531	0.007	118.3	18.36	16.14	13.54	12.21	11.70	11.35	3.93	47.7 ± 15.2	c
SCR 2200−0240.........	22 00 44.45	−02 40 18.9	0.676	0.008	174.2	17.16	15.30	13.94	12.51	11.98	11.74	2.79	97.5 ± 35.2	
SCR 2204−3347.........	22 04 02.28	−33 47 38.9	1.000	0.010	152.0	16.56	14.29	12.96	12.32	11.81	11.60	1.97	[120.6 ± 32.3]	c
SCR 2235−7722.........	22 35 57.78	−77 22 16.2	0.612	0.009	197.6	18.42	16.36	...	14.17	13.67	13.46	2.19	[285.9 ± 76.4]	
SCR 2247−1528.........	22 47 13.08	−15 28 37.8	0.512	0.008	195.4	14.02	12.08	11.31	11.10	10.50	10.34	0.98	77.3 ± 22.5	
SCR 2250−5726AB.......	22 50 45.05	−57 26 01.8	0.714	0.007	117.3	18.07	16.10	13.80	12.63	12.00	11.81	3.48	73.7 ± 21.2	g
SCR 2307−8452.........	23 07 19.88	−84 52 03.8	0.613	0.011	97.2	16.33	14.16	11.83	10.36	9.81	9.47	3.80	20.6 ± 5.9	
SCR 2335−5020.........	23 35 52.96	−50 20 18.9	0.661	0.010	127.0	16.54	15.17	13.97	13.14	12.69	12.47	2.03	[179.4 ± 53.9]	
SCR 2352−6124.........	23 52 29.56	−61 24 23.1	0.848	0.009	167.1	17.10	14.73	12.63	11.52	11.02	10.82	3.21	50.3 ± 14.6	h
					SuperCOSMOS−RECONS sample with μ between $0.4''$ yr^{-1} and $0.5''$ yr^{-1}									
SCR 0000−5029.........	00 00 44.12	−50 29 25.0	0.402	0.017	91.8	15.55	13.44	11.66	11.22	10.73	10.49	2.22	68.3 ± 19.1	
SCR 0122−6400.........	01 22 21.37	−64 00 33.1	0.423	0.012	113.9	15.13	13.23	12.48	12.53	11.93	11.80	0.70	175.9 ± 46.7	
SCR 0128−7104.........	01 28 50.80	−71 04 52.7	0.452	0.010	88.8	17.59	15.45	13.23	12.64	12.13	11.88	2.81	103.5 ± 32.7	

Table 5.3: continued

Name (1)	R.A. (J2000) (2)	Decl. (3)	μ (arcsec) (4)	σ_μ (arcsec) (5)	θ (deg) (6)	B_J (7)	R_{59F} (8)	I_{IVN} (9)	J (10)	H (11)	K_S (12)	$R_{59F}-J$ (13)	Est. Distance (pc) (14)	Notes (15)
			SuperCOSMOS−RECONS sample with μ between $0.4''$ yr^{-1} and $0.5''$ yr^{-1}											
SCR 0133−7200........	01 33 13.09	−72 00 04.6	0.433	0.008	172.2	16.92	14.64	12.16	11.37	10.79	10.50	3.27	43.0 ± 15.6	
SCR 0135−5943........	01 35 46.71	−59 43 14.3	0.412	0.008	81.5	17.36	15.25	13.01	12.01	11.52	11.24	3.24	63.7 ± 18.8	
SCR 0149−8038........	01 49 43.55	−80 38 27.8	0.464	0.008	80.5	18.42	16.35	13.84	11.68	11.11	10.72	4.68	25.3 ± 9.6	
SCR 0210−6252........	02 10 43.99	−62 52 30.1	0.456	0.018	50.0	17.23	14.95	12.92	11.85	11.29	11.02	3.10	56.8 ± 15.6	
SCR 0224−6433........	02 24 10.98	−64 33 02.4	0.448	0.023	107.3	16.26	13.97	11.80	10.94	10.43	10.12	3.03	39.9 ± 12.2	
SCR 0242−5935........	02 42 26.34	−59 35 02.4	0.466	0.007	185.2	16.04	15.02	14.04	13.55	13.00	12.78	1.46	[228.9 ± 64.5]	
SCR 0252−7522........	02 52 45.57	−75 22 44.5	0.496	0.013	63.5	17.10	16.32	16.17	15.77	15.76	15.34	0.55	· · ·	b,f
SCR 0255−7242........	02 55 05.52	−72 42 42.1	0.439	0.013	51.7	17.52	15.44	14.26	13.74	13.23	13.01	1.70	[254.4 ± 70.2]	
SCR 0303−7209........	03 03 44.13	−72 09 59.9	0.430	0.009	85.9	18.77	16.38	14.11	12.72	12.23	11.95	3.66	67.8 ± 19.8	
SCR 0311−6215........	03 11 21.28	−62 15 15.9	0.416	0.015	83.3	15.68	16.05	16.13	16.13	16.31	16.50	−0.08	· · ·	b,d
SCR 0331−8251........	03 31 41.78	−82 51 10.5	0.447	0.007	50.8	18.24	16.43	14.66	13.21	12.69	12.46	3.22	115.2 ± 38.2	
SCR 0525−7425........	05 25 25.36	−74 25 25.8	0.417	0.009	40.2	14.81	12.89	11.35	10.03	9.42	9.21	2.86	28.7 ± 9.4	
SCR 0529−3950........	05 29 40.95	−39 50 25.8	0.406	0.004	57.1	16.58	14.40	13.03	12.46	11.89	11.65	1.94	[124.6 ± 33.5]	
SCR 0533−3908........	05 33 10.28	−39 08 55.5	0.454	0.005	16.5	15.88	13.73	11.58	10.71	10.18	9.90	3.02	37.0 ± 10.8	
SCR 0537−5612........	05 37 53.75	−56 12 17.4	0.402	0.009	122.7	· · ·	14.89	13.12	12.34	11.85	11.57	2.56	96.9 ± 26.0	
SCR 0615−5807........	06 15 05.02	−58 07 43.4	0.410	0.006	314.6	16.63	14.45	12.44	11.48	10.98	10.70	2.97	54.4 ± 15.0	
SCR 0615−1812........	06 15 23.95	−18 12 04.8	0.486	0.006	150.9	18.06	15.85	13.69	12.36	11.82	11.56	3.49	62.4 ± 17.3	
SCR 0618−6704........	06 18 26.01	−67 04 00.3	0.436	0.009	31.4	14.59	12.67	10.74	10.40	9.88	9.60	2.27	45.7 ± 13.4	
SCR 0629−6938........	06 29 56.40	−69 38 13.3	0.473	0.007	153.6	18.14	16.23	14.75	13.66	13.14	12.90	2.57	[183.8 ± 54.6]	
SCR 0630−7643AB.....	06 30 46.63	−76 43 09.2	0.483	0.008	356.8	15.78	13.56	10.74	8.89	8.27	7.92	4.67	6.9 ± 2.0	i
SCR 0654−7358........	06 54 06.34	−73 58 04.0	0.467	0.008	20.2	18.19	16.24	14.79	13.99	13.47	13.28	2.25	[246.7 ± 79.1]	
SCR 0708−4709........	07 08 32.04	−47 09 30.7	0.402	0.006	115.0	14.50	12.48	11.58	11.44	10.90	10.76	1.04	[93.7 ± 26.0]	
SCR 0709−3941........	07 09 37.06	−39 41 52.5	0.426	0.004	190.4	16.55	14.21	12.42	11.77	11.21	10.99	2.44	74.8 ± 20.5	c
SCR 0709−4648........	07 09 37.34	−46 48 58.6	0.413	0.006	10.4	16.03	13.49	12.57	12.20	11.70	11.49	1.29	[131.3 ± 36.2]	c
SCR 0718−4622........	07 18 12.12	−46 22 37.9	0.423	0.007	343.6	17.75	15.52	13.22	11.88	11.33	11.07	3.64	46.6 ± 13.3	
SCR 0727−1421........	07 27 16.46	−14 21 06.3	0.413	0.004	161.8	16.29	13.99	11.56	10.93	10.38	10.11	3.06	39.8 ± 14.7	
SCR 0727−1404........	07 27 40.71	−14 04 59.0	0.484	0.004	141.7	16.78	14.55	11.95	11.35	10.79	10.52	3.20	46.5 ± 18.6	
SCR 0731−0954........	07 31 37.56	−09 54 50.7	0.438	0.003	177.8	18.00	15.68	12.83	11.57	11.03	10.68	4.11	32.8 ± 12.4	
SCR 0736−3024........	07 36 56.69	−30 24 16.3	0.424	0.013	145.7	14.76	12.06	9.46	9.36	8.79	8.49	2.70	20.2 ± 9.0	
SCR 0740−7212........	07 40 00.80	−72 12 27.8	0.481	0.006	3.7	17.25	15.28	13.31	11.77	11.27	11.00	3.51	49.8 ± 15.6	
SCR 0740−0540........	07 40 55.60	−05 40 37.9	0.467	0.003	151.1	18.20	16.04	14.62	13.51	12.96	12.77	2.53	[166.4 ± 47.1]	
SCR 0742−3012........	07 42 41.97	−30 12 39.5	0.418	0.006	134.1	18.34	16.38	14.20	13.00	12.49	12.26	3.38	97.7 ± 27.6	
SCR 0744−6941........	07 44 35.21	−69 41 58.1	0.441	0.007	1.2	17.14	15.05	13.38	12.18	11.70	11.41	2.87	78.8 ± 22.0	
SCR 0745−0725........	07 45 54.24	−07 25 56.1	0.437	0.003	162.8	16.71	14.55	12.92	12.18	11.64	11.42	2.37	96.9 ± 25.6	
SCR 0753−2524........	07 53 56.58	−25 24 01.4	0.426	0.007	300.2	16.18	15.25	15.67	14.75	14.47	14.30	0.50	[365.2 ± 103.9]	b,j
SCR 0754−2338........	07 54 29.56	−23 38 54.5	0.480	0.006	136.8	16.92	14.80	13.52	13.35	12.86	12.69	1.45	[224.3 ± 62.2]	
SCR 0754−3809........	07 54 54.86	−38 09 37.4	0.401	0.011	351.4	16.90	14.68	11.75	10.01	9.42	9.08	4.67	12.0 ± 3.5	
SCR 0756−5434........	07 56 48.71	−54 34 57.1	0.446	0.005	324.2	17.86	15.91	13.56	11.86	11.28	10.98	4.05	38.2 ± 12.2	
SCR 0803−1558........	08 03 30.08	−15 58 30.8	0.493	0.003	153.9	17.00	14.82	12.87	12.24	11.74	11.50	2.58	94.1 ± 26.8	
SCR 0804−1256........	08 04 48.41	−12 56 29.6	0.480	0.003	164.0	17.99	15.66	14.22	13.58	13.05	12.78	2.08	[195.0 ± 51.5]	
SCR 0812−6402........	08 12 23.36	−64 02 24.0	0.409	0.005	340.0	17.08	15.23	13.26	11.80	11.32	11.03	3.43	54.4 ± 17.0	
SCR 0816−2247........	08 16 42.32	−22 47 39.8	0.418	0.006	138.4	18.51	16.26	13.40	12.75	12.21	11.90	3.51	78.5 ± 36.7	
SCR 0823−4444........	08 23 03.57	−44 44 50.2	0.414	0.007	308.1	16.82	14.75	12.48	11.61	11.06	10.81	3.14	54.5 ± 16.5	
SCR 0824−6721........	08 24 03.20	−67 21 50.5	0.403	0.005	288.9	17.54	15.29	13.13	11.55	10.95	10.70	3.74	36.0 ± 10.6	
SCR 0829−3855........	08 29 23.24	−38 55 54.3	0.407	0.005	328.6	17.26	15.43	13.15	11.58	10.95	10.67	3.85	36.8 ± 11.9	
SCR 0835−3400........	08 35 31.73	−34 00 37.4	0.448	0.012	190.1	15.31	12.76	10.25	9.90	9.37	9.08	2.86	25.9 ± 10.9	c
SCR 0837−4639........	08 37 15.70	−46 39 50.2	0.447	0.008	303.5	16.21	13.89	12.86	12.20	11.65	11.44	1.69	[119.5 ± 33.4]	
SCR 0843−5154........	08 43 11.02	−51 54 03.4	0.402	0.008	310.7	16.10	13.94	12.36	11.77	11.22	10.97	2.18	84.6 ± 22.6	
SCR 0843−5209........	08 43 38.80	−52 09 27.5	0.482	0.007	307.3	16.41	14.29	12.57	11.87	11.38	11.11	2.42	84.2 ± 22.6	
SCR 0849−3138........	08 49 38.93	−31 38 22.6	0.405	0.006	344.2	16.55	14.57	12.84	11.69	11.16	10.91	2.88	63.3 ± 17.8	c
SCR 0850−4934........	08 50 24.90	−49 34 23.7	0.469	0.006	295.5	17.42	15.60	13.46	12.22	11.77	11.52	3.38	72.3 ± 21.1	
SCR 0917−3849........	09 17 13.65	−38 49 35.8	0.484	0.007	356.7	16.62	14.37	12.28	11.56	11.12	10.80	2.81	61.3 ± 18.5	c

Table 5.3: continued

Name (1)	R.A. (J2000) (2)	Decl. (3)	μ (arcsec) (4)	σ_μ (arcsec) (5)	θ (deg) (6)	B_J (7)	R_{59F} (8)	I_{IVN} (9)	J (10)	H (11)	K_S (12)	$R_{59F}-J$ (13)	Est. Distance (pc) (14)	Notes (15)
			SuperCOSMOS−RECONS sample with μ between $0.4''$ yr^{-1} and $0.5''$ yr^{-1}											
SCR 0956−8518.........	09 56 14.12	−85 18 01.5	0.478	0.007	319.2	17.11	15.14	13.98	12.49	11.94	11.74	2.64	100.7 ± 38.3	
SCR 1001−2257.........	10 01 06.62	−22 57 04.6	0.426	0.006	142.3	17.99	15.88	14.69	14.28	13.74	13.53	1.60	[328.5 ± 90.3]	
SCR 1011−8106.........	10 11 12.37	−81 06 42.0	0.450	0.008	112.4	16.54	14.50	12.53	10.81	10.24	9.93	3.68	26.7 ± 9.4	
SCR 1014−4428.........	10 14 40.77	−44 28 01.2	0.409	0.008	192.9	18.09	15.71	13.01	12.30	11.84	11.51	3.41	67.2 ± 29.6	
SCR 1054−5159.........	10 54 16.31	−51 59 03.0	0.408	0.006	306.1	17.32	15.38	13.37	11.71	11.10	10.87	3.66	42.7 ± 14.8	
SCR 1104−8352.........	11 04 51.06	−83 52 25.2	0.440	0.015	256.7	...	13.47	12.23	10.53	9.96	9.67	2.94	29.1 ± 13.4	
SCR 1109−4631.........	11 09 28.32	−46 31 09.9	0.467	0.005	279.2	18.17	16.18	14.00	12.35	11.88	11.55	3.83	55.5 ± 17.3	
SCR 1117−3202.........	11 17 29.31	−32 02 09.8	0.448	0.013	204.8	15.90	13.58	11.33	10.34	9.76	9.48	3.24	26.3 ± 8.1	c
SCR 1143−7047.........	11 43 11.44	−70 47 21.4	0.460	0.007	266.5	17.58	15.63	13.81	12.35	11.82	11.59	3.28	72.5 ± 22.9	
SCR 1151−4624.........	11 51 01.63	−46 24 12.0	0.441	0.008	118.8	16.17	13.62	11.68	10.85	10.33	10.04	2.77	40.6 ± 12.1	
SCR 1155−7904.........	11 55 00.07	−79 04 13.1	0.401	0.006	297.3	18.17	16.23	14.99	13.30	12.66	12.44	2.94	119.6 ± 52.7	
SCR 1157−0149.........	11 57 45.56	−01 49 02.4	0.451	0.008	116.4	17.29	15.13	12.62	10.90	10.35	10.02	4.23	22.2 ± 6.5	
SCR 1206−3500.........	12 06 58.52	−35 00 52.2	0.422	0.007	229.3	15.55	13.46	11.19	10.01	9.40	9.13	3.45	21.0 ± 5.9	
SCR 1208−3723.........	12 08 51.06	−37 23 27.6	0.420	0.006	140.5	16.16	13.94	11.77	10.62	10.08	9.78	3.32	29.7 ± 8.3	c
SCR 1211−6849.........	12 11 39.70	−68 49 29.9	0.489	0.008	293.4	16.91	14.73	12.43	11.39	10.91	10.62	3.35	45.4 ± 13.9	
SCR 1213−4820.........	12 13 07.11	−48 20 07.9	0.480	0.006	268.0	16.51	14.24	11.96	11.25	10.72	10.45	2.99	47.9 ± 15.9	
SCR 1223−3654.........	12 23 11.19	−36 54 58.5	0.461	0.006	279.4	16.60	14.53	12.45	10.99	10.42	10.15	3.54	31.9 ± 9.3	c
SCR 1235−4527.........	12 35 34.99	−45 27 03.6	0.485	0.011	317.3	14.97	12.72	11.07	10.57	10.04	9.76	2.15	48.2 ± 13.0	
SCR 1239−4759.........	12 39 51.37	−47 59 07.8	0.401	0.006	268.5	17.26	15.26	12.92	11.57	11.08	10.80	3.69	42.8 ± 12.3	c
SCR 1240−8209.........	12 40 51.09	−82 09 03.4	0.486	0.008	272.4	16.18	14.56	12.30	10.85	10.20	9.93	3.70	29.3 ± 9.8	
SCR 1240−8116.........	12 40 56.05	−81 16 31.1	0.492	0.006	279.8	15.15	13.12	11.25	9.73	9.16	8.89	3.39	19.2 ± 6.1	
SCR 1241−4717.........	12 41 33.13	−47 17 05.9	0.428	0.011	257.9	16.52	14.38	13.43	12.77	12.21	12.06	1.61	[166.2 ± 47.7]	c
SCR 1245−5506.........	12 45 52.60	−55 06 49.9	0.412	0.011	107.0	14.84	12.82	10.34	8.99	8.43	8.12	3.83	11.5 ± 3.4	
SCR 1246−1236.........	12 46 00.70	−12 36 19.4	0.406	0.007	305.4	15.84	15.80	15.86	15.74	15.73	16.13	0.06	...	b,d,k
SCR 1251−1232.........	12 51 34.75	−12 32 59.9	0.450	0.006	264.8	16.89	14.83	13.04	12.18	11.67	11.44	2.65	89.6 ± 24.0	
SCR 1256−1316.........	12 56 31.55	−13 16 07.7	0.402	0.006	249.0	18.24	16.08	13.96	12.89	12.42	12.14	3.19	97.2 ± 27.4	
SCR 1257−5554A	12 57 32.84	−55 54 48.6	0.410	0.012	290.1	14.84	13.47	11.45	10.48	9.90	9.66	2.98	39.1 ± 13.3	l
SCR 1257−5554B	12 57 33.08	−55 54 38.0	0.403	0.006	293.2	17.30	16.94	16.82	...	...	...	...	...	d,m
SCR 1320−7542.........	13 20 47.55	−75 42 51.1	0.434	0.006	249.3	17.88	15.82	14.71	13.93	13.32	13.26	1.89	[270.9 ± 78.5]	
SCR 1331−5138.........	13 31 02.88	−51 38 02.8	0.484	0.007	294.9	16.07	14.10	11.95	10.99	10.50	10.27	3.11	44.5 ± 12.8	
SCR 1340−4427.........	13 40 20.40	−44 27 05.8	0.403	0.005	283.5	17.22	15.18	12.72	11.69	11.16	10.88	3.49	49.0 ± 15.6	
SCR 1342−3544.........	13 42 00.21	−35 44 51.6	0.488	0.006	283.4	18.12	16.02	14.23	13.31	12.80	12.52	2.71	[141.6 ± 37.5]	
SCR 1409−5337.........	14 09 49.48	−53 37 26.4	0.450	0.007	212.4	16.45	14.33	13.06	11.72	11.24	10.96	2.61	70.2 ± 23.0	
SCR 1412−4954.........	14 12 43.89	−49 54 32.4	0.420	0.012	212.9	15.86	13.82	12.25	11.66	11.12	10.89	2.16	83.9 ± 22.8	c
SCR 1420−5106.........	14 20 21.71	−51 06 50.7	0.489	0.010	130.4	14.64	13.02	11.57	10.47	9.92	9.70	2.55	44.5 ± 14.8	
SCR 1433−3847.........	14 33 03.37	−38 47 00.6	0.465	0.006	256.6	18.45	16.40	15.53	14.37	13.78	13.59	2.03	[295.4 ± 103.4]	c
SCR 1443−5502.........	14 43 25.99	−55 02 53.0	0.477	0.017	277.5	15.08	13.22	11.57	10.28	9.71	9.49	2.94	32.4 ± 10.2	c
SCR 1444−3426.........	14 44 06.58	−34 26 47.3	0.451	0.014	187.7	15.01	12.49	10.47	9.74	9.18	8.88	2.75	24.0 ± 7.5	c
SCR 1445−5046.........	14 45 23.96	−50 46 06.4	0.435	0.007	244.1	17.10	15.52	13.64	12.02	11.50	11.30	3.49	63.1 ± 24.4	c
SCR 1450−3742.........	14 50 02.86	−37 42 10.1	0.449	0.017	212.2	15.41	13.23	11.30	9.95	9.37	9.07	3.28	21.2 ± 6.0	c
SCR 1457−3904.........	14 57 49.06	−39 04 51.4	0.423	0.009	196.6	17.98	15.86	14.82	13.69	13.21	12.98	2.17	[215.6 ± 68.8]	
SCR 1507−3611.........	15 07 50.51	−36 11 49.7	0.407	0.005	271.6	17.67	15.51	13.67	11.55	11.05	10.78	3.96	35.2 ± 16.0	
SCR 1510−4259.........	15 10 42.34	−42 59 25.4	0.430	0.008	229.0	17.18	15.09	12.46	11.19	10.60	10.35	3.90	31.2 ± 10.0	n
SCR 1512−4354.........	15 12 52.33	−43 54 12.3	0.419	0.011	214.2	16.00	13.69	11.47	10.57	9.96	9.75	3.12	31.6 ± 9.8	c
SCR 1529−4238.........	15 29 56.31	−42 38 38.9	0.447	0.015	243.2	16.75	14.72	13.00	11.53	10.96	10.68	3.19	47.7 ± 15.5	c
SCR 1532−3622.........	15 32 13.90	−36 22 31.0	0.438	0.007	235.4	15.48	13.50	11.96	10.10	9.54	9.28	3.40	23.0 ± 10.3	o
SCR 1547−2751.........	15 47 36.68	−27 51 20.9	0.440	0.007	156.8	16.02	14.25	12.51	11.32	10.80	10.55	2.93	55.2 ± 16.9	c
SCR 1550−4718.........	15 50 55.19	−47 18 48.4	0.413	0.013	247.6	16.12	14.24	13.23	11.79	11.19	10.98	2.45	77.2 ± 30.6	o
SCR 1552−7052.........	15 52 46.95	−70 52 02.4	0.468	0.006	216.0	16.33	14.18	11.92	10.81	10.28	10.07	3.37	34.5 ± 10.1	
SCR 1559−4442.........	15 59 00.74	−44 42 12.3	0.434	0.012	220.3	15.97	14.81	14.04	12.78	12.16	11.98	2.03	[125.4 ± 53.1]	
SCR 1601−4442.........	16 01 37.48	−44 42 01.4	0.439	0.010	240.3	17.17	15.50	13.71	11.68	11.18	10.93	3.82	44.7 ± 21.9	
SCR 1608−4229.........	16 08 34.77	−42 29 37.8	0.408	0.008	221.3	16.97	15.81	15.23	13.57	13.01	12.87	2.24	[147.6 ± 70.1]	

Table. 5.3: continued

Name (1)	R.A. (J2000) (2)	Decl. (3)	μ (arcsec) (4)	σ_μ (arcsec) (5)	θ (deg) (6)	B_J (7)	R_{59F} (8)	I_{IVN} (9)	J (10)	H (11)	K_S (12)	$R_{59F}-J$ (13)	Est. Distance (pc) (14)	Notes (15)
			SuperCOSMOS−RECONS sample with μ between $0.4''$ yr^{-1} and $0.5''$ yr^{-1}											
SCR 1621−2810	16 21 06.94	−28 10 24.5	0.465	0.007	163.9	17.48	16.01	15.64	13.80	13.26	13.03	2.21	[197.3 ± 103.8]	
SCR 1627−7337	16 27 37.13	−73 37 06.2	0.439	0.007	235.8	15.71	13.89	13.26	12.65	12.02	11.95	1.23	[151.7 ± 46.1]	
SCR 1630−3633	16 30 27.29	−36 33 56.0	0.413	0.011	249.2	15.94	14.39	11.88	10.04	9.50	9.03	4.35	14.8 ± 5.9	
SCR 1631−2805	16 31 33.44	−28 05 28.0	0.468	0.008	220.7	17.46	15.67	13.82	11.90	11.36	11.06	3.77	46.3 ± 20.7	
SCR 1634−3112	16 34 05.78	−31 12 02.4	0.420	0.010	248.1	16.92	14.69	12.94	11.47	10.94	10.70	3.22	46.3 ± 14.0	
SCR 1637−4016	16 37 03.35	−40 16 00.1	0.444	0.008	234.2	16.82	16.03	12.97	12.97	12.51	12.24	3.06	128.5 ± 58.3	
SCR 1637−3014	16 37 57.54	−30 14 57.3	0.462	0.014	245.1	15.39	13.36	11.65	10.89	10.34	10.11	2.47	52.4 ± 14.1	
SCR 1717−6916	17 17 52.66	−69 16 43.2	0.466	0.005	320.9	17.45	15.04	12.86	11.48	10.94	10.67	3.56	38.4 ± 11.0	
SCR 1724−5637	17 24 36.47	−56 37 02.9	0.421	0.008	154.5	15.18	13.11	11.42	10.39	9.86	9.63	2.72	37.2 ± 10.0	
SCR 1739−8222	17 39 45.45	−82 22 02.3	0.465	0.008	211.8	17.06	15.04	14.21	12.90	12.38	12.19	2.14	[151.7 ± 56.6]	
SCR 1740−5646	17 40 46.93	−56 46 57.9	0.448	0.005	229.5	18.48	15.90	14.44	13.83	13.33	13.19	2.07	[232.9 ± 64.3]	
SCR 1748−7211	17 48 51.85	−72 11 53.1	0.428	0.008	191.0	16.99	14.85	12.88	11.57	10.99	10.75	3.28	46.9 ± 13.0	
SCR 1800−0431B	18 00 20.05	−04 32 01.7	⋯	⋯	⋯	⋯	⋯	⋯	13.41	12.83	12.66	⋯	⋯	p
SCR 1800−0431A	18 00 21.33	−04 31 47.8	0.402	0.004	227.4	17.26	16.40	15.93	13.10	12.50	12.29	3.30	96.1 ± 71.5	
SCR 1808−0341	18 08 48.40	−03 41 54.6	0.424	0.004	197.2	16.74	16.07	15.40	11.72	11.19	11.03	4.35	49.4 ± 41.0	
SCR 1811−5510	18 11 34.94	−55 10 37.9	0.482	0.006	197.9	17.39	15.16	12.87	11.62	11.06	10.78	3.54	42.6 ± 12.2	
SCR 1821−5549	18 21 45.87	−55 49 17.5	0.424	0.007	181.0	16.97	14.63	12.61	11.57	11.00	10.74	3.06	50.2 ± 13.9	
SCR 1822−4542	18 22 58.78	−45 42 45.9	0.436	0.006	216.2	17.86	15.13	13.76	13.65	13.10	12.88	1.48	[228.7 ± 67.2]	
SCR 1832−4217	18 32 59.19	−42 17 20.3	0.466	0.009	200.7	15.43	13.64	12.54	12.19	11.57	11.38	1.45	[121.6 ± 33.4]	
SCR 1856−1951	18 56 15.32	−19 51 19.5	0.400	0.010	201.1	15.69	13.81	13.13	13.09	12.58	12.47	0.72	[227.2 ± 67.4]	
SCR 1857−4309	18 57 33.21	−43 09 24.9	0.403	0.020	169.5	12.32	11.83	11.33	11.09	10.75	10.69	0.74	⋯	f
SCR 1910−4338	19 10 23.58	−43 38 37.5	0.494	0.010	177.1	18.33	16.13	13.39	11.86	11.28	10.99	4.27	34.6 ± 10.5	
SCR 1912−5034	19 12 45.01	−50 34 34.4	0.447	0.005	233.7	18.24	16.03	13.70	12.19	11.67	11.35	3.84	48.3 ± 13.8	
SCR 1913−2312	19 13 06.05	−23 12 05.4	0.416	0.006	159.2	17.89	15.81	13.40	11.43	10.87	10.52	4.38	26.0 ± 9.1	c
SCR 1918−3323	19 18 53.29	−33 23 56.8	0.437	0.010	221.0	17.20	15.05	12.41	11.37	10.88	10.58	3.68	39.3 ± 14.2	
SCR 1926−5218	19 26 48.73	−52 18 17.4	0.494	0.007	191.2	16.97	15.22	14.39	13.54	12.97	12.87	1.68	[229.7 ± 75.0]	
SCR 1928−3634	19 28 33.60	−36 34 30.1	0.470	0.012	166.4	16.36	14.12	11.92	10.61	10.06	9.81	3.51	27.4 ± 7.7	
SCR 1931−5840	19 31 21.58	−58 40 37.2	0.402	0.007	135.7	16.83	14.69	13.32	12.18	11.67	11.44	2.51	91.7 ± 26.7	
SCR 1948−5914	19 48 58.82	−59 14 23.3	0.415	0.008	151.7	16.60	14.63	12.39	11.11	10.58	10.28	3.52	35.9 ± 10.2	c
SCR 1958−5609	19 58 31.28	−56 09 10.6	0.494	0.007	161.9	17.60	15.55	14.41	13.30	12.77	12.52	2.25	[169.1 ± 53.2]	
SCR 1959−3631	19 59 21.03	−36 31 03.9	0.436	0.014	158.1	11.58	9.44	8.40	8.24	7.62	7.41	1.20	19.8 ± 5.4	
SCR 1959−5549	19 59 58.76	−55 49 29.6	0.413	0.011	169.9	16.19	13.95	11.82	10.47	9.88	9.63	3.48	25.0 ± 7.0	
SCR 2007−3551	20 07 41.36	−35 51 46.6	0.428	0.010	225.3	17.58	15.59	12.97	11.53	10.96	10.67	4.06	33.8 ± 10.1	
SCR 2009−6005	20 09 23.44	−60 05 43.3	0.414	0.010	154.3	18.17	15.87	13.71	12.11	11.58	11.27	3.76	46.5 ± 13.6	
SCR 2016−7945	20 16 49.73	−79 45 53.0	0.434	0.007	128.4	16.75	16.09	15.75	15.11	15.03	14.64	0.99	[482.5 ± 130.7]	b
SCR 2018−4836	20 18 13.66	−48 36 51.9	0.410	0.007	147.2	17.38	15.20	13.33	12.08	11.62	11.37	3.12	69.0 ± 18.8	
SCR 2018−6606	20 18 28.69	−66 06 44.5	0.462	0.008	191.3	17.72	15.76	14.71	13.68	13.14	12.99	2.08	[228.0 ± 72.1]	
SCR 2044−4123	20 44 27.89	−41 23 51.6	0.429	0.012	142.5	16.12	14.03	12.52	11.75	11.16	10.99	2.28	82.4 ± 22.1	
SCR 2046−4321	20 46 27.46	−43 21 06.3	0.405	0.011	173.4	14.70	13.63	13.23	12.83	12.40	12.30	0.80	169.4 ± 44.2	
SCR 2059−4615	20 59 10.74	−46 15 19.7	0.400	0.009	123.8	16.40	14.39	12.12	11.33	10.79	10.54	3.06	50.8 ± 15.6	
SCR 2059−4302	20 59 23.19	−43 02 29.7	0.448	0.009	163.7	17.38	16.03	13.49	12.75	12.21	11.96	3.28	104.4 ± 37.3	c
SCR 2104−5229	21 04 00.61	−52 29 43.4	0.400	0.009	233.7	17.60	15.42	14.42	13.44	12.94	12.76	1.98	[207.2 ± 62.9]	
SCR 2123−3653	21 23 14.36	−36 53 27.2	0.446	0.010	133.7	17.44	15.56	13.38	12.34	11.86	11.58	3.22	78.5 ± 22.5	q
SCR 2151−8604	21 51 37.56	−86 04 33.4	0.454	0.012	192.7	16.57	14.48	13.57	12.74	12.23	12.03	1.74	[160.6 ± 48.3]	
SCR 2155−7330	21 55 01.97	−73 30 24.5	0.459	0.011	202.0	15.78	13.97	11.85	10.60	10.05	9.78	3.38	31.6 ± 9.2	r
SCR 2212−7337	22 12 05.47	−73 37 17.2	0.419	0.008	122.9	17.43	15.32	12.90	11.39	10.85	10.48	3.92	31.6 ± 9.1	
SCR 2249−6324	22 49 47.16	−63 24 37.7	0.454	0.009	174.0	18.26	16.28	15.50	14.69	14.04	13.95	1.58	[393.6 ± 125.3]	
SCR 2254−8712	22 54 21.45	−87 12 51.7	0.401	0.011	115.6	16.11	14.13	12.30	11.10	10.54	10.29	3.03	44.2 ± 12.4	
SCR 2305−7729	23 05 01.97	−77 29 12.8	0.429	0.007	193.7	17.04	15.73	13.71	13.82	13.30	13.18	1.91	[238.7 ± 84.9]	
SCR 2317−5140	23 17 08.89	−51 40 19.4	0.446	0.007	192.1	17.04	15.02	13.71	12.82	12.25	12.04	2.19	[139.4 ± 39.8]	
SCR 2329−8758	23 29 02.47	−87 58 06.2	0.429	0.006	111.6	15.79	14.48	13.44	12.70	12.12	11.97	1.77	[144.5 ± 42.3]	

75

Notes.—Units of right ascension are hours, minutes, and seconds, and units of declination are degrees, arcminutes, and arcseconds. Brackets around distance estimates indicate that the distance is likely overestimated because the object is a subdwarf or a white dwarf candidate.

a Common proper motion with LHS 1018.
b Spectroscopically confirmed white dwarf.
c Object detected in the concurrent proper motion survey of Lépine (2005).
d All colors are too blue for distance relations.
e Separation of 2.5$''$ at PA 266.2°.
f No distance estimate is reported because only one color was available within the bounds of the relations.
g Separation of 2.3$''$ at PA 28°.
h Common proper motion with LHS 4031.
i Separation of $\sim$1.0$''$ at PA $\sim$127°.
j Common proper motion with LTT2976.
k K_S has a null error and is unreliable.
l Separation of 11.0$''$ at PA 16°.
m Not detected during automated search due to faint limit but noticed to be a common proper motion companion during the visual inspection; R is $ESO - R$, R_{59F} blended.
n Common proper motion with CD -42 10084.
o Common proper motion with L 408-087.
p Not detected during automated search due to faint limit but noticed to be a common proper motion companion during the visual inspection, blended on all four plates.
q Common proper motion with LTT 8495.
r Common proper motion with HIP 108158.

Table. 5.4: Proper Motion Surveys and Number of New LHS Objects Discovered

Survey	$\mu \geq 1.0''$ yr^{-1}	$\mu = 0.5''-1.0''$ yr^{-1}	Total	# of Publications	Refs.
LHS	528	3074	3602	1	1
LSPM-North	20	181	201	6	2
SCR	9	141	150	4	3,4,5
SIPS	9	59	68	1	6
WTC	2	46	48	7	7,8
Scholz & collaborators . .	8	30	38	8	9,10,11,12
Calan-ESO	3	17	20	3	13,14
LEHPM	unknown	unknown	unknown	2	15

REFERENCES.—(1) Luyten 1979a; (2) Lépine et al. 2002a,b, 2003a,b,c, 2004; (3) Hambly et al. 2004; (4) Henry et al. 2004; (5) Subasavage et al. 2005a,b; (6) Deacon et al. 2005a; (7) Wroblewski & Torres 1989, 1991, 1994, 1996, 1997; (8) Wroblewski & Costa 1999, 2001; (9) Scholz et al. 2000, 2002a,b, 2004a,b; (10) Scholz & Meusinger 2002; (11) Lodieu et al. 2002; (12) Hambaryan et al. 2004; (13) Ruiz & Maza 1987; (14) Ruiz et al. 1993, 2001; (15) Pokorny et al. 2003, 2004

These figures only give upper limits to the completeness of the SCR survey. By the very existence of successful proper motion surveys after the LHS effort (see Table 5.4), it is clear that the LHS Catalogue is also incomplete. While the SCR survey employed minimal machine selected sifts in favor of the human sift to ensure the best possible completeness, the survey is not as complete as we hoped. Blending of objects in crowded fields is the most likely cause for incompleteness within our parameter space. Nonetheless, although we avoid the Galactic plane and Magellanic Clouds, the SCR survey has the most uniform sky coverage for southern hemisphere searches and is consequently the most productive survey at finding new LHS objects in the southern hemisphere.

To combat the blending problem, a more sophisticated technique, such as SU-PERBLINK, is necessary (see description of SUPERBLINK in Lépine & Shara 2005). There are undoubtedly objects remaining to be discovered along the crowded Galactic plane in the southern sky. Lépine and collaborators are currently scouring the southern hemisphere in an identical fashion as their northern hemisphere effort. In

fact, Lépine (2005) presents the results of their search from the southern celestial cap northward to declination $= -30°$. This publication reached press one month before the second installment of our SCR survey (the SCR survey was published in two pieces, the first between declinations $-90°$ and $-47°$ and the second between declinations $-47°$ and $00°$). Lépine (2005) and Subasavage et al. (2005b) have a total of 61 overlapping objects (of which 43 have $\mu \geq 0.5'' \text{ yr}^{-1}$). When we include the southern hemisphere efforts of Lépine and collaborators, and count each object only once giving the count to the first publication, we see that the LSPM-South effort has discovered 111 objects with $\mu \geq 0.5'' \text{ yr}^{-1}$ (of which four have $\mu \geq 1.0'' \text{ yr}^{-1}$) (Lépine 2005; Lépine et al. 2005). Thus, the LSPM effort has discovered a total of 312 objects with $\mu \geq 0.5'' \text{ yr}^{-1}$ (of which 24 have $\mu \geq 1.0'' \text{ yr}^{-1}$) and the SCR effort has discovered a total of 107 objects with $\mu \geq 0.5'' \text{ yr}^{-1}$ (of which six have $\mu \geq 1.0'' \text{ yr}^{-1}$). Figure 5.3 is a plot of all the new LHS objects discovered since the effort of Luyten and reflects the shift in new discoveries from the SCR survey to the LSPM survey. Note that while the LSPM effort uses a superior blinking algorithm (SUPERBLINK), objects detected by the SCR survey are occasionally missed by SUPERBLINK. This is evident in Figure 5.3 in which there are ∼10 SCR discoveries (*filled triangles*) not detected by SUPERBLINK in the region of sky between declinations $-47°$ and $-30°$. Also evident is a void at right ascension ∼6 hours, declination ∼-20°. This position happens to be the antapex of solar motion where one would expect to find few HPM objects (as discussed in § 2.1.2). A complete list of all duplicates with $\mu \geq 0.5'' \text{ yr}^{-1}$ for which two surveys claim discovery is given in Appendix C.

Figure. 5.3: Sky distribution of new LHS objects from recent proper motion surveys. Only objects with $\mu \geq 0.5''\,\mathrm{yr}^{-1}$ are plotted. Filled triangles are from the SCR survey. Crosses represent objects from the LSPM survey. Other symbols represent objects from Calan-ESO (*open squares*), WTC (*open circles*), SIPS (*open diamonds*), and Scholz et al. (*filled stars*). The curve represents the Galactic plane, where more HPM objects are yet to be revealed.

5.3 Analysis

5.3.1 Distance Estimates for Main-Sequence Stars

Identifying new nearby stars was perhaps the single most important motivation for conducting the SCR proper motion survey. With the wealth of data extracted from both the SSS and 2MASS, we are able to estimate reliable distances without any

further observations. Single, main-sequence stars, that are in the RECONS 10 pc sample were used to develop color-M_{K_S} relations (Hambly et al. 2004). This sample was selected because these objects have high quality trigonometric parallax determinations (only stars with parallax errors less than 5 mas were used) and have been vetted better than any other sample of stars for close companions. Only RECONS stars south of declination = $+3°$ (the SuperCOSMOS plate scan limit as of 2004) that are single and have unblended, unsaturated photographic magnitudes were used. Once this sample was cross-referenced with 2MASS and reliable infrared JHK_S photometry was extracted, a total of 54 main sequence stars were used to generate the relations. An additional object, an L dwarf named LHS 102B, was included even though no B_J magnitude was available.

In total, there are 15 possible color combinations that can be derived from the six bandpasses ($B_J R_{59F} I_{IVN} JHK_S$). Of these, four are not useful ($B_J - R_{59F}$, $J - H$, $J - K_S$, and $H - K_S$) because the range in color is minimal and does not predict reliable M_{K_S} values. The remaining 11 colors are used to generate an ensemble of up to 11 distance estimates for each star (assuming the star's color falls within the range of colors). The resulting distance estimate is taken to be an average of the individual distance estmates and the standard deviation is taken as the internal error. The external error is estimated by running the 55 RECONS stars back through the relations to obtain an average percent error, which amounts to a 26% scatter between the estimated and true distances. Given the uncertainty in photographic magnitudes,

this result is quite surprising and extremely useful as a first guess. The comparison of color to M_{K_S} is useful because practically all undiscovered nearby stars are red dwarfs or brown dwarfs and will have a reliable K_S magnitude in 2MASS. Of course, the relations will not provide a reliable treatment for subdwarfs or WDs. Even for main-sequence stars, the effects of age and metallicity will occasionally render the distance estimate inaccurate by more than 50%, as is the case for 7 of the 55 stars used in the relations. Details of the relations (i.e., applicable color range, coefficients for the 4th order fits, and the RMS in magnitudes) are presented in Hambly et al. (2004).

The distance estimates derived for the new SCR discoveries are given in Table 5.3 column 14. In a few cases, no distance estimate is given; the colors are too blue and the relations are not applicable, or the photometry is corrupted. Note that brackets enclose several distance estimates indicating that the estimates are likely erroneous, either because the object is a suspected (or confirmed) WD or subdwarf (our procedure for identifying suspected subdwarfs is discussed in detail in the next section).

5.3.2 Reduced Proper Motion Diagram

The magnitude and color information from the SSS database is far superior to earlier efforts because of the rigorous photometric calibration procedures undertaken by the SSS. In fact, all objects in the LHS Catalogue that are fainter than $m_{\text{pg}} = 10.0$

Figure. 5.4: Reduced proper motion diagram for the SCR systems with $\mu \geq 0.4''$ yr^{-1} (the size of the points splits the SCR sample into stars with μ more or less than $0.5''$ yr^{-1}) and known systems with $\mu \geq 0.5''$ yr^{-1} recovered during the SCR survey. Reduced proper motion (*vertical axis*) has units of magnitudes. The X-axis is color, using plate R_{59F} and CCD J from 2MASS. The dashed line serves merely as a reference to distinguish WDs from subdwarfs. Similarly, the shaded region represents the limits within which we identify subdwarf candidates.

(e.g. including all WDs) have quoted magnitudes that are a by-eye estimate performed by the author (Luyten 1979a). As such, many of the known objects that were recovered by the SCR survey now have reliable magnitude and color information that can constrain their positions in the RPM diagram (hence their luminosity classes).

5.3.2.1 Subdwarfs

Shown in Figure 5.4 is the RPM diagram for new SCR discoveries as well as the known objects with $\mu \geq 0.5'' \text{ yr}^{-1}$ recovered during the SCR survey (the details outlining the technique of RPM can be found in Section 3.3). It is apparent that most of the new SCR stars are main-sequence red dwarfs, while there is a substantial sample of new subdwarf candidates; note the bifurcated population of circles running from the upper left to the lower right. The shaded area just above the dashed line maps out the subdwarf region. We identify subdwarf candidates with $R_{59\text{F}} - J > 1.0$ and having RPM (H_R) within 4.0 mag of the somewhat arbitrary dashed line separating the WDs from the subdwarfs. Because subdwarfs are underluminous for a given color with respect to main-sequence dwarfs, their distance estimates will be erroneously large (hence the brackets around distance estimates of subdwarf candidates in Table 5.3). A large distance estimate ($d \sim 200$ pc or larger) is another indication that the object is likely a K- or M-type subdwarf. A complete list of 65 new SCR subdwarf candidates (including 27 that have been spectroscopically confirmed, courtesy of Dr. Wei-Chun Jao) can be found in Appendix D.

5.3.2.2 White Dwarfs

There are ten SCR discoveries that fall within the WD region below the dashed line of Figure 5.4. Of these nine have been spectroscopically confirmed (*filled triangles*) and one is a spectroscopically confirmed subdwarf (*filled star*). All but two of the

known objects in the WD region are spectroscopically confirmed, in most cases, by past researchers but in a few cases by our efforts using the better magnitude and color information from the SSS database. The two that are unconfirmed lie just below the dashed line and their photometry (particularly the JHK_S) indicate that both are unlikely to be single WDs (i.e., near-infrared colors are too red) but rather are likely to be subdwarfs. Details of the observations both for spectroscopic identification as well as follow-up observations is deferred to later chapters.

What is interesting to note is the nearby WD detection sensitivity limit by imposing a magnitude limit of $R_{59F} = 16.5$. Using a sample of 98 of the 109 known WDs within 25 pc, an H-R diagram can be constructed to determine what fraction of nearby WDs are detectable above this magnitude limit. Figure 5.5 illustrates two distances (10 pc and 25 pc) within which the SCR survey is sensitive to detections. Thus, all WDs above the dashed line are detectable within 25 pc (i.e., all but the coolest and thus reddest WDs), and all WDs above the dashed-dotted line are detectable within 10 pc (i.e., *all known nearby WDs*).

5.3.3 SCR 1845−6357

The most exceptional object discovered during the entire SCR survey, SCR 1845−6357 (SCR 1845), deserves a section of its own. Found relatively early in the survey, this object has the largest proper motion of all the new SCR discoveries with $\mu = 2.558'' \text{ yr}^{-1}$. In fact, both of the fastest movers, this object and SCR 1138−7721 ($\mu = 2.141'' \text{ yr}^{-1}$),

Figure. 5.5: H-R Diagram illustrating the SCR magnitude limit's (i.e., $R_{59F} = 16.5$) nearby WD detection sensitivity. Open circles correspond to 98 of the 109 known WDs within 25 pc. The dashed line represents the sensitivity for WDs within 25 pc. The dashed-dotted line represents the sensitivity for WDs within 10 pc.

were discovered on the same day. I began to think we were going to discover tens of objects with $\mu > 2.0''$ yr^{-1} in the gold mine of the undersampled southern hemisphere. As it turns out, I was having a lucky day; no other new objects were found with $\mu > 2.0''$ yr^{-1} throughout the rest of the survey. Also exceptional, SCR 1845 is the reddest object of the new discoveries. With a $R_{59F} - J = 6.79$, SCR 1845 is the furthest point to the right on Figure 5.4.

Perhaps most exceptional, SCR 1845 had the closest distance estimate of 3.5 ± 1.2 pc (from Table 5.3) using the color-M_{K_S} relations. To verify SCR1845's proximity,

we obtained optical CCD photometry so that we could remove the large uncertainties inherent in plate photometry (e.g., non-linearity). Using more precise CCD photometry and a set of CCD color-M_{K_S} relations generated in an identical manner to those using the plate photometry, we obtained a distance estimate of 4.63 ± 0.75 pc (Henry et al. 2004). In an attempt to further constrain the distance, collaborators Nigel Hambly and Niall Deacon scanned all plate material available to the SSS in that region of the sky to obtain a crude trigonometric parallax. In total, there were eight epochs of plate data that was reduced to obtain a trigonometric parallax of 282 ± 23 mas (3.55 ± 0.32 pc, Deacon et al. 2005b). Needless to say, this object became priority #1 on our parallax program, the Cerro Tololo Inter-American Observatory Parallax Investigation (CTIOPI, to be discussed in § 8.1). After two years of intense observation, we obtained a precise CCD trigonometric parallax of 259.45 ± 1.11 mas (3.85 ± 0.02 pc, Henry et al. 2006). Taking into account another nearby M dwarf discovered by Teegarden et al. (2003), known as SO 025300.5+165258 and ranks as the 23rd nearest system to the Sun, SCR 1845 is the 24th nearest system. Prior to these two discoveries, the only system found to be closer in the past 30 years was GJ 1061 (Henry et al. 1997), which ranks as the 20th nearest system.

To further enhance our amazement at the exceptional nature of SCR 1845, Biller et al. (2006) discovered that it has a brown dwarf companion, seen in Figure 5.6. Montagnier et al. (2006) confirmed that the companion shares the proper motion of the primary, ruling out the highly unlikely possibility that the brown dwarf is an

Figure. 5.6: Optical image (*left*) of SCR 1845 from CTIOPI data taken in July 2003 and the infrared *H*-band image (*right*) taken by Montagnier et al. (2006). The B component, indicated by an arrow, has a separation of $1.17''$ at position angle $170.2°$.

unbound background source. This discovery marks the first T-type brown dwarf to be found orbiting a low mass star. In addition, SCR 1845 is the second closest system that contains a brown dwarf, second only to the binary brown dwarf ϵ Indi Ba-Bb at a distance of 3.63 ± 0.01 pc.

5.3.4 Comments on Individual Systems

SCR 0005−6103 ($\mu = 0.504''$ yr^{-1} at position angle $84.3°$) is a common proper motion companion to LHS 1018 ($\mu = 0.519''$ yr^{-1} at position angle $85.7°$), for which there is no trigonometric parallax available. The distance estimates for SCR 0005−6103 and LHS 1018 are 43.2 ± 13.7 pc and 34.0 ± 9.1 pc, respectively, consistent within the errors.

SCR 0006−6617 ($\mu = 0.559''$ yr^{-1} at position angle 161.7°) at first appears to be a very widely separated ($\sim27'$) common proper motion companion to LHS 1019 ($\mu = 0.576''$ yr^{-1} at position angle 158.9°). However, the estimated distance for SCR 0006−6617 is 63.2 ± 18.6 pc, whereas the trigonometric parallax from *Hipparcos* for LHS 1019 indicates a distance of 17.6 ± 0.80 pc. In addition, SCR 0006−6617 ($H_{R_{59F}} = 18.85$, $R_{59F}-J = 3.10$) does not fall within the subdwarf region of Figure 5.4, rendering it unlikely that this object is a subdwarf with an overestimated distance. We conclude that this is a rare case of two physically unassociated objects of similar proper motion being found in the same region of the sky.

SCR 0630−7643 AB ($\mu = 0.483''$ yr^{-1} at position angle 356.8°) is a close binary. CCD images indicate two sources with a constant separation of $\sim 1.0''$ at PA $\sim127°$ over 5 months and brightness ratio of 0.8 at I_{KC}. The combined photometry taken from the photographic plates, which do not resolve the system, gives an underestimated distance of 6.9 ± 2.0 pc. Combined CCD photometry and the relations of Henry et al. (2004) give a distance estimate of 5.2 ± 0.9 pc. Reliable brightness ratios at V_J and R_{KC} are not available because the system is less resolved in images mostly because of the degraded seeing at shorter wavelengths. However, the system has been confirmed to be a member of the RECONS 10 pc sample with a true distance of 8.76 ± 0.14 pc (Henry et al. 2006) and is a promising target for future astrometric mass determinations.

SCR 0640−0552 ($\mu = 0.592''$ yr^{-1} at position angle 170.5°) is the brightest new detection, with $R_{59F} = 8.8$ and an estimated distance of 8.5 ± 2.3 pc. CCD photometry from three nights indicates $V_J = 10.22$, $R_{KC} = 9.22$, and $I_{KC} = 8.03$, confirming that it is a very bright object. These values, when combined with the 2MASS JHK_S magnitudes, yield a distance estimate of 9.4 ± 1.5 pc using the CCD relations of Henry et al. (2004).

SCR 0753−2524 ($\mu = 0.426''$ yr^{-1} at position angle 300.2°) is a common proper motion companion to LTT 2976 ($\mu = 0.361''$ yr^{-1} at position angle 303.7°), which has a *Hipparcos* parallax of $0.05116'' \pm 0.00157''$ (distance $= 19.5 \pm 0.6$ pc). The separation of the two stars is $\sim400''$ (projected separation ~8000 AU) at position angle 208.9°. SCR 0753−2524 is confirmed to be a WD (with a full discussion found in Section 6.3), for which we estimate a distance of 16.2 ± 3.2 pc using the crude linear photographic plate $B_J - R_{59F}$ relation for WDs of Oppenheimer et al. (2001b). Although the sizes of the proper motions do not match perfectly, the better determined position angles are consistent, so we conclude that the two stars form a system.

SCR 0818−3110 ($\mu = 0.842''$ yr^{-1} at position angle 162.6°) is a new nearby cool WD with an estimated distance of 13.1 pc using the photographic plate $B_J - R_{59F}$ relation for WDs of Oppenheimer et al. (2001b). This distance is likely underestimated because this object is a DZ with strong Ca II K & H absorption at 3933Å and 3968Å (see § 6.3.2), in the spectral region covered by the B_J filter (3650Å to 4150Å). The suppressed flux at B_J causes the $B_J - R_{59F}$ color to be too red (i.e., too cool) so that the distance relation does not provide a reliable estimate.

SCR 0821$-$6703 ($\mu = 0.758''$ yr^{-1} at position angle 327.6°) is a new nearby cool WD with an estimated distance of 10.9 ± 2.2 pc using the photographic plate $B_J - R_{59F}$ relation for WDs of Oppenheimer et al. (2001b).

SCR 1138$-$7721 ($\mu = 2.141''$ yr^{-1} at position angle 286.8°) has the second largest proper motion of objects discovered in the SCR survey. It has a distance estimate of 8.8 ± 2.7 pc, consistent with its trigonometric distance of 8.18 ± 0.20 pc (Henry et al. 2006).

SCR 1257$-$5554 AB ($\mu_A = 0.410''$ yr^{-1} at position angle 290.1° and $\mu_B = 0.403''$ yr^{-1} at position angle 293.2°) is a probable red dwarf/WD pair. The B component was too faint to be picked up in the SCR search but was noticed on frames that were blinked to confirm its primary. Infrared data are not available because this object exceeds the faint limit of 2MASS. We suspect that it is a hot WD because of its plate colors and because its companion is a modestly bright M star estimated to be at 39.1 ± 13.2 pc. The B component is not plotted on Figure 5.4 because of the lack of the $R_{59F} - J$ color.

SCR 1510$-$4259 ($\mu = 0.430''$ yr^{-1} at position angle 229.0°) is a common proper motion companion to CD -42 10084 ($\mu = 0.436''$ yr^{-1} at position angle 228.1°), which has a *Hipparcos* parallax of $0.03999'' \pm 0.00241''$ (distance $= 25.0 \pm 1.6$ pc). The separation of the two stars is $88''$ at position angle 123.5°. The distance estimate for SCR 1510$-$4259, 31.2 ± 10.0 pc, is consistent within the errors and the proper motions are a match. We conclude that the two stars form a system.

SCR 1529−4238 ($\mu = 0.447''$ yr^{-1} at position angle 243.2°) is a probable common proper motion companion to L408-87 ($\mu = 0.285''$ yr^{-1} at position angle 235.0°; NLTT Catalogue) for which there is no trigonometric parallax available. The separation of the two stars is 45$''$ at position angle 159.0°. The sizes of the proper motions do not match well, but the position angles are a fair match. Given the incomplete information in the NLTT (no photographic R magnitude), presumably because of the very crowded field, the proper motion for L408-87 is suspect. In fact, we cannot estimate a distance for L408-87 because it is blended on several plates, precluding reliable plate magnitudes. We tentatively conclude that the two stars form a system.

SCR 1608−2913 AB ($\mu = 0.540''$ yr^{-1} at position angle 231.0°) is a close double system with separation 2.5$''$ at position angle 266.2°, determined using frames acquired during CTIOPI. The magnitude differences are 0.56, 0.49, and 0.37 mag at V_J, R_{KC}, and I_{KC}, respectively.

SCR 1800−0431 AB ($\mu = 0.402''$ yr^{-1} at position angle 227.4°) is a common proper motion pair with a separation of 24$''$ at position angle 234.0°. While investigating the primary, the B component was noticed on images extracted from all four available plates; however, it is blended with other sources in all four cases, so no reliable plate photometry or distance estimate are available.

SCR 2012−5956 ($\mu = 1.440''$ yr^{-1} at position angle 165.6°) is a new nearby cool WD with an estimated distance of 18.0 ± 3.6 pc using the photographic plate $B_J - R_{\mathrm{59F}}$ relation for WDs of Oppenheimer et al. (2001b). Follow-up analyses will be discussed in Section § 8.4.3 (listed as WD 2008−600).

SCR 2123−3653 ($\mu = 0.446''$ yr^{-1} at position angle 133.7°) is a possible common proper motion companion to LTT 8495 ($\mu = 0.417''$ yr^{-1} at position angle 134.1°), for which there is no trigonometric parallax available. The separation of the two stars is 50″ at position angle 168.0°. The proper motions are consistent, indicating that the two stars almost certainly form a system. However, from plate + JHK_S photometry, distance estimates are 25.9 ± 8.3 pc and 78.5 ± 28.5 pc for LTT 8495 and SCR 2123−3653, respectively, which indicates that if the two are a pair, LTT 8495 is likely to be an unresolved multiple.

SCR 2155−7330 ($\mu = 0.459''$ yr^{-1} at position angle 202.0°) is a common proper motion companion to HIP 108158 ($\mu = 0.477''$ yr^{-1} at position angle 204.0°). The *Hipparcos* parallax for this object is $0.02510'' \pm 0.00074''$ (distance $= 39.8 \pm 1.1$ pc), which is reasonably consistent with the photometric distance estimate for SCR 2155−7330 of 31.6 ± 9.2 pc.

SCR 2250−5726 AB ($\mu = 0.714''$ yr^{-1} at position angle 117.3°) is noticeably peanut-shaped in the SuperCOSMOS frames. CCD frames taken at the CTIO 0.9 m confirm it to be a close binary source with separation 2.3″ at position angle 28°.

SCR 2352−6124 ($\mu = 0.848''$ yr^{-1} at position angle 167.1°) is a common proper motion companion to LHS 4031 ($\mu = 0.839''$ yr^{-1} at position angle 168.2°), which has a *Hipparcos* parallax of $0.02070'' \pm 0.00120''$ (distance $= 48.3 \pm 2.6$ pc), which is consistent with our photometric distance for SCR 2352−6124 of 50.3 ± 14.6 pc.

5.4 Conclusions

One of the primary motivations for HPM surveys is, of course, the promise of detecting new nearby stars. The new nearby discoveries are typically red dwarfs and, occasionally, WDs. The output list of sources detected, once culled for false hits, also include subdwarfs of very high intrinsic velocity that are generally not as near as their main-sequence counterparts but are nevertheless interesting in their own right as tracers of the Galactic halo population.

Listed in Table 5.5 is a summary of the number of SCR systems with distance estimates within each of our two target horizons (10 pc and 25 pc) and beyond. New common proper motion objects that are companions to known objects are not included in the counts, nor are confirmed WDs (because their distance estimates require different relations than applied here).

In total, we have found 43 new candidate systems within 25 pc of the Sun. There remain several likely subdwarfs with overestimated distances that may fall in closer bins than indicated in Table 5.5. Perhaps the most surprising result of this survey is the discovery that the slowest proper motion group ($0.6'' \, \text{yr}^{-1} > \mu \geq 0.4'' \, \text{yr}^{-1}$) contains the largest number (26) of new candidates for systems within 25 pc. In fact, we have found equal numbers of 10 pc candidates with $\mu > 1.0'' \, \text{yr}^{-1}$ as we have with $0.6'' \, \text{yr}^{-1} > \mu \geq 0.4'' \, \text{yr}^{-1}$. The presence of so many new nearby stars with relatively low proper motions hints that there may be large numbers of even slower moving

Table. 5.5: Distance Estimate Statistics for New SCR Systems

Proper Motion	$d \leq 10$ pc	10 pc $< d \leq 25$ pc	$d > 25$ pc
$\mu \geq 1.0''$ yr^{-1}	2	0	6
$1.0''$ yr$^{-1} > \mu \geq 0.8''$ yr^{-1}	0	3	3
$0.8''$ yr$^{-1} > \mu \geq 0.6''$ yr^{-1}	1	11	48
$0.6''$ yr$^{-1} > \mu \geq 0.4''$ yr^{-1}	2	24	188
Total	5	38	245

NOTE.—Excludes WDs and new wide companions.

stars that remain hidden in the solar neighborhood. Thus, searches for nearby stars buried in large samples with smaller proper motions are warranted, in particular given the availability of large photometric databases that allow the derivation of accurate distance estimates when optical and infrared data are combined, such as done here.

In summary, we have revealed a total of 299 new SCR proper motion systems in the southern sky. Of these, 148 have $\mu \geq 0.5''$ yr^{-1} (less the 43 that overlap with Lépine 2005, discussed in Section 5.2), making them new members of the classic LHS sample. Among the new discoveries, we anticipate that most are main-sequence M dwarfs, nine are confirmed WDs, at least five are new binary systems, and 65 are K or M type subdwarf candidates. Seven additional proper motion companions to previously known HPM stars were also found. Five of the nine WDs are anticipated to be within 25 pc. Worthy of note are the eight new SCR stars brighter than R_{59F} = 12, six of which have $\mu \geq 0.5''$ yr^{-1}, hinting at the possibility of relatively bright nearby stars that have not yet been identified.

All three sets of stars — WDs, red dwarfs, and subdwarfs — provide important contributions to these intrinsically faint, neglected samples. Undoubtedly, objects fainter than our survey cutoff of $R_{59F} = 16.5$ remain to be found, as well as a small number of stars meeting our survey criteria that fell in crowded regions or were simply missed because of the stringent limits required for SCR star veracity. Finally, we are delighted to have discovered during the SCR survey five new systems that are likely new members of the RECONS 10 pc sample, and are actively determining accurate parallaxes for them, as well as for many of the 38 other SCR systems within 25 pc, via our parallax program in Chile, CTIOPI.

5.5 Ongoing SCR Efforts

The success of the SCR survey has surpassed expectations. In fact, the results have hinted at the value of continuing the survey to slower proper motions (and perhaps to fainter magnitude limits). The decision was made to take the next step and evaluate the slower proper motion detections. Because the sample size in this parameter space is significantly larger, only the region of sky reaching from the south celestial pole northward to $\delta = -47°$ (the same region of focus for the first installment of the original SCR survey) was evaluated. A total of 1606 new proper motions systems with $0.40'' \, \mathrm{yr}^{-1} > \mu \geq 0.18'' \, \mathrm{yr}^{-1}$ was discovered in this region of the sky (Finch et al. 2007, as well as Charlie Finch's masters thesis). Of these, two are anticipated to be within 10 pc, and an additional 29 are estimated to be within 25 pc. With a

RPM diagram, 12 objects are identified as WD candidates as well as one additional blue object that was not detected by the survey but was noticed to be a common proper motion companion to a detection. Of these 13 WD candidates, three have been spectroscopically confirmed and will be discussed in detail in § 6.3.2.

There remains a large chunk of southern sky ($\delta = -47°$ to $00°$) yet to be sifted for new discoveries with $0.40'' \, \text{yr}^{-1} > \mu \geq 0.18'' \, \text{yr}^{-1}$ and $R_{59F} \leq 16.5$. Sifting this sample will be a huge undertaking, easily worthy of a masters thesis. To date, there are no volunteers. Also currently untouched, the sample of faint detections ($16.5 < R_{59F} < \sim 19$) over the entire southern sky is yet another significant increase in sample size. Astrometry for objects in this magnitude regime is not as good nor are there likely to be as many nearby WDs but there could exist a few gems should it ever get sifted. One could also extend the proper motion cutoff to even slower proper motions. The limiting factor here would be the amount of time between epochs but it is likely that a proper motion constraint of $0.10'' \, \text{yr}^{-1}$ could be achieved for most of the southern hemisphere using SSS data. Most likely, Lépine and collaborators will have completed the LSPM-South survey in the southern hemisphere far sooner and will reach just as faint and to slower proper motions. As noted previously, the LSPM effort occasionally misses objects detected by the SCR search; however, the significance of the few missed detections likely will not warrant the immense effort necessary to sift the data.

Chapter 6

Spectroscopy for New WD Candidates

With a sample of WD candidates reliably vetted using RPM diagrams based on recent HPM surveys (e.g., SCR, LEHPM), it is necessary to obtain spectroscopic observations to confirm WD status. This is particularly important for objects near the arbitrary line separating WDs from subdwarfs in the RPM diagram, where there is subdwarf contamination (albeit minimal).

6.1 Spectroscopy Observations

Observations were obtained using the 1.5 m telescope at Cerro Tololo Inter-American Observatory (CTIO) and operated by the Small and Moderate Aperture Research Telescope System (SMARTS) consortium. Data were collected on six separate observing runs in 2003 October and December, 2004 March and September, and 2006 May and December. The Ritchey-Chrétien Spectrograph and Loral 1200×800 CCD detector were used with grating 09 (in first order), providing 8.6 Å resolution and wavelength coverage from 3500 Å to 6900 Å. Bias, dome flats, and sky flats were collected each evening prior to sunset. A series of five dark frames with exposures of 30 minutes each were taken once at the beginning of each run. Target observations consisted of two exposures (typically 20 - 30 minutes each) to permit cosmic ray rejection, followed by a comparison Helium-Argon (HeAr) lamp exposure (typically 10 seconds) to calibrate wavelength coverage for each object. Flux standards were observed nightly to flux calibrate the data.

A slit width of 2″ was used for the 2003 and 2004 observing runs. Some of these data have flux calibration problems because the slit was not rotated to be aligned along the direction of atmospheric refraction. In conjunction with telescope "jitter", light was sometimes lost preferentially at the red or the blue end for these data.

A slit width of 6″ was used for the 2006 observing runs, eliminating most of the flux calibration problems even though the slit was not rotated. All observations were taken at an airmass of less than 2.0. Within our wavelength window, the maximum atmospheric differential refraction is less than 3″ (Filippenko 1982). Because of a concept called "anamorphic demagnification" (a detailed summary can be found in Schweizer 1979), which occurs when there is a large angle between the optical axes of the collimator and camera as well as a large grating tilt, no resolution should be lost because of the larger slit width. Such is the case for the spectrograph on the CTIO 1.5 m using the setup described above. A test was performed to verify that no resolution was lost by taking spectra of a F dwarf with sharp absorption lines from slit widths of 2″ to 10″ in 2″ increments. Indeed, no resolution was lost although the background flux increased with increasing slit width. Note, resolution of the comparison lamp spectrum *is* lost when the slit is opened because the comparison lamp is a resolved source (unlike stars that are unresolved point sources). A comparison of the data using the increased slit width showed no noticeable adverse effects (i.e., more noise because of the increased background flux) and seemed to correct the flux calibration problems.

6.2 Spectroscopy Data Reduction

Figure. 6.1: Raw image of a stellar spectrum. Various features that are described in the text as well as the axes are labeled. The stellar spectrum is the narrow dark band that spans the dispersion axis.

Basic calibration of the data utilized the Image Reduction and Analysis Facility (IRAF) following the procedure outlined in Massey (1997). The data were bias subtracted, flat-fielded, and dark corrected using IRAF package *ccdproc*. Because the lamp used to illuminate the dome flat does not emit light at all wavelengths equally, the "shape" of the lamp along the dispersion axis (see Figure 6.1) was removed with the IRAF task *response* using a cubic spline curve fit (of order 25 - 50). To fine tune the flat-fielding, the sky flats were combined and used as an illumination correction that corrected any sky variations along the spatial axis of the CCD (this step is really only necessary on long exposures when sky counts are significant but was performed on all the data for the sake of consistency). A bad pixel mask was generated using a set of long and short dome flats but was unsuccessful at removing the prominent bad column at dispersion axis pixel value 239. This artifact was removed from each

spectrum individually after final processing but before combining spectra of the same target.

Final reduction of the spectra followed the procedure outlined in Massey et al. (1992). For each target image, the background sky is defined manually using the IRAF task *background* and consists of two regions, one on each side of the stellar spectrum, as near to the spectrum (with respect to the dispersion axis) as possible without including any starlight. A first order Legendre polynomial is fit to these regions and then subtracted from the rest of the image. The apertures containing the stellar spectra are then extracted using IRAF task *apsum* by defining the peak when the image is viewed as a slice along the spatial axis. An identical aperture is extracted for each image's comparison HeAr lamp image for the purpose of wavelength calibration. By calibrating the wavelength using only the same region of the CCD that contains the stellar spectrum, we avoid any effects caused by variations along the spatial axis. For example, pixel 240 of the dispersion axis will not correspond to 4417 Å along the entire spatial axis because of an imperfect alignment of the slit with respect to the CCD. Prominent lines (three or four) from a comparison lamp are identified by eye to serve as a frame of reference for the weaker lines to be matched to a library of lines using IRAF task *identify*. Matches with large residuals are discarded until there are $\sim$40 marked lines and the RMS of all the match values compared with library values is $< 20\%$. The matches from this comparison lamp serve as a reference for matching all other comparison lamps for a given night using IRAF

task *reidentify*. A dispersion solution is then calculated for each target spectrum using a third order cubic spline fit via the IRAF task *dispcor*. The final calibration necessary is the flux calibration. Raw flux values are integrated over flux bandpasses and divided by the exposure time using IRAF task *standard*, which outputs a single file of bandpass counts and standard star fluxes. Using this output, a sixth order cubic spline sensitivity function is fit to account for the non-uniform sensitivity of the chip over all wavelengths using IRAF task *sensfunc*. The sensitivity function is applied to all target spectra using IRAF task *calibrate*. The data are then cleaned of any cosmic rays and bad columns by comparing the two spectra for each object manually. Lastly, the two spectra for each object are combined using iraf task *sarith*.

6.3 Spectroscopy Results

Once a WD candidate is spectroscopically confirmed, it is given a "WD" designation. The traditional naming convention for WDs uses the object's epoch 1950 equinox 1950 coordinates. Coordinates for new WD discoveries from both search phases were extracted from 2MASS along with the Julian date of observation. These coordinates were adjusted to account for proper motion from the epoch of 2MASS observation to epoch 2000 (hence epoch 2000 equinox 2000). The coordinates were then transformed to equinox 1950 coordinates using the IRAF task *precess*. Finally, the coordinates were again adjusted (opposite the direction of proper motion) to obtain epoch 1950 equinox 1950 coordinates.

Proper motions were taken from various proper motion surveys in addition to unpublished values obtained via the SCR proper motion survey while recovering previously known HPM objects. These values, as well as J2000 coordinates and alternate names, are tabulated in the following sections separated by the search phase of discovery. Phase One includes all objects observed during the 2003 and 2004 spectroscopic runs and one star from the May 2006 run (WD 1105−340, also known as SCR 1107−3420 A). Phase Two includes all other objects observed during the 2006 runs.

6.3.1 Phase One

Phase One data (with exception of WD 1105−340) were acquired using a $2''$ slit width. In total, 33 new nearby WD systems were discovered and were published in Subasavage et al. (2007). Of these new systems, 26 are DA (hydrogen rich) including 1 DAB (hydrogen rich with helium), 4 are DC (featureless), 2 are DZ (helium rich with metals), and 1 is DQ (helium rich with carbon). The DA spectra are separated into two plots, those with $T_{eff} \geq 10,000$ K (Figure 6.2), and those with $T_{eff} < 10,000$ K (Figure 6.3) as determined from spectral energy distribution (SED) fitting to the photometry (see § 7.3.2). The only noticeable features are broad absorption at the Balmer lines (in the cooler cases, only Hα). These lines are broadened because of the extreme pressures found in the WD atmospheres that are caused by high surface gravities and is known as Stark broadening.

The four featureless DC spectra are plotted in Figure 6.4. A handful of unusual WDs were discovered and require additional data to characterize fully. As such, the

spectral plots will be shown here but a detailed discussion will be deferred until §
8.4.3.

WD 0622−329 is a DA WD that has a few weak He I lines making its formal
classification a DAB. The top panel of Figure 6.5 shows the spectral plot and identifies
the spectral features.

WD 0121−429 is a DA WD that exhibits Zeeman splitting of the Balmer lines
(evident in Hα and Hβ) because of the presence of a magnetic field (seen in the
bottom panel of Figure 6.5). Blueward of Hβ, the absorption lines are difficult to
identify because of the distortions caused by the magnetic field.

WD 0840−136 is a cool DZ WD that exhibits absorption caused by Ca II H & K
(3933 Å and 3968 Å) as well as Ca I at 4227 Å. The spectrum is plotted in the top
panel of Figure 6.6.

WD 2138−332 is another DZ WD that exhibits absorption caused by Mg I and Fe
I in addition to the Ca I and Ca II absorption. The spectrum is plotted in the bottom
panel of Figure 6.6.

WD 1149−272 is the only DQ WD discovered during phase one. It is characterized
as having mild Swan band features at 4737, 5165, and 5636 Å because of the presence
of C$_2$. The spectrum is plotted in Figure 6.7.

A complete list of the new WD discoveries from Phase One as well as J2000
coordinates and alternate names is found in Table 6.1.

Figure. 6.2: Spectral plots of the hot ($T_{\text{eff}} \geq 10{,}000$ K) DA WDs from Phase One, normalized at 5200 Å and plotted in descending T_{eff} as derived from the SED fits to the photometry (see § 7.3.2). The first five Balmer series lines are labeled. Note that some of the flux calibrations are not perfect, in particular, at the blue end.

Figure. 6.3: Spectral plots of the cool (T_{eff} < 10,000 K) DA WDs from Phase One, normalized at 5200 Å and plotted in descending T_{eff} as derived from the SED fits to the photometry (see § 7.3.2). The first five Balmer series lines are labeled. Note that some of the flux calibrations are not perfect, in particular, at the blue end.

Figure. 6.4: Spectral plots of the four featureless DC WDs from Phase One, normalized at 5200 Å and plotted in descending T_{eff} as derived from the SED fits to the photometry (see § 7.3.2). Note that some of the flux calibrations are not perfect, in particular, at the blue end.

Figure. 6.5: (*Top panel*) Spectral plot of DAB WD 0622−329. Indicated above the spectrum are the hydrogen Balmer lines (*filled stars*) and the visible He I lines (*open diamonds*). (*Bottom panel*) Spectral plot of DAH WD 0121−429. Indicated above the spectrum are the hydrogen Balmer lines (*filled stars*), although the Zeeman splitting associated with a magnetic field has rendered the lines blueward of Hβ difficult to identify. Horizontal bars over the Hα and Hβ regions indicate the spread of the split lines.

Figure. 6.6: (*Top panel*) Spectral plot of DZ WD 0840−136. The visible absorption features of Ca ɪ and Ca ɪɪ are labeled. (*Bottom panel*) Spectral plot of DZ WD 2138−332. In addition to the Ca ɪ and Ca ɪɪ features, this object displays absorption caused by Mg ɪ (*open circles*) and Fe ɪ (*small filled circles*). The source of the large feature at 5175 Å is currently unknown.

Figure. 6.7: Spectral plot of the only DQ WD from Phase One. Indicated above the spectrum are the three Swan band features caused by C_2.

Table. 6.1: Astrometry and Alternate Designations for Phase One New WDs.

WD Name	R.A. (J2000.0)	Decl.	μ (arcsec yr^{-1})	θ (deg)	Ref.		Alternate Names		
(1)	(2)	(3)	(4)	(5)	(6)		(7)		
0034−602	00 36 22.31	−59 55 27.5	0.280	69.0	L	NLTT 1993	= LP 122-4	= LP 991-16	= ...
0121−429	01 24 03.98	−42 40 38.5	0.538	155.2	L	LHS 1243	= NLTT 4684	= LP 992-99	= ...
0216−398	02 18 31.51	−39 36 33.2	0.500	78.6	L	LHS 1385	= NLTT 7640	= ...	= ...
0253−755	02 52 45.64	−75 22 44.5	0.496	63.5	S	SCR 0252-7522	= ...	= ...	= ...
0310−624	03 11 21.34	−62 15 15.7	0.416	83.3	S	SCR 0311-6215	= ...	= ...	= ...
0344+014	03 47 06.82	+01 38 47.5	0.473	150.4	S	LHS 5084	= NLTT 11839	= LP 593-56	= ...
0404−510	04 05 32.86	−50 55 57.8	0.320	90.7	P	LEHPM 1-3634	= ...	= ...	= ...
0501−555	05 02 43.43	−55 26 35.2	0.280	191.9	P	LEHPM 1-3865	= ...	= ...	= ...
0511−415	05 13 27.80	−41 27 51.7	0.292	4.4	P	LEHPM 2-1180	= ...	= ...	= ...
0525−311	05 27 24.33	−31 06 55.7	0.379	200.7	P	NLTT 15117	= LP 892-45	= LEHPM 2-521	= ...
0607−530	06 08 43.81	−53 01 34.1	0.246	327.6	P	LEHPM 2-2008	= ...	= ...	= ...
0622−329	06 24 25.78	−32 57 27.4	0.187	177.7	P	LEHPM 2-5035	= ...	= ...	= ...
0821−669	08 21 26.70	−67 03 20.1	0.758	327.6	S	SCR 0821-6703	= ...	= ...	= ...
0840−136	08 42 48.45	−13 47 13.1	0.272	263.0	S	NLTT 20107	= LP 726-1	= ...	= ...
1016−308	10 18 39.84	−31 08 02.0	0.212	304.0	L	NLTT 23992	= LP 904-3	= LEHPM 2-5779	= ...
1054−226	10 56 38.64	−22 52 55.9	0.277	349.7	P	NLTT 25792	= LP 849-31	= LEHPM 2-1372	= ...
1105−340	11 07 47.89	−34 20 51.4	0.287	168.0	S	SCR 1107-3420A	= ...	= ...	= ...
1149−272	11 51 36.10	−27 32 21.0	0.199	278.3	P	LEHPM 2-4051	= ...	= ...	= ...
1243−123	12 46 00.69	−12 36 19.9	0.406	305.4	S	SCR 1246-1236	= ...	= ...	= ...
1316−215	13 19 24.72	−21 47 55.0	0.467	179.2	S	NLTT 33669	= LP 854-50	= WT 2034	= ...
1436−781	14 42 51.54	−78 23 53.6	0.409	272.0	S	NLTT 38003	= LP 40-109	= LTT 5814	= ...
1452−310	14 55 23.47	−31 17 06.4	0.199	174.2	P	LEHPM 2-4029	= ...	= ...	= ...
1647−327	16 50 44.32	−32 49 23.2	0.526	193.8	L	LHS 3245	= NLTT 43628	= LP 919-1	= ...
1742−722	17 48 31.21	−72 17 18.5	0.294	228.2	P	LEHPM 2-1166	= ...	= ...	= ...
1946−273	19 49 19.78	−27 12 25.7	0.213	162.0	L	NLTT 48270	= LP 925-53	= ...	= ...
2008−600	20 12 31.75	−59 56 51.5	1.440	165.6	S	SCR 2012-5956	= ...	= ...	= ...
2008−799	20 16 49.66	−79 45 53.0	0.434	128.4	S	SCR 2016-7945	= ...	= ...	= ...
2035−369	20 38 41.42	−36 49 13.5	0.230	104.0	L	NLTT 49589	= L 495-42	= LEHPM 2-3290	= ...
2103−397	21 06 32.01	−39 35 56.7	0.266	151.7	P	LEHPM 2-1571	= ...	= ...	= ...
2138−332	21 41 57.56	−33 00 29.8	0.210	228.5	P	NLTT 51844	= L 570-26	= LEHPM 2-3327	= ...
2157−574	22 00 45.37	−57 11 23.4	0.233	252.0	P	LEHPM 1-4327	= ...	= ...	= ...
2218−416	22 21 25.37	−41 25 27.0	0.210	143.4	P	LEHPM 1-4598	= ...	= ...	= ...
2231−387	22 33 54.47	−38 32 36.9	0.370	220.5	P	NLTT 54169	= LP 1033-28	= LEHPM 1-4859	= ...

NOTE.—Units of right ascension are hours, minutes, and seconds, and units of declination are degrees, arcminutes, and arcseconds.
REFERENCES.—(L) Luyten 1979a,b; (P) Pokorny et al. 2004; (S) Subasavage et al. 2005a,b, this work

6.3.2 Phase Two

The second phase results were all obtained during the 2006 runs for which the wider 6″ slit width was used. In total, 23 new WD systems (a total of 24 WDs) were spectroscopically confirmed. Of those, 14 are DA (hydrogen rich), 7 are DC (featureless), 2 are DZ (helium rich with metals), and 1 is a DB (helium rich). Physical parameters have not yet been estimated for this entire sample because additional data are necessary. However, a better flux calibration using the wider slit width allows us to determine reliable relative effective temperatures. Figure 6.8 contains the spectral plots for the hot ($T_{\text{eff}} \geq 10,000$ K) DA WDs while Figure 6.9 contains the spectral plots for cool ($T_{\text{eff}} < 10,000$ K) DA WDs. As discussed previously, the only features are absorptions at the Balmer lines (in the cooler cases, only Hα).

The seven featureless DC spectra are plotted in Figure 6.10. The two calcium-rich DZ spectra are plotted in Figure 6.11. Prominent in both spectra are the Ca II H and K lines that are labeled in the top panel. Additional absorption features prominent in the bottom panel arise from Mg I (designated by open circles) and Fe I (designated by small filled circles). The lone helium-rich DB spectrum is plotted in Figure 6.12. All absorption features present in this spectrum arise from He I and are labeled.

A complete list of the new WD discoveries from Phase Two as well as J2000 coordinates and alternate names is found in Table 6.2.

Figure. 6.8: Spectral plots of the hot ($T_{\text{eff}} \geq 10{,}000$ K) DA WDs from Phase Two, normalized at 5200 Å and plotted in descending T_{eff} as estimated by the slopes of the continua and the strengths of the absorption lines. Notice the flux calibration problems are not present in these data.
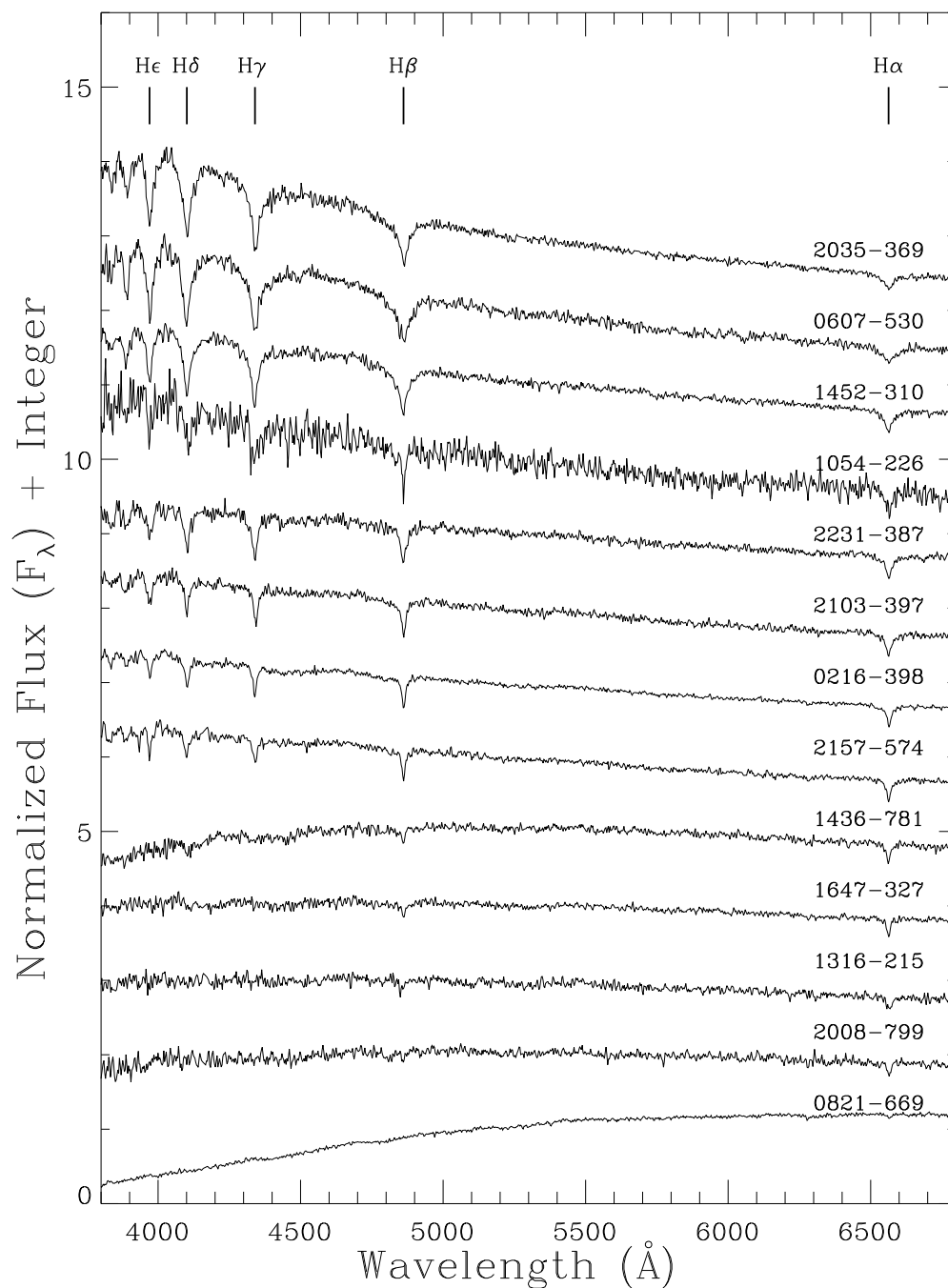
Figure. 6.9: Spectral plots of the cool (T_{eff} < 10,000 K) DA WDs from Phase Two, normalized at 5200 Å and plotted in descending T_{eff} as estimated by the slopes of the continua and the strengths of the absorption lines. Notice the flux calibration problems are not present in these data.

Figure. 6.10: Spectral plots of the seven featureless DC WDs from Phase Two, normalized at 5200 Å and plotted in descending T_{eff} as estimated by the slopes of the continua. Notice the flux calibration problems are not present in these data.

Figure. 6.11: Spectral plots of the two calcium-rich DZ WDs from Phase Two. The most prominent absorption features in both spectra are the Ca II H and K lines and Ca I (labeled in top panel). Additional features in the bottom panel arise from Mg I (*open circles*) and Fe I (*small filled circles*).

Table 6.2: Astrometry and Alternate Designations for Phase Two New WDs.

WD Name	R.A. (J2000.0)	Decl. (J2000.0)	μ (arcsec yr^{-1})	θ (deg)	Ref.	Alternate Names
(1)	(2)	(3)	(4)	(5)	(6)	(7)
0011−721......	00 13 49.91	−71 49 54.2	0.326	141.3	S	NLTT 681 = LP 50-73 = ...
0102−579......	01 04 12.14	−57 42 48.6	0.239	91.1	S	SCR 0104-5742 = ... = ...
0123−460......	01 25 18.03	−45 45 31.1	0.759	137.8	S	SCR 0125-4545 = ... = ...
0134−177......	01 37 15.16	−17 27 22.6	0.319	189.3	S	NLTT 5424 = LP 768-192 = ...
0149−723......	01 50 38.49	−72 07 16.7	0.334	223.9	S	SCR 0150-7207 = ... = ...
0311−649......	03 12 25.68	−64 44 10.8	0.190	105.6	S	WT 106 = LEHPM 1-3159 = ...
0431−360......	04 32 55.87	−35 57 28.9	0.301	84.1	S	LEHPM 2-1182 = SCR 0432-3557 = ...
0431−279......	04 33 33.58	−27 53 24.8	0.403	92.4	S	NLTT 13532 = LP 890-39 = LEHPM 2-405
0620−402......	06 21 41.64	−40 16 18.7	0.379	166.0	S	LEHPM 2-505 = SCR 0621-4016 = ...
0651−398A.....	06 53 30.21	−39 54 29.1	0.227	344.4	S	WT 202 = ... = ...
0651−398B.....	06 53 35.34	−39 55 33.3	0.229	344.7	S	WT 201 = ... = ...
0655−390......	06 57 05.90	−39 09 35.7	0.340	242.6	S	NLTT 17220 = L 454-9 = ...
0708−670......	07 08 52.28	−67 06 31.4	0.246	246.3	S	SCR 0708-6706 = ... = ...
0707−320......	07 09 25.07	−32 05 07.3	0.551	338.2	L	LHS 1898 = NLTT 17486 = LP 896-18
0709−252......	07 11 14.39	−25 18 15.0	0.223	334.4	S	SCR 0711-2518 = ... = ...
0751−252......	07 53 56.61	−25 24 01.4	0.426	300.2	S	SCR 0753-2524 = ... = ...
0816−310......	08 18 40.26	−31 10 20.3	0.842	162.6	S	SCR 0818-3110 = ... = ...
0856−007......	08 59 12.91	−00 58 42.9	0.202	125.8	S	NLTT 20690 = LP 606-32 = ...
1116−470......	11 18 27.20	−47 21 57.0	0.322	275.1	S	SCR 1118-4721 = ... = ...
1817−598......	18 21 59.54	−59 51 48.5	0.365	194.9	S	SCR 1821-5951 = ... = ...
1916−362......	19 20 02.83	−36 11 02.7	0.208	132.0	S	SCR 1920-3611 = ... = ...
2009−471......	20 12 48.75	−46 59 02.5	0.244	136.3	S	WT 689 = ... = ...
2118−388......	21 22 05.59	−38 38 34.7	0.186	113.5	S	SCR 2122-3838 = ... = ...
2133−135......	21 36 16.38	−13 18 34.5	0.297	120.2	S	NLTT 51636 = Ross 203 = ...

NOTE.—Units of right ascension are hours, minutes, and seconds, and units of declination are degrees, arcminutes, and arcseconds.
REFERENCES.—(L) Luyten 1979a,b; (S) Subasavage et al. 2005a,b; Finch et al. 2007, this work

Figure 6.13 is an RPM diagram illustrating the effectiveness of identifying the new WD discoveries (*asterisks*) presented here. New WD identifications are from the SCR, NLTT, WTC, and LEHPM surveys. The filled circles represent new HPM discoveries from the SCR proper motion survey discussed in Chapter 5. Note that there are four new WDs that lie to the right of the arbitrary WD-subdwarf boundary. These objects were selected for spectroscopic follow-up based on their 2MASS colors (discussed in § 7.3.1) in addition to their positions on the RPM diagram.

Including the spectroscopically confirmed discoveries from both phases, a total of 56 new WD systems containing 57 WDs in the southern hemisphere were identified in this effort. Separating objects by spectral type, 40 are DA (including 1 DAB), 11 are DC, 4 are DZ, 1 is DB, and 1 is DQ.

As it became increasingly evident that there is no shortage of relatively bright WDs to be discovered in the southern hemisphere, our priority for spectroscopic follow-up shifted to identifying nearby WDs only. During the Phase Two search, once WD candidates were vetted via the RPM diagram, a distance was estimated using the linear plate color relation of Oppenheimer et al. (2001b). Only candidate WDs whose distance estimate was within $\sim$30 pc were targeted for spectroscopic follow-up, which biased this sample toward cooler WDs. This bias is the reason that more DC WDs (see Figures 6.4 and 6.10) and fewer hot DA WDs were identified (see Figures 6.2 and 6.8) in Phase Two than in Phase One, because hot DAs are inherently more luminous and can be detected at greater distances.

Figure. 6.13: Reduced proper motion diagram for new WD discoveries (*asterisks*). New HPM discoveries from the SCR proper motion survey are also plotted (*filled circles*). The solid line marks an arbitrary boundary between WDs and subdwarfs. The encircled point labeled "sd" is a confirmed subdwarf that happens to lie just inside the WD region.

In order to target the new WDs that are actually nearby, we would like to constrain their distance estimates. With more precise CCD photometry, we are able to estimate distances using two independent methods, via an empirical color-magnitude relation and via WD modeling. The first step is to obtain CCD photometry for the newly discovered WDs.

Chapter 7

Photometry for New and Known WDs

CCD photometry is far superior to plate magnitudes because the recorded flux in an exposure is linearly related to the exposure time (to first order as long as the flux does not approach the saturation limit of the CCD). Conversely, the emulsions on a photographic plate do not respond linearly to the stellar fluxes and a more indirect series of corrections and calibrations are necessary, which introduce additional uncertainties. CCD magnitudes are determined to better than 0.03 mag routinely with one observation, while plate magnitudes are determined to 0.3 mag (see Table 5.2) and are dependent on the brightness of the object. Of course, any properties derived from these quantities will be better constrained if the magnitudes are better constrained – in this case, typically by a factor of 10.

7.1 Photometry Observations

Optical $V_J R_{\mathrm{KC}} I_{\mathrm{KC}}$ for new and known WD systems was obtained using the CTIO 0.9 m telescope during several observing runs from 1999 to 2003 as part of the NOAO Surveys Program and from 2003 through 2007 as part of the SMARTS Consortium. The 2048 × 2046 Tektronix CCD camera was used with the Tek 2 $V_J R_{\mathrm{KC}} I_{\mathrm{KC}}$ filter set. Only the central quarter of the chip was used, providing a 6.8′ square field of view. Bias frames and dome flats in each filter were taken prior to sunset each night.

One photometry observing run was completed using the CTIO 1.0 m telescope. The 4064 × 4064 STA CCD camera (known as the Y4KCam) was used with a $B_JV_JR_{KC}I_{KC}$ filter set. The field of view was $20'$ square. Bias frames and dome flats in each filter were taken prior to sunset each night.

Several standard stars from Graham (1982), Bessel (1990), and Landolt (1992) that are free from significant background contamination within a $7''$ radius were observed nightly. Each standard was observed at three airmasses, typically $\sim$1.1, $\sim$1.4, and $\sim$2.0 airmasses. At least one very red standard is observed each night to properly calibrate the magnitudes for the nearby red dwarfs on the CTIOPI program. These observations enabled us to calibrate fluxes to the Johnson-Kron-Cousins system and to calculate extinction corrections.

Target objects are usually observed at the lowest possible airmasses and, with exception to a few targets in the northern and the extreme southern hemispheres, are less than 1.6 airmasses. Ideally, each target object will have at least three independent observations (i.e., observed on at least three nights) before the results are definitive. However, if only two measurements are available and they agree within a few sigma, the results are deemed publishable. Of the 33 systems discovered during Phase One, all have at least two observations and 12 systems have three or more observations (Subasavage et al. 2007).

7.2 Photometry Data Reduction

Photometry reductions were performed using standard IRAF packages except that they have been conveniently bundled into 0.9 m CTIOPI data-specific IRAF scripts called *redpi* and *apercorr*, written by Dr. Wei-Chun Jao. Bias subtraction and dome flat-fielding were performed using the IRAF task *ccdproc* via the *redpi* script. The remainder of the reductions utilized the *apercorr* script.

Each night's data were separated into two groups, the standard stars and the science (target) stars. The standard star frames were evaluated first, with a check of the region around each standard star for cosmic ray contamination using the *display* and *imexam* tasks. If cosmic rays were found within a 7″ radius (14″ diameter, which is consistent with the aperture used by Landolt 1992, for standard stars), the IRAF task *cosmicray* was used to remove the cosmic ray. In a few cases, the task had to be run multiple times, with a slight tweak in the parameters, to sufficiently remove the cosmic ray. Once all standard star regions were free of cosmic rays, the stars were tagged and the flux calculated within a 14″ diameter. A background level was determined using an annulus around each standard that had an inner radius of 20″ and a width of 3″ to be subtracted from the flux of the stellar aperture using the task *phot*. These data were compiled into usable text files using the tasks *mkimset* and *mknobsfile*. The transformation equation used to determine apparent magnitude is

$$m_{standard} = m_{inst} + a_1 + a_2 x + a_3(color) + a_4(color)x, \qquad (7.1)$$

where m_{inst} is the instrumental magnitude derived from the background subtracted flux within the stellar aperture, a_1 through a_4 are transformation coefficients, *color* is the color term (usually $V_J - I_{\mathrm{KC}}$ but can be any permutation consisting of $V_J R_{\mathrm{KC}} I_{\mathrm{KC}}$ magnitudes), x is the airmass and $m_{standard}$ is the standard magnitude from either Graham (1982), Bessel (1990), or Landolt (1992). The task *fitparam* computes the transformation coefficients using a least squares method.

The science star frames were then evaluated in a similar manner. While checking for cosmic rays, an appropriate aperture was determined. If the field was uncrowded, a $14''$ diameter aperture was used. In a crowded field, or if the science star is near a companion, an aperture ranging from $4''$ to $12''$ in diameter was applied using the largest aperture possible without including contamination from neighboring sources. In these cases, an aperture correction was calculated by selecting other stars (typically five) in the frame that are uncontaminated and sufficiently exposed and was applied to the flux within the smaller science star aperture. Aperture corrected instrumental magnitudes were then applied to Eq. 7.1, now with the coefficients determined using the standard stars, to determine the apparent magnitudes. A custom perl script was written for this task by Dr. Wei-Chun Jao, identical in function to the IRAF task *evalfit*, but instead generates an output that facilitates easy inclusion into our large master photometry database.

7.3 Analysis

Our basic understanding of the physics of WDs is often sufficient to reproduce the variety of spectral features seen in WDs (although our perspicacity of the details in the physics necessary for precise WD modeling is far from complete). Also, WD luminosities for a given effective temperature (hence color, in all but the coolest WDs) are consistent except for slight (and important) variations that arise primarily because of mass differences. As previously discussed, WDs are degenerate objects and as such, the mass is inversely related to its size (i.e., more massive WDs are smaller and less luminous). Nonetheless, the vast majority of WDs in the solar neighborhood are of average mass (i.e., 0.6 $M_\odot$) and therefore of average temperature-dependent luminosity, so that empirical color-magnitude relations, similar to those used for red dwarfs in § 5.3.1, can be generated for WDs.

7.3.1 Empirical Distance Relations

With reliable CCD photometry available for a sample of WDs that have accurate trigonometric parallax measurements, a suite of photometric distance relations can be generated. Data taken from Bergeron et al. (2001) were used for this purpose. In order to prevent unnecessary contamination because of observational uncertainties, only those WDs that have trigonometric parallaxes placing them within 25 pc and parallax errors less than 10 mas were used in the fits. In addition, any object that is known or suspected to be an unresolved multiple (e.g. a double degenerate) was removed. Of the 152 objects contained in Bergeron et al. (2001), 68 met these criteria.

Optical $B_J V_J R_{\mathrm{KC}} I_{\mathrm{KC}}$ and infrared JHK (CIT) photometry for the 68 objects was extracted from the publication. Color transformations to the 2MASS system were applied as described in Carpenter (2001). JHK_S magnitudes and errors from 2MASS were also extracted via Aladin, but were disregarded if the error was null. A weighted mean of each infrared magnitude was calculated for objects having both measurements. Magnitude errors were propogated through each step, and the resulting errors were $J \leq 0.04$ mag, $H \leq 0.06$ mag, and $K_S \leq 0.09$ mag.

M_V magnitudes were calculated and ranges in color were determined for each of the 21 colors available. To better constrain M_V for a given color, any color that had less than a one magnitude range for all M_V was excluded from the final suite of relations used to determine distances. Thirteen useful relations remained. After comparing fits of order 2, 3, 4, and 5 for each color, we used 3rd order fits, which minimized RMS values without introducing erroneous "bumps" in the fits. Coefficients for the fits of the 13 useful colors are presented in Table 7.1.

Table. 7.1: Details for photometric distance relations relative to M_V

Color (1)	Applicable Range (2)	# Stars (3)	Coeff. #1 ($\times$ color^3) (4)	Coeff. #2 ($\times$ color^2) (5)	Coeff. #3 ($\times$ color) (6)	Coeff. #4 (constant) (7)	RMS (mag) (8)
$(B-V)$.......	0.10 to 1.84	68	+1.82E-01	−1.47E-00	+4.10E-00	+12.52	0.49
$(B-R)$.......	0.16 to 2.45	68	+1.69E-01	−1.04E-00	+3.17E-00	+12.27	0.45
$(B-I)$........	0.15 to 2.99	67	+7.11E-02	−5.43E-01	+2.30E-00	+12.26	0.46
$(B-J)$.......	0.16 to 3.57	68	−3.28E-03	−5.00E-02	+1.18E-00	+12.63	0.46
$(B-H)$.......	0.14 to 3.88	68	+7.12E-03	−7.11E-02	+1.08E-00	+12.64	0.47
$(B-K)$.......	0.04 to 4.06	68	−1.48E-03	−1.16E-02	+9.38E-01	+12.69	0.47
$(V-I)$........	−0.03 to 1.41	67	−7.05E-02	+1.16E-00	+2.20E-00	+12.57	0.50
$(V-J)$.......	0.00 to 1.98	68	−9.24E-02	+3.14E-01	+1.33E-00	+12.76	0.49
$(V-H)$.......	−0.04 to 2.08	68	+1.57E-01	−3.53E-01	+1.51E-00	+12.74	0.50
$(V-K)$.......	−0.14 to 2.22	68	+1.40E-01	−2.90E-01	+1.34E-00	+12.79	0.51
$(R-J)$.......	−0.05 to 1.28	68	−8.05E-01	+1.93E-00	+1.06E-00	+12.98	0.51
$(R-H)$.......	−0.03 to 1.45	68	+4.03E-01	−4.62E-01	+1.79E-00	+12.88	0.54
$(R-K)$.......	−0.12 to 1.61	68	+3.16E-01	−3.28E-01	+1.56E-00	+12.89	0.54

Figure. 7.1: Example color-M_V plot displaying the 68 known WDs from Bergeron et al. (2001) and the corresponding $B_J - J$ relation (curved line). The vertical lines indicate the limits of the color within which the relation is useful.

A sample fit for the M_V versus $B_J - J$ relation is illustrated in Figure 7.1. For this particular color, the relation to M_V is as follows:

$$M_V = -3.28\text{E}-03(B_J - J)^3 - 5.00\text{E}-02(B_J - J)^2 + 1.18(B_J - J) + 12.62. \tag{7.2}$$

For a given WD, the distance estimate was taken to be the average of the distance estimates using each color. The standard deviation of the average with respect to the individual color's distance estimates was taken to be the internal error. By estimating distances to the 68 WDs used to generate the relations and comparing those to the true distances, a percent error of 13% was obtained and was adopted as the external error in these relations. The internal and external errors are added in quadrature for each object to give a total error.

To better constrain the distance estimates, colors that incorporate infrared magnitudes with errors greater than 0.16 mag (somewhat arbitrarily selected based on the error distribution of the 2MASS photometry of our WD discoveries) have been automatically excluded from the averaged distance estimate. Also, to avoid extrapolation when using the fits to evaluate a WD whose distance is unknown, color limits are set beyond which there are no stars in the standard sample to support the relation. Note, one point in Figure 7.1 with $B_J - J \sim 0$ is not within the color limits. Applicable colors correspond to effective temperatures between $\sim$5,000 K and $\sim$11,000 K. While it may seem that the relations are only applicable to a small range in T_{eff}, it is in this range that we find the cooler and less luminous WDs. In a magnitude limited survey, the less luminous objects are the ones that are nearby and are primary targets of this effort.

An interesting trend was noticed when evaluating which colors were suitable for distance estimates. When plotting infrared colors, it became clear that all of them are

degenerate for all M_V. For instance, the spread in color for $J - K_S$ is less than 0.5 for all M_V such that a fit would produce a nearly vertical line when plotting color (X-axis) vs. M_V (Y-axis). This effect is shown in Figure 7.2. While not useful for distance estimates, an infrared color constraint is useful as an additional discriminant for WD candidates, particularly for objects in the region of the RPM diagram bordering the WD - subdwarf boundary around which contamination will likely occur. Subdwarfs in this region typically have $J - K_S \sim 0.7$ or larger and thus there exists a significant color gap to distinguish between the two luminosity classes. Indeed a few new WDs were spectroscopically identified that are found in the subdwarf region of the RPM diagram and are plotted in Figure 6.13.

After using these relations to estimate distances to new WDs from Phase One, collaborator (and committee member) Pierre Bergeron noticed a flaw. Upon modeling the physical parameters of the new WDs (discussed in the next section) and obtaining independent distance estimates, there existed a systematic disagreement between the two estimates. The discrepancy was greatest at higher T_{eff} ($\sim$10,000 K) and among the DA WDs (see Figure 7.3).

The most likely cause for the discrepancy among hot DAs is the strength of the broad Balmer absorption lines in the optical. All optical filters used with exception of the I_{KC} (i.e.,$B_J V_J R_{\text{KC}}$) incorporate one or more of these features so that the measured flux integrated over the filter bandpass is suppressed. Any color that utilizes an optical magnitude and an infrared magnitude (including I_{KC}) will thus appear redder thereby implying the WD is cooler and less luminous.

Figure. 7.2: Plot of infrared $J - K_S$ color vs. M_V for WDs used to generate the distance relations. Notice how the spread in color is less than 0.5 mag over all M_V and is degenerate (i.e., there is no unique M_V for a given color value).

Hotter WDs are more luminous and farther away than cooler WDs, in general. Thus, most of the hotter DA WDs did not meet our distance criterion, by which the sample used to generate the relations was selected. As such, the color-M_V relations are biased against hot DA WDs and do not provide an accurate treatment for these

Figure. 7.3: Color-magnitude plot that contains the entire sample of Bergeron et al. (2001). The curved line represents the $B_J - J$ relation illustrated in Figure 7.1. Notice the deviation from the curve for DA WDs (*filled circles*) at blue colors and the agreement with the non-DA WDs (*open circles*). Plot generated by P. Bergeron.

objects. Admittedly, the flaw is problematic for the analysis of all our new WD discoveries but the relations still hold merit for estimating distances to cool DA WDs and all non-DA WDs (e.g. most nearby WDs). In fact, we often use the distances estimated by the relations to select nearby candidates for trigonometric parallax determinations. To analyze the entire new WD sample, physical modeling is necessary.

7.3.2 Modeling of Physical Parameters

If significant S/N spectra are available, WDs can be modeled by fitting the absorption lines to glean a T_{eff} and a $\log g$, where g is surface gravity. The relative strengths of the absorption lines are sensitive to T_{eff} and the widths of the absorption lines (i.e., broadness) are sensitive to $\log g$. For this technique to be applicable, the spectrum must have absorption lines. For the cool DAs that show only weak Hα and the featureless DCs, another method that uses photometry must be applied.

In order to evaluate all the new WD discoveries in a homogeneous manner, the photometry alone was used for modeling. Collaborators Pierre Bergeron and Patrick Dufour are responsible for modeling the WD discoveries. Briefly, the optical $V_J R_{\text{KC}} I_{\text{KC}}$ and infrared JHK_S magnitudes were transformed to average stellar fluxes f_λ^m received at Earth using the calibration of Holberg & Bergeron (2006) for photon counting devices. The resulting SEDs were compared with those predicted from model atmosphere calculations. One of a handful of model atmospheres was selected, either the pure hydrogen, pure helium, or mixed hydrogen and helium models (as described in Bergeron et al. 2001, and references therein) or the helium-rich models modified to account for carbon or metals (as described in Dufour et al. 2005, 2007). Both the observed and model fluxes are dependent on T_{eff}, $\log g$, and atmospheric composition, and are related by the following equation

$$f_\lambda^m = 4\pi (R/D)^2 H_\lambda^m, \tag{7.3}$$

where R/D is the ratio of a star's radius to its distance from Earth, and H_λ^m is the Eddington flux that depends on $T_{\rm eff}$, $\log g$ and $N({\rm He})/N({\rm H})$, properly averaged over the corresponding filter bandpass. The fitting technique uses the Levenberg-Marquardt nonlinear least-squares method (Press et al. 1992), which is based on a steepest descent method. The value of χ^2 is taken as the sum over all bandpasses of the difference between both sides of Eq. 7.3, weighted by the corresponding photometric uncertainties. Only $T_{\rm eff}$ and the solid angle $[4\pi(R/D)^2]$ are considered to be free parameters, and the covariance matrix of the fit directly determines the uncertainties of both parameters. The canonical value of $\log g = 8.0$ is assumed for all WDs, and its validity has been tested by Bergeron et al. (1992b) in which a sample of 129 DA WDs was spectroscopically fit and a $\log g$ directly determined. The mean for this sample is $\log g = 7.91$ with a dispersion of 0.26 dex.

The main atmospheric constituent, hydrogen or helium, is determined by the presence of Hα in the spectrum. If the spectrum is featureless (i.e., DC), the fits obtained with both compositions are compared to the observed flux values and the better fit is selected. For DQ (carbon) and DZ (calcium) stars, the first estimates of the atmospheric parameters are obtained by fitting the SED with an assumed value of metal abundances. The optical spectrum is then fit to better determine the metal abundances, and improve the atmospheric parameters from the SED. This procedure (outlined in Dufour et al. 2005, 2007) is iterated until a self-consistent photometric and spectroscopic solution is achieved. The DQ and DZ WDs discovered in Phase

Two, as well as the known WDs without distances (see § 7.4.2), were modeled using a pure helium model. Once additional data are collected, a more careful assessment using the appropriate models for DQ and DZ WDs will be employed for these objects.

Once the effective temperature and the atmospheric composition are determined, the absolute visual magnitude is determined. This is done by combining the new calibration of Holberg & Bergeron (2006) with evolutionary models similar to those described in Fontaine et al. (2001). Modifications include using C/O cores, $q(\text{He})$ $\equiv \log M_{\text{He}}/M_\star = 10^{-2}$ and $q(\text{H}) = 10^{-4}$ (representative of hydrogen-atmosphere WDs), and $q(\text{He}) = 10^{-2}$ and $q(\text{H}) = 10^{-10}$ (representative of helium-atmosphere WDs). By comparing the absolute visual magnitude with the V_J magnitude, a first estimate of the distance to each star is derived. Errors on the SED estimated distances incorporate the errors of the photometry values (~ 0.03 mag for optical magnitudes and usually larger for near-infrared magnitudes) as well as an error of 0.26 dex in log g (as discussed above).

7.4 Photometry Results

7.4.1 New WD Discoveries

Photometric magnitudes, derived values for T_{eff}, and distance estimates determined from both the empirical relations as well as the SED fit as well as the total errors (i.e., both internal and external) for the 57 new WD discoveries are listed in Table 7.2.

Spectral types for the new WD discoveries were deferred until this section because the DA WD (most of the sample) sub-types are dependent on the T_{eff}, which was determined via photometry. These objects have been assigned a half-integer temperature index as defined by McCook & Sion (1999), where the temperature index equals $50{,}400/T_{\text{eff}}$.

As an external check, a subset of DA WDs from the phase one search were analyzed by fitting the observed Balmer line profiles using the spectroscopic technique developed by Bergeron et al. (1992b), and recently improved by Liebert et al. (2003). The resulting effective temperatures were then compared to those derived via SED fitting and are plotted in Figure 7.4. The uncertainties of the spectroscopic technique are typically 0.038 dex in log g and 1.2% in T_{eff} according to Liebert et al. (2003). A larger uncertainty of 1.5% in T_{eff} was adopted here because of the problematic flux calibrations of the Phase One spectra. The agreement is excellent, except perhaps at high temperatures where the photometric determinations become more uncertain. It is possible that the significantly elevated point in Figure 7.4, WD 0310−624 (labeled), is an unresolved double degenerate with very different component effective temperatures (see § 8.4.3).

Table. 7.2: Photometry and Derived Parameters for 57 New WDs from Phase One and Phase Two

WD Name (1)	V_J (2)	R_{KC} (3)	I_{KC} (4)	# Obs. (5)	J (6)	σ_J (7)	H (8)	σ_H (9)	K_S (10)	σ_{K_S} (11)	T_{eff} (K) (12)	Comp. (13)	Dist$_{REL}$ (pc) (14)	Dist$_{SED}$ (pc) (15)	SpT (16)	Search Phase (17)	Notes (18)
0011−721	···	···	···	0	14.21	0.03	13.97	0.04	13.92	0.05	···±···	···	···±···	···±···	DA	II	a
0034−602	14.08	14.19	14.20	3	14.37	0.04	14.55	0.06	14.52	0.09	14655±1413	H	···±···	35.8±5.7	DA3.5	I	b
0102−579	···	···	···	0	15.67	0.07	15.57	0.16	15.76	null	···±···	···	···±···	···±···	DA	II	a
0121−429	14.83	14.52	14.19	4	13.85	0.02	13.63	0.04	13.53	0.04	6369±137	H	12.6±1.5	···±···	DAH	I	c,d
0123−460	16.31	15.94	15.56	1	15.11	0.04	14.84	0.06	14.91	0.10	5863±157	H	21.6±2.9	24.7±4.0	DA8.5	II	a
0134−177	···	···	···	0	15.34	0.04	15.26	0.07	15.20	0.14	···±···	···	···±···	···±···	DA	II	a
0149−723	···	···	···	0	15.65	0.05	15.64	0.12	15.42	0.18	···±···	···	···±···	···±···	DC	II	
0216−398	15.75	15.55	15.29	3	15.09	0.04	14.83	0.06	14.89	0.14	7364±241	H	23.9±3.1	29.9±4.7	DA7.0	I	
0253−755	16.70	16.39	16.08	2	15.77	0.07	15.76	0.15	15.34	null	6235±253	He	33.2±4.5	34.7±5.5	DC	I	
0310−624	15.92	15.99	16.03	2	16.13	0.10	16.31	0.27	16.50	null	13906±1876	H	···±···	21.0±3.7	DA3.5	II	b,c
0311−649	13.27	13.34	13.36	2	13.45	0.02	13.46	0.03	13.57	0.05	11945±557	H	19.4±2.5	···±···	DA4.0	I	b
0344+014	16.52	16.00	15.54	2	15.00	0.04	14.87	0.09	14.70	0.12	5084±91	He	19.9±3.1	···±···	DC	I	
0404−510	15.81	15.76	15.70	2	15.74	0.06	15.55	0.13	15.59	null	10052±461	H	36.5±5.2	53.5±8.5	DA5.0	I	
0431−360	···	···	···	0	15.48	0.06	15.17	0.08	15.23	0.18	···±···	···	···±···	···±···	DA	II	a
0431−279	···	···	···	0	15.37	0.05	15.11	0.07	14.92	0.12	···±···	···	···±···	···±···	DA	II	a
0501−555	16.35	16.17	15.98	2	15.91	0.08	15.72	0.15	15.82	0.26	7851±452	He	37.2±4.9	44.8±6.9	DC	I	
0511−415	16.00	15.99	15.93	2	15.96	0.08	15.97	0.15	15.20	null	10393±560	H	42.7±5.6	61.8±10.8	DA5.0	I	
0525−311	15.94	16.03	16.03	2	16.20	0.12	16.21	0.25	14.98	null	12941±1505	H	···±···	76.3±13.6	DA4.0	I	b
0607−530	15.99	15.92	15.78	3	15.82	0.07	15.66	0.14	15.56	0.21	9395±426	H	37.2±4.9	51.7±9.0	DA5.5	I	
0620−402	···	···	···	0	15.27	0.04	15.13	0.09	15.24	0.17	···±···	···	···±···	···±···	DZ	II	a
0622−329	15.47	15.41	15.36	2	15.44	0.06	15.35	0.11	15.53	0.25	···±···	···	32.7±4.1	···±···	DAB	I	c,e
0651−398A	16.07	15.76	15.44	2	15.10	0.05	14.90	0.08	14.71	0.13	7222±219	H	20.2±2.5	25.1±4.3	DA7.0	II	
0651−398B	15.46	15.23	14.98	2	14.71	0.04	14.55	0.05	14.49	0.11	6450±220	H	22.3±2.9	26.9±4.5	DA8.0	II	
0655−390	15.11	14.80	14.48	1	14.15	0.03	13.88	0.04	13.89	0.07	6442±163	H	14.6±1.8	17.2±2.9	DA8.0	II	
0707−320	15.61	15.57	15.49	2	15.49	0.06	15.43	0.11	15.38	0.20	9900±440	H	33.3±4.3	47.8±8.2	DA5.0	II	
0708−670	16.22	15.71	15.21	2	14.71	0.03	14.65	0.05	14.47	0.07	5108±74	He	17.5±2.6	17.5±2.7	DC	II	
0709−252	···	···	···	0	14.39	0.03	14.39	0.04	14.49	0.09	···±···	···	···±···	···±···	DA	II	a
0751−252	16.27	15.78	15.31	4	14.75	0.03	14.47	0.03	14.30	0.09	5159±107	H	15.8±2.1	17.8±2.9	DA10.0	II	a
0816−310	15.43	15.21	15.05	3	14.92	0.04	14.73	0.07	14.83	0.12	7477±285	H	23.8±3.1	27.1±4.3	DZ	II	
0821−669	15.34	14.82	14.32	3	13.79	0.03	13.57	0.03	13.34	0.04	5160±95	H	10.2±1.4	11.5±1.9	DA10.0	I	
0840−136	15.72	15.36	15.02	3	14.62	0.03	14.42	0.05	14.54	0.09	···±···	···	18.5±2.6	···±···	DZ	II	f
0856−007	16.31	15.82	15.36	2	14.83	0.04	14.58	0.05	14.69	0.13	5309±126	H	18.0±2.7	19.3±3.2	DA9.5	I	b
1016−308	14.67	14.75	14.81	2	15.05	0.04	15.12	0.08	15.41	0.21	16167±1598	H	···±···	50.6±9.2	DA3.0	I	b
1054−226	16.02	15.82	15.62	2	15.52	0.05	15.40	0.11	15.94	0.26	8266±324	H	31.4±3.9	41.0±7.0	DA6.0	I	g
1105−340	13.66	13.72	13.79	2	13.95	0.03	13.98	0.04	14.05	0.07	13926±988	H	···±···	28.2±4.8	DA3.5	I	b,h
1116−470	15.52	15.18	14.85	1	14.45	0.03	14.37	0.06	14.35	0.09	5859±140	He	17.6±2.3	17.8±2.8	DC	II	
1149−272	15.87	15.59	15.37	4	15.17	0.05	14.92	0.06	14.77	0.11	6188±194	He (+C)	24.3±3.4	24.0±3.8	DQ	I	
1243−123	15.57	15.61	15.64	2	15.74	0.07	15.73	0.11	16.13	null	12608±1267	H	···±···	62.6±10.7	DA4.0	I	b
1316−215	16.67	16.33	15.99	2	15.56	0.05	15.33	0.08	15.09	0.14	6083±201	H	26.0±3.7	31.6±5.3	DA8.5	I	
1436−781	16.11	15.82	15.49	2	15.04	0.04	14.88	0.08	14.76	0.14	6246±200	H	21.7±2.9	26.0±4.3	DA8.0	I	
1452−310	15.85	15.77	15.63	2	15.58	0.06	15.54	0.09	15.50	0.22	9206±375	H	34.1±4.2	46.8±8.1	DA5.5	I	
1647−327	16.21	15.85	15.49	3	15.15	0.05	14.82	0.08	14.76	0.11	6092±193	H	21.7±2.8	25.5±4.2	DA8.5	I	
1742−722	15.53	15.62	15.70	2	15.85	0.08	15.99	0.18	15.65	null	15102±2451	H	···±···	71.7±12.9	DA3.5	I	b
1817−598	···	···	···	0	15.20	0.05	15.01	0.10	14.91	0.14	···±···	···	···±···	···±···	DC	II	a
1916−362	13.61	13.70	13.79	1	14.10	0.08	14.22	0.04	14.21	0.07	14661±2686	He	···±···	30.0±5.2	DB	II	b,i
1946−273	14.19	14.31	14.47	2	14.72	0.04	14.77	0.09	14.90	0.13	21788±3304	H	···±···	52.0±9.9	DA2.5	II	b
2008−600	15.84	15.40	14.99	4	14.93	0.05	15.23	0.11	15.41	null	5078±221	He	25.1±7.6	···±···	DC	I	j
2008−799	16.35	15.96	15.57	3	15.11	0.04	15.03	0.08	14.64	0.09	5807±161	H	21.3±3.4	24.5±4.1	DA8.5	II	
2009−471	···	···	···	0	15.38	0.05	15.00	0.05	15.08	0.12	···±···	···	···±···	···±···	DA	I	a
2035−369	14.94	14.85	14.72	2	14.75	0.04	14.72	0.06	14.84	0.09	9640±298	H	24.1±3.1	33.1±5.7	DA5.0	I	
2103−397	15.31	15.15	14.91	2	14.79	0.03	14.63	0.04	14.64	0.08	7986±210	H	21.8±2.7	28.2±4.8	DA6.5	I	
2118−388	···	···	···	0	15.16	0.04	14.92	0.07	15.05	0.12	···±···	···	···±···	···±···	DC	II	a

Table 7.2: continued

WD Name (1)	V_J (2)	R_{KC} (3)	I_{KC} (4)	# Obs. (5)	J (6)	σ_J (7)	H (8)	σ_H (9)	K_S (10)	σ_{K_S} (11)	$T_{\rm eff}$ (K) (12)	Comp. (13)	Dist$_{\rm REL}$ (pc) (14)	Dist$_{\rm SED}$ (pc) (15)	SpT (16)	Search Phase (17)	Notes (18)
2133−135	13.69	13.63	13.55	2	13.60	0.03	13.58	0.04	13.69	0.06	10182± 281	H	14.4±1.8	20.4±3.5	DA5.0	II	
2138−332	14.47	14.30	14.16	3	14.17	0.03	14.08	0.04	13.95	0.06	7188± 291	He (+Ca)	17.2±2.2	17.3±2.7	DZ	I	
2157−574	15.96	15.73	15.49	3	15.18	0.04	15.05	0.07	15.28	0.17	7220± 246	H	25.4±3.3	32.0±5.4	DAZ	I	
2218−416	15.36	15.35	15.24	2	15.38	0.04	15.14	0.09	15.39	0.15	10357± 414	H	30.5±4.4	45.6±8.0	DA5.0	I	
2231−387	16.02	15.88	15.62	2	15.57	0.06	15.51	0.11	15.11	0.15	8155± 336	H	30.4±4.9	40.6±6.9	DA6.0	I	

NOTES.—"Dist$_{\rm REL}$" refers to the distances estimated using the empirical relations while "Dist$_{\rm SED}$" refers to the distances estimated using SED fitting.

a Object could not be modeled because optical magnitudes have not yet been obtained.

b Object is too blue for the empirical distance relations.

c If available, distance(s) underestimated. Object is likely an unresolved double degenerate (see § 8.4.3).

d Zeeman splitting of the Balmer lines seen in spectrum (signified with an 'H' appended to the spectral type, see § 8.4.3).

e Temperature is not listed because this object cannot be characterized by a single temperature (see § 8.4.3).

f Object is likely cooler than $T_{\rm eff}$ ~5,000 K and the theoretical models appropriate for DZ WDs do not provide an accurate treatment at these temperatures (see § 8.4.3).

g Our noisy spectrum classifies this object as a DA but recent high S/N spectra indicate that it is a DAZ (Bergeron, private communication).

h Distance of 19.1 ± 3.0 pc is estimated using $V_J R_{KC} I_{KC} J H K_S$ for the CPM companion M dwarf and the relations of Henry et al. (2004). System is possibly within 25 pc.

i Object's temperature is hotter than the grid of models; therefore, the SED fit is an extrapolation.

j Distance is likely overestimated because object is a very cool WD with collision-induced absorption in the infrared, thereby affecting its colors.

Figure. 7.4: Comparison plot of the values of T_{eff} derived from photometric SED fitting vs. those derived from spectral fitting for 25 of the DA WDs from the phase one search. The solid line represents equal temperatures. The elevated point, WD $0310-624$, is discussed in § 8.4.3.

With the realization that the distances estimated via empirical color relations are problematic for certain objects, the distances estimated via SED fitting to the photometry are given priority. In the cases when the SED estimated distance is unavailable, the empirical distance estimate will be used in the statistics. By a quick count of column 15 (or column 14 if column 15 is blank), of the 56 new WD systems (a total of 57 new WDs), at least 15 have distance estimates within 25 pc. Eleven objects do not yet have photometry observations (all were discovered during Phase Two) and as such, no reliable distance estimates are available. One object, WD $1105-340$, has a distance estimate of 28.2 ± 4.8 pc. This object has a CPM companion M dwarf whose distance estimate using $V_J R_{\mathrm{KC}} I_{\mathrm{KC}} JHK_S$ and the relations of Henry et al. (2004) is 19.1 ± 3.0 pc. Thus, this system may lie within 25 pc. Also, WD $2008-600$

is a very cool WD with infrared continuum collision-induced absorption (CIA). This phenomemon occurs in hydrogen-atmosphere or mixed-atmosphere WDs that have cooled enough for molecular hydrogen to exist ($T_{\text{eff}} \lesssim 5000$ K). These molecules then collide with other H (hydrogen-atmosphere) and He (mixed-atmosphere) atoms and molecules. The collisions induce a temporary dipole moment in the H_2 molecule that creates permitted dipole transitions that significantly increase the opacity in the red and near-infrared wavelength regime (see Harris et al. 1999, and references therein). Thus, the empirical relations do not provide an accurate treatment of this object. It too, is likely within 25 pc. Additionally, several objects have distance estimates just beyond 25 pc and it is possible that some may prove to be just within 25 pc when a true distance (i.e., trigonometric parallax) is measured.

7.4.2 Known WDs Without True Distances

In recent years, several new nearby WDs have been identified by other researchers (i.e., Lépine et al. 2005; Kawka & Vennes 2006). A primary aim of this effort is to further complete the nearby WD sample and as such, known WDs without trigonometric parallaxes were targeted for photometry so that nearby targets could be identified. The results of the analyses, identical to those performed on the new WD discoveries, are listed in Table 7.3.

Of the 23 systems in the known sample, 12 are estimated to be within 25 pc (see Table 7.3 column 15). A few more have distance estimates just beyond 25 pc using

the SED fitting but just within 25 pc using the empirical relations, leaving open the possibility that some are within 25 pc. Combining the new and known WD samples, a total of 27 are estimated to be within 25 pc and several are just beyond 25 pc. A true distance via trigonometric parallax is vital to confirm the proximity of these objects.

Table. 7.3: Photometry and Derived Parameters for 24 Known WDs

WD Name (1)	V_J (2)	R_{KC} (3)	I_{KC} (4)	# Obs. (5)	J (6)	σ_J (7)	H (8)	σ_H (9)	K_S (10)	σ_{K_S} (11)	T_{eff} (K) (12)	Comp. (13)	$Dist_{REL}$ (pc) (14)	$Dist_{SED}$ (pc) (15)	SpT (16)	Notes (17)
0024−556	15.17	15.15	15.07	2	15.01	0.04	15.23	0.10	15.09	0.14	10007± 378	H	27.6±3.7	39.8±6.8	DA5.0	
0141−675	13.82	13.52	13.23	3	12.87	0.02	12.66	0.03	12.58	0.03	6484± 128	H	8.2±1.0	9.7±1.6	DA8.0	
0150+256	15.70	15.52	15.33	2	15.07	0.04	15.08	0.09	15.16	0.14	7880± 280	H	26.6±3.6	33.0±5.6	DA6.5	
0255−705	14.08	14.03	14.00	2	14.04	0.03	14.13	0.04	13.99	0.06	10541± 326	H	17.3±2.2	25.8±4.5	DA5.0	
0442−304	16.03	15.93	15.86	2	15.94	0.09	15.81	null	15.21	null	9949± 782	He	41.4±5.1	55.1±9.1	DQ	
0806−661	13.73	13.66	13.61	3	13.70	0.02	13.74	0.03	13.78	0.04	10753± 406	He	15.3±1.9	21.1±3.5	DQ	
0928−713	15.11	14.97	14.83	3	14.77	0.03	14.69	0.06	14.68	0.09	8836± 255	H	23.0±2.8	30.7±5.3	DA5.5	
1009−184	15.44	15.18	14.91	3	14.68	0.04	14.52	0.05	14.31	0.07	6449± 194	H	19.4±2.6	20.9±3.2	DZ	a
1036−204	16.24	15.54	15.34	3	14.63	0.03	14.35	0.04	14.04	0.07	4948± 70	He	15.6±3.0	16.2±2.5	DQ	b
1143−013	16.39	16.08	15.79	1	15.54	0.06	15.38	0.08	15.18	0.16	6824± 250	H	29.2±3.6	34.4±5.8	DA7.5	
1202−232	12.80	12.66	12.52	3	12.40	0.02	12.30	0.03	12.34	0.03	8623± 168	H	7.7±1.0	10.2±1.7	DA6.0	
1237−230	16.53	16.13	15.74	2	15.35	0.05	15.08	0.08	14.94	0.11	5841± 173	H	23.3±2.9	26.9±4.5	DA8.5	
1314−153	14.82	14.89	14.97	2	15.17	0.05	15.26	0.09	15.32	0.21	15604±2225	H	. . . ± · · ·	52.7±9.5	DA3.0	c
1315−781	16.16	15.73	15.35	2	14.89	0.04	14.67	0.08	14.58	0.12	5720± 162	H	19.2±2.3	21.6±3.6	DC	d
1339−340	16.43	16.00	15.56	2	15.00	0.04	14.75	0.06	14.65	0.10	5361± 138	H	18.7±2.4	21.2±3.5	DA9.5	
1418−088	15.39	15.21	15.01	2	14.76	0.04	14.73	0.06	14.76	0.10	7872± 243	H	22.5±2.8	28.5±4.8	DA6.5	
1447−190	15.80	15.59	15.32	2	15.06	0.04	14.87	0.07	14.78	0.11	7153± 235	H	23.2±3.0	29.1±4.9	DA7.0	
1607−250	15.19	15.12	15.09	2	15.08	0.08	15.08	0.08	15.22	0.15	10241± 457	H	29.1±3.8	41.2±7.2	DA5.0	
1756+143	16.30	16.12	15.69	1	14.93	0.04	14.66	0.06	14.66	0.08	5466± 151	H	18.7±5.1	22.4±3.4	DA9.0	e
1814+134	15.85	15.34	14.86	2	14.38	0.04	14.10	0.06	14.08	0.06	5313± 115	H	14.2±1.8	15.6±2.5	DA9.5	
2040−392	13.74	13.77	13.68	2	13.78	0.02	13.82	0.03	13.81	0.05	10811± 325	H	15.4±2.1	23.1±4.0	DA4.5	
2211−392	15.91	15.61	15.24	2	14.89	0.03	14.64	0.05	14.56	0.08	6243± 167	H	19.8±2.5	23.5±4.0	DA8.0	
2226−754A	16.57	15.93	15.33	2	14.66	0.04	14.66	0.06	14.44	0.08	4230± 104	H	15.7±2.4	12.8±2.0	DC	f
2226−754B	16.88	16.17	15.51	2	14.86	0.04	14.82	0.06	14.72	0.12	4177± 112	H	17.7±2.8	14.0±2.2	DC	f

NOTES.—"$Dist_{REL}$" refers to the distances estimated using the empirical relations while "$Dist_{SED}$" refers to the distances estimated using SED fitting.

a Identified as a DC/DQ WD by Henry et al. (2002). We obtained a blue spectrum that show Ca II H & K absorption and classify this object as a DZ.

b The SED fit to the photometry is marginal. This object displays deep Swan band absorption that significantly affects its measured magnitudes.

c Object is too blue for the empirical distance relations.

d Not listed in McCook & Sion (1999) but identified as a WD by Luyten (1949). Spectral type is derived from our spectrum.

e As of mid-2004, object has moved onto a background source. Photometry is probably contaminated, which is consistent with the poor SED fit for this object.

f Spectral type was determined using the spectrum published by Scholz et al. (2002b).

Chapter 8

Trigonometric Parallaxes for New and Known WDs

Trigonometric parallax measurements are the only direct geometrical determinations of stellar distances. The only underlying assumptions are that the Earth orbits the Sun and that we know Earth's position relative to the Sun accurately. Using current ground-based techniques, a star's distance can be measured out to $\sim$100 pc with a certainty of 10% or better, i.e., $\pi_{\mathrm{trig}} = 10 \pm 1$ mas (space-based missions such as *Hipparcos* have measured distances out to $\sim$200 pc with similar certainties). While a distance of 100 pc is miniscule relative to the size of the Galaxy and insignificant relative to the size of the Universe, there remain many secrets to uncover about our closest neighbors.

A precise distance determination is crucial to accurately model the physical parameters of WDs. Distance determinations constrain luminosities, which then constrain radii. If we assume the theoretical mass-radius relation for WDs is accurate, masses can be fairly well constrained. Thus, gravity can be determined directly for all WDs (not just DAs), instead of assuming a canonical value of $\log g = 8.0$. In addition, any unresolved double degenerates will present themselves unambiguously because they will appear overluminous by roughly a factor of two. Such systems provide empirical evidence for stellar evolution, in particular for close binary systems as they evolve off the main-sequence.

A complete volume-limited sample of WDs is extremely useful for statistical analyses, such as an estimate of the fraction of dark matter in our Galaxy made up of WDs. In addition, as discussed briefly in § 1.3.3, the nearest WDs are superb candidates to detect astrometric perturbations caused by orbiting planets. To date, no planets have been detected around WDs, but the likely explanation is that no one is looking. Not only do trigonometric parallaxes directly determine the distance, the same dataset can be used (usually over longer timescales) to detect long period "wobbles" caused by unseen companions if the astrometric signature is large enough. For a given system, the astrometric signature is inversely related to distance, thus the closer the WD, the larger the signal (all else being equal). As of the writing of this thesis, our CTIOPI data reduction pipeline only solves for the parallax and proper motion of an object. With reductions for more than 200 targets completed thus far, a few objects display probable perturbations that are witnessed in the residuals of the fit. In this chapter, I discuss trigonometric parallax measurements for 62 WDs targeted in this dissertation.

8.1 Parallax Observations

Parallax measurements are carried out as part of the CTIOPI program, a southern hemisphere parallax program that began in 1999 under the auspices of the NOAO Surveys Program and has continued since 2003 under the auspices of the SMARTS Consortium. Observations are carried out at the CTIO 0.9 m telescope and the

instrument setup is identical to that used for the photometry observations outlined in § 7.1. Briefly, the 2048×2046 Tektronix CCD camera was used with the Tek 2 $V_J R_{KC} I_{KC}$ filter set. To minimize off-axis optical distortions, only the central quarter of the chip was used, providing a 6.8′ square field of view. Bias frames and dome flats in each filter were typically taken prior to sunset each night.

Before long-term parallax observations begin, a suitable reference field and filter must be selected. In general, the reference field is selected so that ∼10 reference stars are distributed around the target star (hereafter referred to as the pi star). In a few cases when the field is sparse, the best possible number and distribution of reference stars is selected. The filter is selected so that the pi star and the reference field are sufficiently exposed. In the case of WDs, the R_{KC} is almost always selected because WDs are fairly colorless and the CCD is most sensitive in the R_{KC} band. In the case of late-type M dwarfs or brown dwarfs, the I_{KC} is selected because late-type stars are very red and emit little flux in the V_J band. An example setup field is shown in Figure 8.1.

Once the pointing and filter are selected, a rough exposure time (for a given quality of seeing) is noted as well as the pixel coordinates for the pi star. Finally, the brightest star (usually the pi star but in the case of faint WDs, a reference star) is labeled as the exposure setter to avoid saturation while observing under various atmospheric conditions.

08:21:26.70 -67:03:20.1

SCR0821-6703

Figure. 8.1: Setup field for a parallax target taken at the CTIO 0.9 m telescope. The pi star is labeled with two arrows and the reference stars are labeled with diagonal dashes.

During a night of observing, a pi star within 30 minutes (or up to 1 hour for faint targets) of the meridian is selected to minimize the effects of differential color refraction (DCR, discussed in § 8.2). The observer then points the telescope and applies an offset so that the pi star is within ∼5 pixels of the original setup pixel coordi-

nates. The exposure time is adjusted as needed, depending on seeing, atmospheric transparency, and how recently the mirror was cleaned, and a series of five to ten exposures are taken in sequence, ideally half east of the meridian and half west of the meridian. This process is repeated throughout the night so that 10 - 20 pi stars are observed each night. Since August 1999, CTIOPI has typically had one week a month to acquire data for the 427 pi stars (as of 08 May 2007) on the program.

8.2 Parallax Reductions

The reduction pipeline *redpi* was developed by Dr. Wei-Chun Jao and is described in Jao et al. (2005). Briefly, the IRAF task *ccdproc* is responsible for basic calibrations (i.e., bias subtraction, flat-fielding). The calibrated data are then stored in a directory specific to each pi star. Once enough data are available, a parallax reduction is performed (see § 8.3).

Optical $V_J R_{\mathrm{KC}} I_{\mathrm{KC}}$ photometry is necessary for each reference star as well as the pi star and serves two purposes, (1) to correct for the effect of DCR and, (2) to correct from relative to absolute parallax. Photometry reductions are identical to those discussed in § 7.2 and are completed prior to finalizing a parallax reduction.

First, an examination of each parallax frame is necessary to discard frames of poor quality. In a few cases, telescope guiding problems create a smear in the image and are not useful for high-precision astrometry. Another problem that has arisen involves a filter being positioned incorrectly in the filter wheel such that the images

were taken in the wrong filter (unbeknownst to the observer and not discovered until months or years later when a parallax reduction is performed). Once a subset of good quality images is collected, the reference field and pi star are individually tagged for centroiding. In practice, only one frame from each observing night needs to be tagged and those pixel coordinates are very similar to the rest of the frames taken that night during the same telescope pointing. Centroids for the reference field and pi stars are extracted using *SExtractor* (Bertin & Arnouts 1996).

Precise coordinates for the pi star are extracted from the 2MASS database (when available) and the position is proper motion adjusted from the epoch of observation to epoch 2000. At this point the centroids are corrected for DCR based on the color of each reference and pi star and a quality control of all the reference stars in each frame is performed.

Refraction occurs because light is bent when passing through the Earth's atmosphere. Differential refraction occurs because blue light is refracted more than red light. For a given filter bandpass, an A0 type star will appear to refract more than an M0 type star because it emits more blue light through a $V_J R_{KC} I_{KC}$ filter. The details of the DCR correction can be found in Jao et al. (2005) but typically this correction shifts the stars' positions by no more than a few mas.

Constraints on ellipticity, elongation, and full width at half maximum (FWHM) eliminate any star outside of these constraints. Ellipticity must be below 20%, elongation must be below 1.2, and FWHM must be below 2.5″. A suitable trail plate is

selected and must contain all of the reference and pi stars, have an hour angle (HA)

of observation less than 5 minutes, and have reasonably good seeing.

In the next phase of reduction, the trail plate is rotated so that the X-axis is due

east-west by comparison with the Guide Star Catalog 2.2 using the IRAF task *imwcs*.

The remainder of the image centroids are recalibrated to account for different scaling

in both the X and Y directions, as well as the different amounts of translation in

both directions. A least squares reduction via the Gaussfit program[1] is performed,

assuming the reference star grid has $\Sigma_i \Pi_i = 0$ and $\Sigma_i \mu_i = 0$. Parallaxes and proper

motions for the reference stars are calculated individually after the pi star reduction.

If a reference star is found to have a considerable parallax and/or proper motion, it is

removed from the final reduction. If a reference star is found to have abnormally high

residuals, because of photocentric contamination by a neighboring source or even a

bad column on the CCD, it is also removed from the final reduction. After a few

iterations to ensure the reference field is of good quality, the final reduction produces

a relative trigonometric parallax for the pi star.

Even the reference stars trace out small parallax ellipses because these stars are not

infinitely far away. Thus, a correction to absolute parallax must be performed. This is

accomplished in one of (at least) three different ways, (1) using statistical methods, (2)

spectroscopic parallaxes for each of the reference stars, or (3) photometric parallaxes

for each of the reference stars. Statistical methods rely on the apparent magnitude of

---

[1]Available from the *HST* Astrometry Team at *ftp://clyde.as.utexas.edu/pub/gaussfit/*.

the pi star and its Galactic coordinates. Assumptions are made about the Galactic component (i.e., disk, halo) membership of the reference stars based on their apparent magnitudes. In turn, an estimate of the distance provides an estimate of the sizes of the parallax ellipses of the reference stars, which can then be converted to an average ellipse size for the reference star set and added back into the pi star's ellipse size to give an absolute parallax. Using spectroscopic parallaxes to correct to absolute is probably the most reliable method because it removes any uncertainty about the luminosity classes of the reference field stars. However, a significant amount of observing time is necessary to obtain spectra for $\sim$10 reference stars around each of the 427 pi stars on CTIOPI. Therefore, photometric distances are used for CTIOPI targets to correct to absolute parallax under the assumption that all reference stars are single main-sequence stars so that the CCD distance relations of Henry et al. (2004) are applicable. Because the photometry is already available from the DCR correction, no further telescope time is necessary to make this modest (typically $\sim$1.5 mas) correction. Of course, contamination from evolved stars or unresolved double stars in the reference field, as well as reddening, has not been taken into account.

8.3 Parallax Results

A trigonometric parallax determination takes a significant amount of time. A fair assumption is that a parallax takes one integrated night spread over at least 2 years. WD targets for this project are currently at various stages of completion. The current criteria that define a definitive parallax are:

- the relative parallax error is less than 3 mas

- the target has been observed for at least 2 years

- there is a reasonable balance between images with positive and negative parallax factors (usually consisting of a minimum of 30 frames each)

- $V_J R_{KC} I_{KC}$ photometry has been obtained for the field (at least 2 independent observations)

A total of 62 WDs are on the CTIOPI program; including 10 known to be within 10 pc placed on the program as part of the Astrometric Search for Planets Encircling Nearby Stars (ASPENS) project. ASPENS is targeting all red dwarfs and WDs within 10 pc, south of declination $= 0°$, that are not enshrouded by a bright primary (a total of 54 systems). This study is aimed at detecting photocenter shifts induced by low mass companions orbiting around nearby stars. In many cases, the CTIOPI determined parallax is significantly better than previous measurements using photographic plates. Astrometric results for WDs on CTIOPI with enough data to obtain at least a preliminary parallax are found in Table 8.1.

In Table 8.1, I list all 62 WDs on CTIOPI as of 08 May 2007 even if no parallax reduction is yet possible. The samples are broken into five categories, definitive results, preliminary results, no results, ASPENS WDs, and companions to WDs whose parallaxes were measured by CTIOPI (for the sake of taking weighted means as prescribed in Appendix A). The filter used for the parallax determination is listed

in column 3. The number of seasons and the number of frames are listed in columns 4 and 5, respectively. In column 4, the appended 's' implies that the seasons have scattered observations (usually indicating two or fewer epochs per season) and the appended 'c' implies that the seasons have continuous observations (i.e., three or more epochs per season). The number of reference stars used is listed in column 7. The relative parallax and error is listed in column 8. Column 9 lists the correction to absolute parallax that has been applied to the relative parallax to give the absolute parallax and error listed in column 10. The proper motion and position angle is listed in columns 11 and 12, respectively. The tangential velocity, calculated from the absolute parallax when available, otherwise calculated from the relative parallax, is given in column 13.

As an external check for consistency, a sample of known nearby objects have been observed since 1999 and are now part of ASPENS. These objects have well-determined parallaxes via CTIOPI that can be compared to previous parallax determinations. Several comparisons are displayed in Jao et al. (2005); shown in Figure 8.2 are two exemplary objects for which the CTIOPI data coverage spans more than six years.

Table 8.1: Astrometric Results for WD Systems on CTIOPI

Name (1)	R.A. (J2000) (2)	Decl.	Filter (3)	N_{sea} (4)	N_{frm} (5)	Years (6)	N_{ref} (7)	π(rel) (mas) (8)	π(corr) (mas) (9)	π(abs) (mas) (10)	μ (arcsec yr^{-1}) (11)	θ (deg) (12)	V_{tan} (km s^{-1}) (13)	Notes (14)
							Definitive WD Parallaxes and Proper Motions							
0034−602	00 36 22.31	−59 55 27.5	R	3s	29	2.89	9	42.45 ± 1.80	1.12 ± 0.15	43.57 ± 1.81	0.2780 ± 0.0019	62.9 ± 0.75	30.2	
0121−429	01 24 03.98	−42 40 38.5	R	4s	53	3.06	6	54.37 ± 1.00	0.54 ± 0.03	54.91 ± 1.00	0.5936 ± 0.0009	150.9 ± 0.17	51.2	a
0141−675	01 43 00.98	−67 18 30.3	V	7c	142	6.05	8	101.41 ± 1.08	1.18 ± 0.08	102.59 ± 1.08	1.0761 ± 0.0006	198.9 ± 0.06	49.7	b
0150+256	01 52 51.93	+25 53 40.7	R	4s	35	2.67	11	29.94 ± 2.56	0.82 ± 0.06	30.76 ± 2.56	0.2162 ± 0.0027	76.9 ± 1.17	33.3	
0226−329	02 28 27.20	−32 42 33.9	R	4s	31	2.91	9	20.75 ± 1.81	1.00 ± 0.13	21.75 ± 1.81	0.2258 ± 0.0014	200.2 ± 0.68	49.2	
0628−020	06 30 38.60	−02 05 50.6	I	4s	58	2.66	7	42.51 ± 1.89	3.08 ± 0.30	45.59 ± 1.91	0.2087 ± 0.0028	213.0 ± 1.48	21.7	
0806−661	08 06 53.76	−66 18 16.6	R	4s	60	2.94	9	50.79 ± 1.69	1.63 ± 0.14	52.42 ± 1.70	0.4451 ± 0.0025	130.4 ± 0.64	40.2	
0821−669	08 21 26.70	−67 03 20.1	R	4c	76	3.83	10	93.15 ± 1.09	0.90 ± 0.07	94.05 ± 1.09	0.7634 ± 0.0009	329.5 ± 0.14	38.5	
0851−246	08 53 57.69	−24 46 56.0	I	5s	64	3.87	10	36.42 ± 0.83	1.05 ± 0.09	37.47 ± 0.83	0.6365 ± 0.0006	75.7 ± 0.09	80.5	c
0928−713	09 29 07.97	−71 33 58.8	R	4c	57	2.99	11	36.52 ± 1.01	1.91 ± 0.11	38.43 ± 1.02	0.4426 ± 0.0010	319.8 ± 0.26	54.6	
1009−184	10 12 01.88	−18 43 33.2	I	5s	70	4.91	10	53.57 ± 1.01	0.64 ± 0.05	54.21 ± 1.01	0.5144 ± 0.0006	269.0 ± 0.09	45.0	
1016−308	10 18 39.84	−31 08 02.0	R	4s	34	3.18	12	20.80 ± 1.64	0.84 ± 0.04	21.64 ± 1.64	0.1980 ± 0.0014	294.7 ± 0.79	43.4	
1202−232	12 05 26.66	−23 33 12.1	R	4s	66	3.07	8	91.07 ± 0.92	1.62 ± 0.12	92.69 ± 0.93	0.2457 ± 0.0010	16.3 ± 0.40	12.6	
1314−153	13 16 43.59	−15 35 58.3	V	5s	56	4.29	7	9.71 ± 1.86	0.79 ± 0.11	10.50 ± 1.86	0.6952 ± 0.0010	197.5 ± 0.13	313.8	d
1436−781	14 42 51.51	−78 23 53.6	R	4c	56	3.59	12	39.13 ± 0.82	0.76 ± 0.05	39.89 ± 0.82	0.4105 ± 0.0008	274.8 ± 0.18	48.8	
1814+134	18 17 06.48	+13 28 25.0	V	3s	60	2.38	10	75.17 ± 1.17	1.99 ± 0.14	77.16 ± 1.18	1.1940 ± 0.0015	201.9 ± 0.14	73.3	
2007−219	20 10 17.51	−21 46 45.6	V	7s	146	6.05	10	40.58 ± 0.94	0.73 ± 0.05	41.31 ± 0.94	0.3315 ± 0.0005	162.0 ± 0.16	38.0	e
2008−600	20 12 31.75	−59 56 51.5	V	4s	84	3.06	13	59.42 ± 0.86	1.00 ± 0.05	60.42 ± 0.86	1.4276 ± 0.0010	166.1 ± 0.07	112.0	f
2040−392	20 43 49.21	−39 03 18.0	R	4c	72	3.26	11	43.29 ± 0.98	1.02 ± 0.15	44.31 ± 0.98	0.3389 ± 0.0008	182.1 ± 0.19	36.3	
2226−754B	22 30 33.55	−75 15 24.2	V	5s	57	4.36	12	66.12 ± 1.31	0.32 ± 0.03	66.44 ± 1.31	1.8666 ± 0.0011	167.6 ± 0.16	133.2	
2226−754A	22 30 40.00	−75 15 55.3	V	5s	57	4.36	12	65.87 ± 1.29	0.32 ± 0.03	66.19 ± 1.29	1.8625 ± 0.0011	167.7 ± 0.06	133.4	
2351−335	23 54 01.14	−33 16 30.3	I	3c	67	2.30	5	36.91 ± 3.01	2.49 ± 0.11	39.40 ± 3.01	0.4982 ± 0.0036	220.2 ± 0.84	59.9	
							Preliminary WD Parallaxes and Proper Motions							
0222−291	02 24 32.18	−28 54 09.6	R	4c	29	3.01	8	21.84 ± 4.88	... ± ...	... ± ...	0.4823 ± 0.0040	92.7 ± 0.69	104.7	
0255−705	02 56 17.22	−70 22 10.8	R	3s	25	1.93	10	42.06 ± 2.54	0.92 ± 0.06	42.98 ± 2.54	0.6585 ± 0.0022	101.0 ± 0.33	72.6	
0311−649	03 12 25.69	−64 44 10.8	R	2s	19	1.03	9	30.20 ± 2.10	... ± ...	... ± ...	0.1735 ± 0.0033	102.0 ± 1.85	27.2	g
0419−487	04 21 05.56	−48 39 07.1	R	3s	54	3.21	7	47.56 ± 1.68	... ± ...	... ± ...	0.5370 ± 0.0016	178.2 ± 0.28	53.5	
0651−398A	06 53 35.34	−39 55 33.3	R	2s	18	0.93	13	39.88 ± 1.41	1.60 ± 0.11	41.48 ± 1.41	0.2414 ± 0.0048	342.6 ± 1.92	27.6	
0651−398B	06 53 30.21	−39 54 29.1	R	2s	18	0.93	13	39.72 ± 1.52	1.60 ± 0.11	41.32 ± 1.52	0.2373 ± 0.0052	343.1 ± 2.11	27.2	
0751−252	07 53 56.61	−25 24 01.5	R	3s	44	1.85	11	55.81 ± 0.88	0.53 ± 0.03	56.34 ± 0.88	0.3596 ± 0.0017	304.8 ± 0.54	30.3	
0816−310	08 18 40.26	−31 10 20.3	R	2s	19	0.98	8	54.68 ± 1.49	0.60 ± 0.03	55.28 ± 1.49	0.8194 ± 0.0034	163.4 ± 0.42	70.3	
1036−204	10 38 55.57	−20 40 56.7	R	4s	43	2.83	8	69.96 ± 0.78	... ± ...	... ± ...	0.6101 ± 0.0007	333.9 ± 0.13	41.3	
1105−340	11 07 47.89	−34 20 51.4	R	2s	30	0.96	8	42.42 ± 2.32	... ± ...	... ± ...	0.2613 ± 0.0035	170.8 ± 1.13	29.2	
1149−272	11 51 36.10	−27 32 21.0	R	3s	29	1.83	10	35.79 ± 1.44	1.60 ± 0.22	37.39 ± 1.46	0.2081 ± 0.0020	282.6 ± 0.98	26.4	
1223−659	12 26 42.02	−66 12 18.6	V	4s	37	2.95	11	65.05 ± 2.00	... ± ...	... ± ...	0.1842 ± 0.0018	186.5 ± 0.89	13.4	
1237−230	12 40 24.18	−23 17 43.8	R	4s	27	2.83	9	19.18 ± 2.45	... ± ...	... ± ...	1.0850 ± 0.0016	224.1 ± 0.17	268.1	g
1241−798	12 44 52.67	−80 09 27.8	V	5s	24	4.06	8	67.56 ± 4.09	3.36 ± 0.81	70.92 ± 4.17	0.5284 ± 0.0022	311.8 ± 0.47	35.3	
1242−105	12 44 52.70	−10 51 08.7	V	5s	26	3.64	8	24.03 ± 2.68	... ± ...	... ± ...	0.3427 ± 0.0017	258.7 ± 0.47	67.6	
1315−781	13 19 25.63	−78 23 28.3	R	3s	39	1.85	10	44.68 ± 4.66	1.36 ± 0.11	46.04 ± 4.66	0.4704 ± 0.0043	139.5 ± 1.04	48.4	g
1339−340	13 42 02.88	−34 15 19.4	R	2s	32	0.94	10	45.04 ± 1.11	1.26 ± 0.08	46.27 ± 1.11	2.5647 ± 0.0031	297.2 ± 0.13	262.7	g
1447−190	14 50 11.93	−19 14 08.7	R	3s	35	1.87	9	16.47 ± 1.75	... ± ...	... ± ...	0.2703 ± 0.0024	286.7 ± 0.92	77.8	
1647−327	16 50 44.32	−32 49 23.2	R	2c	33	1.17	9	31.51 ± 1.20	... ± ...	... ± ...	0.5077 ± 0.0027	192.9 ± 0.51	76.4	
2008−799	20 16 49.74	−79 45 53.0	R	3s	33	1.72	10	40.12 ± 2.31	0.74 ± 0.12	40.86 ± 2.31	0.4240 ± 0.0041	128.5 ± 1.11	49.2	
2035−369	20 38 41.42	−36 49 13.5	R	2s	30	1.72	9	26.62 ± 2.01	0.77 ± 0.07	27.39 ± 2.01	0.2159 ± 0.0029	105.4 ± 1.38	36.4	
2138−332	21 41 57.56	−33 00 29.8	V	2s	35	1.76	11	60.52 ± 1.67	... ± ...	... ± ...	0.2219 ± 0.0037	242.3 ± 1.82	17.4	
2211−392	22 14 34.75	−38 59 07.3	R	2s	21	1.03	9	50.35 ± 1.32	... ± ...	... ± ...	1.0786 ± 0.0033	110.6 ± 0.32	101.5	
2336−079	23 38 50.74	−07 41 19.9	R	4s	51	3.34	8	69.45 ± 2.23	... ± ...	... ± ...	0.0361 ± 0.0016	122.4 ± 4.82	2.5	h

Table. 8.1: continued

Name (1)	R.A. Decl. (J2000) (2)	Filter (3)	N_{sea} (4)	N_{frm} (5)	Years (6)	N_{ref} (7)	π(rel) (mas) (8)	π(corr) (mas) (9)	π(abs) (mas) (10)	μ (arcsec yr^{-1}) (11)	θ (deg) (12)	$V_{\tan}$ (km s^{-1}) (13)	Notes (14)
WDs on CTIOPI with no Parallax Reduction to Date													
0123−460.....	01 25 18.03 −45 45 31.1	R	...	...	...	...	... ± ...	... ± ...	... ± ...	... ± ...	... ± ...	...	
0708−670.....	07 08 52.28 −67 06 31.4	R	...	...	...	...	... ± ...	... ± ...	... ± ...	... ± ...	... ± ...	...	
0840−136.....	08 42 48.45 −13 47 13.1	R	...	...	...	...	... ± ...	... ± ...	... ± ...	... ± ...	... ± ...	...	
0856−007.....	08 59 12.91 −00 58 42.9	R	...	...	...	...	... ± ...	... ± ...	... ± ...	... ± ...	... ± ...	...	
1116−470.....	11 18 27.20 −47 21 57.0	R	...	...	...	...	... ± ...	... ± ...	... ± ...	... ± ...	... ± ...	...	
1916−362.....	19 20 02.83 −36 11 02.7	R	...	...	...	...	... ± ...	... ± ...	... ± ...	... ± ...	... ± ...	...	
2133−135.....	21 36 16.38 −13 18 34.5	R	...	...	...	...	... ± ...	... ± ...	... ± ...	... ± ...	... ± ...	...	
2216−657.....	22 19 48.32 −65 29 17.6	R	...	...	...	...	... ± ...	... ± ...	... ± ...	... ± ...	... ± ...	...	
Parallaxes and Proper Motions for ASPENS WDs													
2359−434.....	00 02 10.72 −43 09 55.5	R	4s	65	2.84	7	121.74 ± 1.36	... ± ...	... ± ...	0.8870 ± 0.0015	138.5 ± 0.19	34.5	i
0038−226.....	00 41 26.03 −22 21 02.3	R	8s	64	7.28	7	109.02 ± 1.37	1.24 ± 0.07	110.26 ± 1.37	0.6045 ± 0.0005	232.6 ± 0.09	26.0	j
0046+051.....	00 49 09.91 +05 23 19.1	R	...	...	...	...	... ± ...	... ± ...	... ± ...	... ± ...	... ± ...	...	
0435−088.....	04 37 47.41 −08 49 10.6	R	4s	62	3.23	6	105.10 ± 2.99	0.89 ± 0.20	105.99 ± 3.00	1.5738 ± 0.0015	172.0 ± 0.08	70.4	
0552−041.....	05 55 09.53 −04 10 07.1	I	4c	142	3.25	9	152.90 ± 0.86	... ± ...	... ± ...	2.3754 ± 0.0009	166.8 ± 0.03	73.6	
0738−172.....	07 40 20.78 −17 24 49.2	R	4c	90	3.14	11	108.72 ± 1.09	... ± ...	... ± ...	1.2610 ± 0.0009	116.5 ± 0.08	55.0	
0752−676.....	07 53 08.16 −67 47 31.5	R	4s	54	3.23	13	125.02 ± 1.57	... ± ...	... ± ...	2.0959 ± 0.0010	135.8 ± 0.06	79.5	k
0839−327.....	08 41 32.42 −32 56 32.8	V	4c	77	3.21	9	110.97 ± 2.41	... ± ...	... ± ...	1.7017 ± 0.0015	322.3 ± 0.10	72.7	
1142−645.....	11 45 42.93 −64 50 29.7	V	8s	165	7.01	10	215.50 ± 1.27	1.64 ± 0.19	217.14 ± 1.28	2.6928 ± 0.0005	97.4 ± 0.02	58.8	l
2251−070.....	22 53 53.35 −06 46 54.5	R	4s	65	3.11	9	115.38 ± 1.17	... ± ...	... ± ...	2.5709 ± 0.0009	105.6 ± 0.03	105.6	
Parallaxes and Proper Motions for CPM Companions to WDs													
LP 600−43.....	06 30 38.80 −02 05 54.0	I	4s	60	2.66	7	46.82 ± 1.45	3.08 ± 0.30	49.90 ± 1.48	0.1972 ± 0.0021	215.2 ± 1.21	18.7	
LHS 234.......	07 40 19.36 −17 24 46.0	I	4c	90	3.14	11	107.95 ± 1.09	... ± ...	... ± ...	1.2701 ± 0.0009	116.0 ± 0.08	55.8	
LHS 2067......	08 53 56.35 −24 46 56.5	I	5s	64	3.87	10	38.79 ± 0.75	1.05 ± 0.09	39.84 ± 0.76	0.6345 ± 0.0005	75.5 ± 0.08	75.5	
SCR 1107B.....	11 07 50.25 −34 21 00.6	R	2s	20	0.87	8	39.00 ± 2.40	... ± ...	... ± ...	0.2656 ± 0.0036	170.6 ± 1.15	32.3	
LHS 4039......	23 54 01.11 −33 16 22.7	I	3c	67	2.30	5	41.25 ± 1.99	2.49 ± 0.11	43.74 ± 1.99	0.5194 ± 0.0024	217.9 ± 0.52	56.3	

NOTE.—Units of right ascension are hours, minutes, and seconds, and units of declination are degrees, arcminutes, and arcseconds.

a. A new DA WD that is likely a double degenerate with a magnetic DA and a DC component.
b. Object shows hints of a perturbation in the RA residuals.
c. Object is underluminous and has a common proper motion metal-poor M-type subdwarf companion.
d. Object is overluminous and has the largest tangential velocity of the CTIOPI WD sample. Further modeling is necessary but it is possible that this object is a double degenerate halo candidate.
e. Object shows hints of a perturbation in both the RA and DEC residuals.
f. A new cool DC WD that exhibits CIA in the near-infrared based on the 2MASS magnitudes.
g. Object is overluminous and is suspected to be an unresolved double degenerate.
h. Known WD that has the slowest proper motion of any WD within 25 pc.
i. Parallax is significantly improved, previous trigonometric parallax error is 6.8 mas.
j. Parallax is significantly improved, previous trigonometric parallax error is 10.4 mas.
k. Parallax is significantly improved, previous trigonometric parallax error is 8.4 mas.
l. Parallax is significantly improved, previous trigonometric parallax error is 9.7 mas.

Figure. 8.2: Comparison plot of CTIOPI parallaxes with parallaxes measured from the ground (YPC = Yale Parallax Catalog) and space (HST = *Hubble Space Telescope*, HIP = *Hipparcos*). The units on the Y-axis are arcseconds.

Not all of the WDs on CTIOPI currently have photometry. However, there is a sizeable sample for which photometry does exist – via CTIOPI for newly discovered WDs or elsewhere in the literature for ASPENS WDs. Photometry coupled with parallax data enables the construction of a H-R diagram. Plotted in Figure 8.3 is a H-R diagram for 50 WD systems on CTIOPI (large open and filled circles), for which the error bars are smaller than the points. The large open circles that are labeled will be discussed in § 8.4.3. The small open circles represent 98 of the 109 systems previously known to be within 25 pc, for which error bars are generally larger but vary. Large uncertainties for known systems arise primarily from the trigonometric parallaxes and

Figure. 8.3: H-R diagram for CTIOPI WDs that have photometry, a total of 50, including ASPENS targets. CTIOPI parallaxes are grouped by those that are within 25 pc (*large filled circles*) and those that are beyond 25 pc (*large open circles*). For comparison, 98 of the 109 WDs previously known to be within 25 pc are plotted (*small open cirlces*). Labeled objects are discussed in the text.

will thus effect the absolute magnitude determinations (i.e., Y-axis) more significantly.

Eleven known systems are missing because no photometry is available (e.g. Sirius B, Procyon B).

8.3.1 Comparison of Distance Estimates with True Distances

As a check of the reliability of the two distance estimation techniques (empirical relations and SED fitting), a sample of 20 WDs with new trigonometric parallaxes was

Figure. 8.4: Comparison plots of WD distance estimation techniques vs. trigonometric parallaxes. (*a*) Comparison of the empirical relations distance estimates vs. those of the SED fitting technique. (*b*) Comparison of the empirical relations distance estimates vs. trigonometric parallax distances. (*c*) Comparison of the distance estimates via SED fitting vs. trigonometric parallax distances. Equal values are represented by the diagonal line in each plot. Filled circles represent absolute parallaxes and open circles represent relative parallaxes in plots *b* and *c*.

selected, excluding the elevated objects in Figure 8.3. First, the distance estimates obtained by using the empirical relations were compared to those obtained by SED fitting. As discussed in § 7.3.1, the empirical relations are problematic so we might expect some discrepancy in this comparison. This is indeed the case, and is illustrated

in Figure 8.4*a*. A similar trend is also witnessed when the distance estimates via the empirical relations are compared to trigonometric parallax distances (Figure 8.4*b*). Not so surprising, the distance estimates via SED fitting agree quite well with the trigonometric parallax distances (Figure 8.4*c*). The filled circles represent absolute parallax values while the open circles represent relative parallax values. Corrections to absolute will decrease the distances (by less than 1 pc) thereby sliding the open points on Figures 8.4*b* and 8.4*c* down slightly. Thus, the empirical relations serve a purpose in that they provide a reasonable first guess of a WD's distance but SED fitting provides greater confidence of a WD's proximity. One possibility that may strengthen the confidence in the empirical relations is to separate the DA WDs from the non-DA WDs and generate independent relations for the two samples. Spectral types are not always known and an all-encompassing approach was favored for this effort. Also, revised criteria are necessary to select a DA sample with trigonometric parallaxes so that enough stars will comprise the sample.

8.4 Discussion

8.4.1 Statistics

A breakdown of the status of WDs on the CTIOPI program is listed in Table 8.2. Thus far, CTIOPI has measured a trigonometric parallax for 38 WDs within 25 pc, including eight ASPENS WDs previously known to be within 25 pc. There remain

nine stars (seven new WDs, one known WD, and one ASPENS WD) that do not yet have enough data for a parallax reduction. These WDs have been added recently and are some of the most promising nearby candidates, as our selection process of parallax targets has been refined. One major change is that we have opted to measure a trigonometric parallax only for those WDs with distance estimates less than 20 pc to avoid targets with distance estimates near the 25 pc boundary.

Table. 8.2: Parallax Status for WDs on CTIOPI

Sample	Total	Definitive Parallax	Preliminary Parallax	No Parallax	d $\leq$ 25 pc
ASPENS.........	10	3	6	1	9
New WDs........	23	5	11	7	11
Known WDs.....	29	16	12	1	18
Total..........	62	24	29	9	38

Prior to this effort, there were 109 WD systems with trigonometric parallaxes within 25 pc albeit with varying uncertainties, one as large as 24.2 mas (see Appendix A). CTIOPI has measured parallaxes, for the first time, to 29 WD systems (excluding the nine ASPENS targets) within 25 pc, increasing the local WD population by 27%. It is entirely possible that this increase may climb to at least a full 1/3 of the nearby WD sample once enough data are available for the eight new WD systems not yet reduced. With the addition of accurate multi-epoch photometry, we are able to characterize the objects in this sample in a thorough, homogeneous way. In fact, given that the average error for a definitive CTIOPI parallax is ~1.4 mas (from Table 8.1), we may be able to constrain the physical parameters to unprecedented accuracy.

It is interesting to note that of the 109 WDs within 25 pc, there were at least 25 different parallax programs/missions that contributed to this sample. Of course, there is significant overlap between programs, especially for the nearest WDs that may have $\sim$10 independent parallax determinations each. The top five contributors are the US Naval Observatory (USNO, 82 WDs), *Hipparcos* (25 WDs), Lick Observatory (24 WDs), Sproul Observatory (21 WDs), and Yerkes Observatory (19 WDs). While the number of WD parallaxes via CTIOPI is dwarfed by the contributions from USNO, CTIOPI ranks as a decisive second with 38 WD parallaxes (thus far) and in only five years since the WD program began.

One motivation for this project was to evaluate whether the known local WD sample was biased towards large proper motions. In particular, all but one of the WDs in the 10 pc sample have $\mu \geq 1.0''$ yr^{-1} (see § 2.1.1). Curiously enough, the only WD that CTIOPI measured to be within 10 pc for the first time (WD 0141$-$675 at 9.75 $\pm$ 0.10 pc) also has $\mu > 1.0''$ yr^{-1}. The next two nearest WDs on CTIOPI are WD 0821$-$669 (10.63 $\pm$ 0.12 pc), with $\mu = 0.763''$ yr^{-1}, and WD 1202$-$232 (10.79 $\pm$ 0.11 pc) with $\mu = 0.246''$ yr^{-1}. In fact, WD 1202$-$232 is the second slowest moving WD at or within its distance. These results give rise to the notion that the 10 pc WD proper motion distribution is intrinsically skewed toward large proper motions (relative to the 10 pc M dwarf sample) rather than being a result of selection bias. Because these objects are nearby, the tangential velocities are not unusually large, so that halo membership does not offer a valid explanation. In fact, one is at a loss for a

good explanation other than perhaps that the small sample size (19 objects including WD 0141−675) prohibits drawing any significant conclusion from the proper motion distribution.

Table. 8.3: Distance Statistics for CTIOPI WDs

Proper Motion (yr^{-1})	$d \leq 10$ (pc)	$10 < d \leq 25$ (pc)	$d > 25$ (pc)
$\mu \geq 1.0''$...............	1	5	1
$1.0'' > \mu \geq 0.8''$........	0	1	0
$0.8'' > \mu \geq 0.6''$........	0	3	2
$0.6'' > \mu \geq 0.4''$........	0	9	4
$0.4'' > \mu \geq 0.2''$........	0	9	8
$0.2'' > \mu \geq 0.0''$........	0	1	0
Total...............	1	28	15

NOTE.—These statistics exclude the ASPENS WDs on CTIOPI.

This proper motion distribution trend is not nearly as evident in the larger 25 pc sample (see § 2.2.1). In fact, of the 29 WDs on CTIOPI that have distances within 25 pc (excluding ASPENS stars), twice as many objects are found with $\mu \leq 0.6''$ yr^{-1} (19) than with $\mu > 0.6''$ yr^{-1} (10, see Table 8.3). One object, WD 2336−079, has a miniscule proper motion ($\mu = 0.036''$ yr^{-1}) and has a preliminary parallax placing it only 14.40 ± 0.45 pc away. It is unlikely that this trend will cease if proper motions below $0.18''$ yr^{-1} are evaluated, hinting at the possibility of a sizeable sample of nearby WDs with low proper motions yet to be discovered.

Through further evaluations of the astrometric parameter spaces these new systems occupy, future WD hunts can better target nearby WDs. Figure 8.5 shows the distributions of proper motion, distance, and tangential velocity for the new and

Figure. 8.5: Histograms of astrometric properties of the new and known 25 pc WD samples. Plot (a) shows the proper motion distribution, binned by $0.5''$ yr^{-1}. Plot (b) shows the distance distribution, binned by 2 pc. Plot (c) shows the tangential velocity distribution, binned by 20 km s^{-1}. Shaded regions indicate the 29 new 25 pc WD systems as measured during this effort. White regions indicate the 109 known WD systems within 25 pc prior to this effort.

known samples. In all three plots, the new systems are represented by the shadad regions while the known systems are represented by the white regions.

As noted previously (though now in graphical form), it is clear that the majority of the new systems have slower proper motions (see Figure 8.5a), indicating that more

nearby WD systems are likely to be found with slow proper motions. Also, this effort has shown that there is no doubt that the 25 pc sample is incomplete. By evaluating the distributions of the new and known WD systems, as shown in Figure 8.5b, one may reliably conclude that most of the nearby WDs yet to be found are likely beyond 10 pc (though one or more WD discoveries within 10 pc is not beyond reason). Finally, a check of the tangential velocity distribution (Figure 8.5c) shows that most of the new WDs are of average WD velocities. However, there is one new system (WD 1339$-$340) that stands out above the rest with a $V_{\mathrm{tan}} = 262$ km s^{-1}. In fact, Lépine et al. (2005) show that this object's orbit is largely perpendicular to the Galactic plane indicating that it is likely a halo WD. Two WDs from the new sample that are beyond 25 pc (thus, not included in these plots) also have tangential velocities in excess of 200 km s^{-1} (WD 1237$-$230 and WD 1314$-$153). It is entirely possible that they, too, are halo WDs. More detailed analyses (i.e., age determinations) are necessary for confirmation but with the distances greatly constrained, modeling should provide conclusive evidence.

8.4.2 Possible Perturbations

As the time base of the parallax data lengthens, it is possible that these data, once the parallax and proper motion for an object have been fit and removed, will show periodic perturbations in the residuals. The advent of the ASPENS project mentioned earlier focuses on detecting these astrometric photocentric perturbations on

the nearest WDs although objects beyond 10 pc (the horizon of the ASPENS project) may also have substellar or planetary companions. In a few cases already, the parallax data show hints of a perturbation although no exhaustive analysis (i.e., fitting of orbital parameters) has yet been performed.

Figure. 8.6: Nightly mean plot of the residuals for WD 0141−675. Encircled points represent an epoch for which only one frame was taken and the adopted error corresponds to the mean error for epochs with multiple frames. The X-axis is the year of observation.

The first exemplary object that shows a marginal hint of a perturbation is WD 0141−675 for which the parallax data span 6.05 years. This object also happens to be the only WD without a previous trigonometric parallax measurement that was found

162

to be within 10 pc. As can be seen in Figure 8.6, the possible perturbation is only

visible in the nightly means of the RA residuals. It is a bit disconcerting that there

is no hint of a perturbation in the nightly means of the DEC residuals, and calls into

question whether this object is being perturbed.

Figure. 8.7: Nightly mean plot of the residuals of WD 2007−219. Encircled points
represent an epoch for which only one frame was taken and the adopted error corre-
sponds to the mean error for epochs with multiple frames. The X-axis is the year of
observation.

Another exemplary object that shows a more likely perturbation is WD 2007−219

for which parallax data, ironically, also spans 6.05 years. As can be seen in Figure 8.7,

the possible perturbation is visible in both RA and DEC residuals. Furthermore, the

residuals in both directions show similar periodicity. This is a promising candidate for a true perturbation that needs additional follow-up high resolution observations in hopes of resolving the probable pair.

Both of these targets remain on the CTIOPI program and as additional data are collected, a more definitive conclusion will be possible. It is interesting to note that these two objects happen to be the two longest observed WDs on CTIOPI (excluding ASPENS stars). Perhaps, as we collect more data over the next few years for many of the other WD targets, we will find other objects with similar trends. To date, no ASPENS targets shows signs of perturbations; however, the data span only four years or less.

8.4.3 Comments on Individual Systems

With the wealth of data available, including spectroscopy, photometry, and astrometry, the WDs on CTIOPI can be reliably modeled. Upon doing so, a few objects stand out and require additional disscussion. Here we address exceptional objects.

WD 0121−429: A new DA WD that was discovered during the Phase One spectroscopy effort and was found to have Zeeman splitting of the Hα and Hβ absorption lines (the rest of the Balmer lines are not discernable), thereby making its formal classification a DAH. The SED fit to the photometry is superb, yielding a $T_{\rm eff}$ of 6369 $\pm$ 137 K. When we compare the strength of the absorption line trio with that predicted using the $T_{\rm eff}$ from the SED fit, the depth of the absorption appears too shallow. Using the magnetic line fitting procedure outlined in Bergeron et al. (1992a) we must

include a 50% dilution factor to match the observed central line of Hα. Using the trigonometric parallax as a constraint on the luminosity, the SED fit implies a mass of 0.43 ± 0.03 M$_\odot$. Given the age of our Galaxy, the lowest mass WD that could have formed is ~0.47 M$_\odot$ (Iben & Renzini 1984). It is extremely unlikely that this WD formed through single-star evolution. The most likely scenario is that this is a double degenerate binary with a magnetic DA component and a featureless DC component (necessary to dilute the absorption at Hα), similar to G62-46 (Bergeron et al. 1993) and LHS 2273 (see Figure 33 of Bergeron et al. 1997). If this interpretation is correct, any number of component masses and luminosities can reproduce the SED fit.

The spectrum and corresponding magnetic fit to the Hα lines (including the dilution) are shown in Figure 8.8. The viewing angle, $i = 65°$, is defined as the angle between the dipole axis and the line of sight ($i = 0$ corresponds to a pole-on view). The best fit produces a dipole field strength, $B_d = 9.5$ MG, and a dipole offset, $a_z = 0.06$ (in units of stellar radius). The positive value of a_z implies that the offset is *toward* the observer. Only B_d is moderately constrained; both i and a_z can vary significantly yet still produce a reasonable fit to the data (Bergeron et al. 1992a).

WD 0141−675: A known DA WD that is the nearest of the WDs whose parallaxes were measured for the first time and the only one found within 10 pc (9.75 ± 0.10 pc). In addition, this object shows a hint of a perturbation in the residuals of the parallax reduction (see § 8.4.2). Aquisition of parallax data is ongoing in hopes of confirming a perturbation.

Figure. 8.8: Spectral plot of WD 0121−429. The inset plot displays the spectrum (*thin line*) in the Hα region to which a magnetic fit (*thick line*), as outlined in Bergeron et al. (1992a), was performed using the T_{eff} obtained from the SED fit to the photometry. The resulting magnetic parameters are listed below the fit.

WD 0310−624: A new DA WD (spectrum plotted in Figure 6.2) that is one of the hottest new WD discoveries. Because of its elevation significantly above the equal temperature line in Figure 7.4 (*solid line*), it is possible that it is an unresolved double degenerate with very different component effective temperatures. If double, the spectral fit to the Balmer lines will be more heavily influenced by the more luminous component because its spectral features will dominate. The SED fit to the broadband photometry tends to arrive at an intermediate temperature to those of

the components. When the two estimates of $T_{\rm eff}$ are compared, the spectroscopic value is larger than the photometric value beyond the formal uncertainties. In fact, this method has been used to identify unresolved double degenerate candidates (i.e., Bergeron et al. 2001).

WD 0311−649: A new DA WD (spectrum plotted in Figure 6.8) that is over-luminous based on its absolute magnitude and color (see Figure 8.3). This object is likely an unresolved double degenerate with the second WD being responsible for the apparent overluminosity.

WD 0511−415: A new DA WD (spectrum plotted in Figure 6.2) whose spectral fit produces a $T_{\rm eff} = 10{,}813 \pm 219$ K and a log $g = 8.21 \pm 0.10$ using the spectral fitting procedure of Liebert et al. (2003). This object lies near the red edge of the ZZ Ceti instability strip as defined by Gianninas et al. (2006). If variable, this object would help to constrain the cool edge of the instability strip in $T_{\rm eff}$, log g parameter space. Follow-up high-speed photometry is necessary to confirm variability.

WD 0622−329: A new DAB WD that displays Balmer absorption as well as weaker He I at 4472 and 5876 Å. The spectrum (shown in top plot of Figure 6.5) is reproduced best with a spectral fitting model having $T_{\rm eff} \sim 43{,}700$ K. However, the predicted, relatively strong, He II absorption line at 4686 Å for a WD of this $T_{\rm eff}$ is not present in the spectrum. In contrast, the SED fit to the photometry implies a $T_{\rm eff}$ of ∼10,500 K (using either pure H or pure He models). Because the $T_{\rm eff}$ values are vastly discrepant, we explore the possibility that this spectrum is not characterized

Figure. 8.9: Spectral plot of WD 0622−329. The inset plot displays the spectrum (*thin line*) in the region to which the model (*thick line*) was fit, assuming the spectrum is a convolution of a DB component and a slightly cooler DA component. Best-fit physical parameters are listed below the fit for each component.

by a single temperature. We model the spectrum assuming that the object is an unresolved double degenerate. The best fit implies that one component is a DB with $T_{\rm eff} = 14{,}170 \pm 1228$ K and the other component is a DA with $T_{\rm eff} = 9640 \pm 303$ K, similar to the unresolved DA+DB degenerate binary PG 1115+166 analyzed by Bergeron & Liebert (2002). One can see from Figure 8.9 that the spectrum is well modeled under this assumption. We conclude that this object is likely a distant (well beyond 25 pc, hence not on the CTIOPI program) unresolved double degenerate.

WD 0821−668: A new DA WD (spectrum plotted in Figure 6.3) that is the nearest (10.63 ± 0.12 pc) of the 56 new WDs discovered in this effort. Acquisition of parallax data is ongoing to search for unseen companions (even though it is beyond the 10 pc ASPENS horizon).

WD 0840−136: A new DZ WD (spectrum plotted in top panel of Figure 6.6) whose spectrum shows both Ca II (H and K) and Ca I lines. Fits to the photometric data for different atmospheric compositions indicate temperatures of 4800–5000 K. However, fits to the optical spectrum using models of Dufour et al. (2007) cannot simultaneously reproduce all three calcium lines. This problem is similar to that encountered by Dufour et al. (2007), where the atmospheric parameters for the coolest DZ WDs were considered uncertain because of possible high atmospheric pressure effects. A trigonometric parallax via CTIOPI is underway for this object to further constrain its physical parameters.

WD 0851−246: A known DC WD that is underluminous based on its absolute magnitude and color (see Figure 8.3). This object has a common proper motion companion that is a mildly metal-deficient M subdwarf (Jao et al. 2007, in preparation). Systems such as these are rare yet useful for constraining the age of the subdwarf by modeling the WD (e.g., Monteiro et al. 2006). In addition, the WD component is likely very massive thereby making its radius smaller and its luminosity less than a normal WD at that temperature. Detailed modeling is necessary to further unravel the mysteries of this system.

WD 1054−226: Observed spectroscopically as part of the Edinburgh-Cape (EC) blue-object survey and assigned a spectral type of sdB+ (Kilkenny et al. 1997). As is evident in Figure 6.3, the spectrum of this object is one of the noisiest spectra of new WD discoveries and perhaps a bit ambiguous. As an additional check, this object was recently observed by using the ESO 3.6 m telescope and has been confirmed to be a WD. Furthermore, in addition to the Balmer absorption lines, faint absorption due to Ca II (H and K) is evident, thereby making its formal classification DAZ (P. Bergeron, private communication). Possible scenarios that enrich the atmospheres of DAZs include accretion via (1) debris disks, (2) ISM, and (3) cometary impacts (see Kilic et al. 2006, and references therein). The 2MASS K_S magnitude is near the faint limit and is unreliable, but even considering the J and H magnitudes, there appears to be no appreciable near-infrared excess. While this may tentatively rule out the possibility of a hot debris disk, this object would be an excellent candidate for far-infrared spaced-based studies to ascertain the origin of the enrichment.

WD 1149−272: The only DQ WD discovered during this effort. This object was observed spectroscopically as part of the EC blue-object survey for which no features deeper than 5% were detected and was labeled a possible DC (Kilkenny et al. 1997). It is identified as having weak C_2 Swan-band absorption at 4737 Å and 5165 Å and is otherwise featureless. The DQ model reproduces the spectrum reliably and is overplotted in Figure 8.10. This object is characterized as having $T_{\text{eff}} = 6188 \pm 194$ K and log (C/He) $= -7.20 \pm 0.16$. Comparisons with other DQ WDs modeled
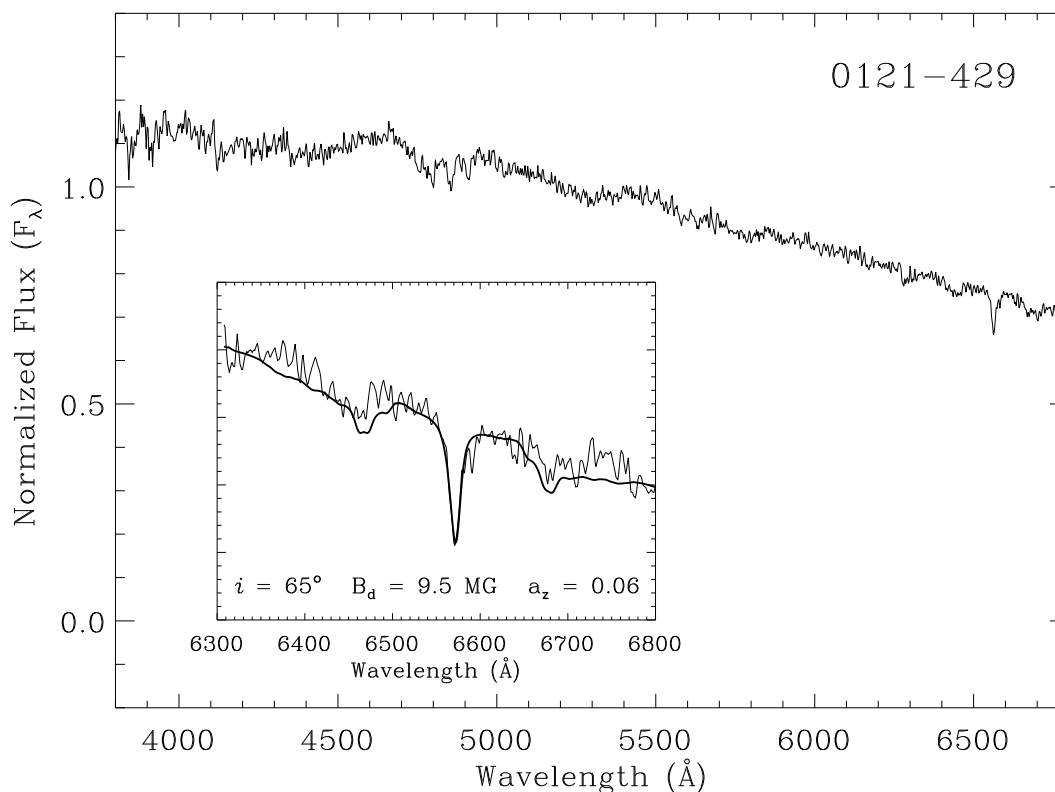
Figure. 8.10: Spectral plot of WD 1149−272. The inset plot displays the spectrum (*thin line*) in the region to which the model (*thick line*) was fit.

in an identical fashion show that this object is one of the coolest and least carbon abundant known (see Figure 12 of Dufour et al. 2005).

WD 1237−230: A known DA WD that is overluminous based on its absolute magnitude and color (see Figure 8.3). This object is likely an unresolved double degenerate where the second WD contributes to the total luminosity and causes an apparent overluminosity.

WD 1242−105: A known DA WD that is overluminous based on its absolute magnitude and color (see Figure 8.3). This object is likely an unresolved double

degenerate where the second WD contributes to the total luminosity and causes an apparent overluminosity.

WD 1314−153: A known DA WD that is overluminous based on its absolute magnitude and color (see Figure 8.3). This object is likely an unresolved double degenerate where the second WD contributes to the total luminosity and causes an apparent overluminosity. In addition, this object has the largest tangential velocity of all objects evaluated in this effort. It is possible, though not probable without additional modeling, that this is a double degenerate halo WD system.

WD 1447−190: A known DA WD that is overluminous based on its absolute magnitude and color (see Figure 8.3). This object is likely an unresolved double degenerate where the second WD contributes to the total luminosity and causes an apparent overluminosity.

WD 2007−219: A known DA WD that has been on the parallax program for ∼6 years. The residuals of the parallax reduction show hints of a perturbation in both axes. Acquisition of parallax data is ongoing in hopes of confirming a perturbation.

WD 2008−600: A new DC WD (spectrum plotted in Figure 6.4) that is flux-deficient in the near-infrared, as indicated by the 2MASS magnitudes. The SED fit to the photometry is a poor match to both the pure hydrogen and pure helium models. A pure hydrogen model provides a slightly better match than a pure helium model and yields a T_{eff} of ∼3100 K, thereby placing it in the relatively small sample of ultracool WDs. However, by using the trigonometric parallax as a constraint, we are able to

Figure. 8.11: SED plot of WD 2008−600 with the luminosity constrained by the trigonometric parallax. Best-fit physical parameters are listed below the fit. Circles represent fit values; error bars are derived from the uncertainties in the magnitudes and the parallax.

discern its true nature. This object is best modeled as having mostly helium with trace amounts of hydrogen [log (He/H) =2.61] in its atmosphere and has a $T_{\text{eff}} = 5078 \pm 221$ K (see Figure 8.11). A mixed hydrogen and helium composition is required to produce sufficient absorption in the infrared as a result of the CIA by molecular hydrogen due to collisions with helium. Such mixed atmospheric compositions have also been invoked to explain the infrared flux deficiency in LHS 1126 (Bergeron et al. 1994), as well as SDSS 1337+00 and LHS 3250 (Bergeron & Leggett 2002). While WD 2008−600 is likely *not* an ultracool WD, it is one of the brightest and nearest
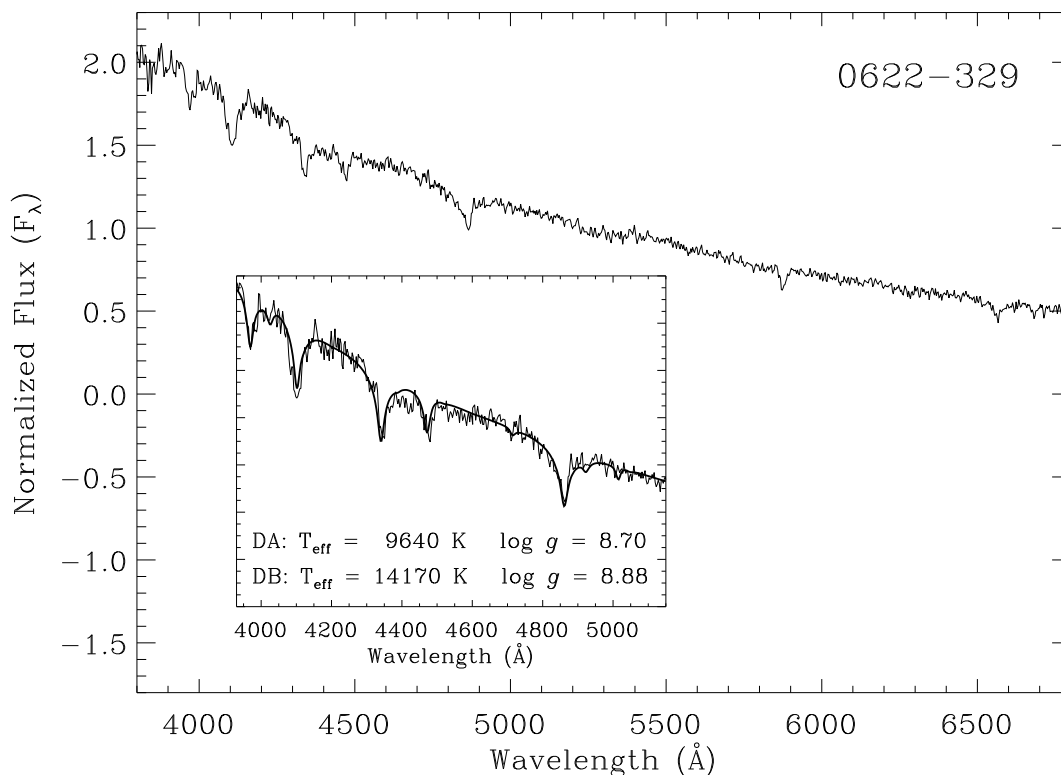
Figure. 8.12: Spectral plot of WD 2138−332. The inset plot displays the spectrum (*thin line*) in the region to which the model (*thick line*) was fit.

cool WDs known. Because the 2MASS magnitudes are not very reliable, it would be useful to obtain additional near-infrared photometry.

WD 2138−332: A new DZ WD for which a calcium-rich model reproduces the spectrum reliably. The spectrum and the overplotted fit are shown in Figure 8.12. The divergence of the spectrum from the fit toward the red end is likely due to an imperfect flux calibration of the spectrum. This object is characterized as having $T_{\text{eff}} = 7188 \pm 291$ K and $\log (\text{Ca/He}) = -8.64 \pm 0.16$. The metallicity ratios are, at first, assumed to be solar (as defined by Grevesse & Sauval 1998), and in this case

the quality of the fit is sufficient without deviation. The corresponding log (Mg/He) $= -7.42 \pm 0.16$ and log (Fe/He) $= -7.50 \pm 0.16$ for this object.

WD 2157−574: A new DA WD (spectrum plotted in Figure 6.3) that displays weak Ca II (H and K) absorption, thereby making its formal classification DAZ. Similar to WD 1054−226, this object would also be an excellent candidate for far-infrared space-based studies so that we can constrain which enrichment mechanism gives rise to these spectral signatures.

Chapter 9

Conclusions

This effort has utilized a broad range of observational techniques. First, plate astrometry of the entire southern sky was sifted to find a total of 299 new HPM systems with $\mu \geq 0.4''$ yr^{-1} as well as seven new companions to known systems. Second, low resolution spectroscopy identified 56 new WD systems gleaned from proper motion data, mainly from our own SCR proper motion survey. Third, optical $V_J R_{KC} I_{KC}$ photometry was obtained at the telescope and near-infrared photometry was extracted from the 2MASS database to accurately model effective temperatures and estimate distances. Lastly, high-precision CCD astrometry has been used to measure trigonometric parallaxes for 53 WD systems (both new and known) thus far with an additional nine systems (for a total of 62 WD systems on CTIOPI) not yet having enough data for parallax determinations. Of these 53 WD systems with parallax determinations, 29 have been measured for the first time to be within 25 pc – a volume that previously contained only 109 WDs with trigonometric parallaxes thus increasing this sample by 27%.

The work presented in this dissertation has converged on several groundbreaking conclusions. First, it appears that the proper motion distribution for the 10 pc WDs is not biased against slower proper motions in any significant way. It is likely that no significant conclusion can be drawn from this distribution because of the small sample size (19 objects).

Figure. 9.1: Missing WDs within 25 pc after CTIOPI WDs are included. The red curve is the expected number density assuming all WDs within 10 pc are known and the density is constant. Dark blue filled circles represent previously measured WD parallaxes within 25 pc. Open light blue circles represent the new CTIOPI WD parallaxes presented here. The solid vertical black lines represent 10 pc and 13 pc (left to right). The dashed vertical black line represents the 25 pc horizon.

Second, the local WD population is significantly incomplete. Other authors (e.g., Holberg et al. 2002) have argued that all WDs out to 13 pc are known and thus the sample is complete. We have already found four WDs within this volume. To the authors' credit, they utilize both trigonometric parallax distances and photometric distance estimates so that they included one of the four (WD 0141−675) in their statistics. However, that leaves three within this volume that were not accounted for and all three are recent discoveries. It is likely that there will be many more new nearby WD discoveries and perhaps a few will fall within this volume. Using only trigonometric parallax distances for WDs within 13 pc, we find a local WD density of 4.4×10^{-3} pc^{-3}, a slightly lower value than that determined by Holberg et al. (2002) of 5.0×10^{-3} pc^{-3}. The discrepancy arises because a few of the objects that Holberg et al. (2002) included in the statistics were later shown not to be WDs but rather F type dwarfs (Kawka et al. 2004). In addition, a few objects whose photometric distances place them within 13 pc were lost when a trigonometric parallax determined they were further away. An updated diagram, similar to Figure 2.6 but now including CTIOPI WDs within 25 pc, is shown in Figure 9.1. Notice how the majority of CTIOPI parallaxes are found beyond 13 pc. However, it seems there is a "kink" in the density curve between 10 pc and 13 pc, indicating that the 13 pc sample may still be incomplete. Thus, the density derived previously is only a lower limit and may increase.

Third, the statistical analyses for proper motion objects from the SCR survey (see § 5.4) as well as the CTIOPI WD sample (see § 8.4.1) indicate that roughly twice as many nearby objects are found with $\mu < 0.6'' \ \mathrm{yr}^{-1}$ than with $\mu \geq 0.6'' \ \mathrm{yr}^{-1}$. There are likely several nearby gems with low proper motions (or none at all) that await discovery. With the amount of time (and money) necessary to obtain a ground-based parallax, a magnitude-limited astrometry initiative, such as the European Space Agency's (ESA) space-based mission *GAIA* or future ground-based efforts such as LSST and Pan-STARRS, will probably be the first to "pluck" these gems from the sky.

9.1 Future Work

The scientific pursuit of answers usually raises as many new questions in the process. Such is the case with this project. Upon reaching the conclusions discussed previously, we find interesting aspects that we had not anticipated. Many of the surprises came about because of the parallax data. Five CTIOPI WDs appear overluminous when plotted in an H-R diagram. Three additional WDs are likely double degenerates based on spectroscopic and/or photometric data. Another two WDs show hints of perturbations in the residuals.

All of these objects are candidates for providing insight into binary evolution. If they can be resolved using high-resolution astrometric techniques (i.e., speckle,

adaptive optics, or interferometry via the *HST*'s FGS), they may provide astrometric masses, which are fundamental calibrators for stellar structure theory and for the reliability of the theoretical WD mass-radius and initial-to-final-mass relationships. To date, only four WD astrometric masses are known to better than $\sim5\%$ (Provencal et al. 1998).

In 2007, we were awarded 16 orbits to use *HST*'s FGS over the next two cycles (years) so that we can resolve WD binaries. The resolution limit of FGS is ~10 mas. Thus far, we have observed four targets, (1) WD 0121$-$429 (magnetic WD with shallow absorption features), (2) WD 1202$-$232 (one of the nearest WDs measured by CTIOPI), (3) WD 2007$-$219 (WD that shows perturbations along both axes of the parallax residuals), and (4) WD 2040$-$392 (WD that appeared overluminous based on a very preliminary parallax). Only WD 0121$-$429 appeared to be mildly resolved but there is a question as to whether the detection is real or an artifact of the FGS. Another orbit is scheduled to observe this object and relinquish any doubt. The remaining orbits have been assigned to four of the five objects that appear overluminous in Figure 8.3, WD 0141$-$675 (the closest WD measured by CTIOPI and also shows a possible perturbation in the parallax residuals), and another WD suspected to be overluminous by other researchers. I plan to work closely with Co-Investigator Ed Nelan of the Space Telescope Science Institute (STScI) to reduce the remaining data in hopes of resolving as many as possible to obtain astrometric masses.

FGS is especially suited to resolve double degenerates because the wavelength range of observation is in the blue end of the visible spectrum, where WDs often have significant flux. Binary evolution predicts that a close binary will actually undergo orbital degradation as the components leave the main-sequence and undergo a common envelope phase. The result is a miniscule separation and orbital periods no more than a few days. If any of the overluminous WDs are not resolved, it is likely that this is the cause. For these objects, we intend to obtain high-dispersion radial velocity measurements in hopes of mapping the orbits and constraining the component masses.

In a few cases, especially those for which a perturbation exists in the parallax residuals, FGS may not be the best instrument to resolve the system. If a perturbation is seen, the two objects cannot be of equal magnitude otherwise there would be no photocentric shift and hence no detected perturbation. Only if the two objects have significantly different luminosities (i.e., a WD and a brown dwarf) will a perturbation be seen. As mentioned, FGS observes in the blue end of the visible spectrum, where substellar companions shine feebly. Because of the magnitude limit of FGS ($V_J \sim$ 17), brown dwarfs would never be seen even if the separations are well beyond the resolution limit. In these cases, we intend to use adaptive optics in the near-infrared. Resolution limits are $\sim$100 mas with adaptive optics, but if the perturbations are real and the periods are on the order of years, these systems should be resolvable.

On to a completely different topic, I would like to extend the same approach of identifying new nearby WDs to the northern hemisphere. While the argument was made and supported in Chapter 2 that the northern hemisphere is better sampled than the southern hemisphere in terms of proper motion, the dearth of WDs within 10 pc north of declination $= +10°$ (only two) is surprising. The exact same methodology presented here (i.e., RPM) can be applied to the northern hemisphere, in particular, to the highly complete dataset of proper motions compiled by Lépine & Shara (2005). What is critical is a dedicated large-scale parallax survey in the northern hemisphere (e.g., the USNO parallax program) focusing on WDs to confirm proximity. Perhaps some involvement in a northern hemisphere parallax program is in my future.

References

Adams, W. S. 1914, PASP, 26, 198

— 1915, PASP, 27, 236

— 1925, Proceedings of the National Academy of Science, 11, 382

Alcock, C., Allsman, R. A., Alves, D. R., Axelrod, T. S., Becker, A. C., Bennett, D. P., Cook, K. H., Dalal, N., Drake, A. J., Freeman, K. C., Geha, M., Griest, K., Lehner, M. J., Marshall, S. L., Minniti, D., Nelson, C. A., Peterson, B. A., Popowski, P., Pratt, M. R., Quinn, P. J., Stubbs, C. W., Sutherland, W., Tomaney, A. B., Vandehei, T., & Welch, D. 2000, ApJ, 542, 281

Anonymous 1877, MNRAS, 37, 193

Auwers, A. 1862, MNRAS, 22, 150

— 1864, MNRAS, 25, 38

— 1873, MNRAS, 34, 25

Bakos, G. Á., Sahu, K. C., & Németh, P. 2002, ApJS, 141, 187

Bergeron, P., & Leggett, S. K. 2002, ApJ, 580, 1070

Bergeron, P., Leggett, S. K., & Ruiz, M. T. 2001, ApJS, 133, 413

Bergeron, P., & Liebert, J. 2002, ApJ, 566, 1091

Bergeron, P., Ruiz, M. T., Hamuy, M., Leggett, S. K., Currie, M. J., Lajoie, C.-P., & Dufour, P. 2005, ApJ, 625, 838

Bergeron, P., Ruiz, M.-T., & Leggett, S. K. 1992a, ApJ, 400, 315

— 1993, ApJ, 407, 733

Bergeron, P., Ruiz, M. T., & Leggett, S. K. 1997, ApJS, 108, 339

Bergeron, P., Ruiz, M.-T., Leggett, S. K., Saumon, D., & Wesemael, F. 1994, ApJ, 423, 456

Bergeron, P., Saffer, R. A., & Liebert, J. 1992b, ApJ, 394, 228

Bertin, E., & Arnouts, S. 1996, A&AS, 117, 393

Bessel, F. W. 1844, MNRAS, 6, 136

Bessel, M. S. 1990, A&AS, 83, 357

Biller, B. A., Kasper, M., Close, L. M., Brandner, W., & Kellner, S. 2006, ApJ, 641, L141

Binney, J., & Merrifield, M. 1998, Galactic astronomy (Princeton, NJ : Princeton University Press)

Burnham, S. W. 1893, MNRAS, 53, 48

Carney, B. W., & Latham, D. W. 1987, AJ, 93, 116

Carpenter, J. M. 2001, AJ, 121, 2851

Dahn, C. C., Harrington, R. S., Riepe, B. Y., Christy, J. W., Guetter, H. H., Kallarakal, V. V., Miranian, M., Walker, R. L., Vrba, F. J., Hewitt, A. V., Durham, W. S., & Ables, H. D. 1982, AJ, 87, 419

Deacon, N. R., & Hambly, N. C. 2007, A&A, 468, 163

Deacon, N. R., Hambly, N. C., & Cooke, J. A. 2005a, A&A, 435, 363

Deacon, N. R., Hambly, N. C., Henry, T. J., Subasavage, J. P., Brown, M. A., & Jao, W.-C. 2005b, AJ, 129, 409

Dufour, P., Bergeron, P., & Fontaine, G. 2005, ApJ, 627, 404

Dufour, P., Bergeron, P., Liebert, J., Harris, H. C., Knapp, G. R., Hall, P. B., Strauss, M. A., Collinge, M. J., & Edwards, M. C. 2007, ArXiv Astrophysics e-prints. `astro-ph/0703758`

Eddington, A. S. 1924, MNRAS, 84, 308

— 1926, The Internal Constitution of the Stars (Cambridge: Cambridge University Press)

Evans, D. W., & Irwin, M. 1995, MNRAS, 277, 820

Filippenko, A. V. 1982, PASP, 94, 715

Finch, C. T., Henry, T. J., Subasavage, J. P., Jao, W.-C., & Hambly, N. C. 2007, AJ, 133, 2898

Fontaine, G., Brassard, P., & Bergeron, P. 2001, PASP, 113, 409

Fowler, R. H. 1926, MNRAS, 87, 114

Gianninas, A., Bergeron, P., & Fontaine, G. 2006, AJ, 132, 831

Giclas, H. L., Burnham, R., & Thomas, N. G. 1971, Lowell proper motion survey Northern Hemisphere. The G numbered stars. 8991 stars fainter than magnitude 8 with motions > 0".26/year (Flagstaff, Arizona: Lowell Observatory)

Giclas, H. L., Burnham, R., Jr., & Thomas, N. G. 1978, Lowell Observatory Bulletin, 8, 89

Gilmore, G., & Reid, N. 1983, MNRAS, 202, 1025

Gliese, W., & Jahreiß, H. 1991, On: The Astronomical Data Center CD-ROM: Selected Astronomical Catalogs, Vol. I; L.E. Brotzmann, S.E. Gesser (eds.), NASA/Astronomical Data Center, Goddard Space Flight Center, Greenbelt, MD, Tech. rep.

Gould, A., & Chanamé, J. 2004, ApJS, 150, 455

Graham, J. A. 1982, PASP, 94, 244

Green, R. F. 1976, PASP, 88, 665

Green, R. F., Schmidt, M., & Liebert, J. 1986, ApJS, 61, 305

Greenstein, J. L., Oke, J. B., & Shipman, H. L. 1971, ApJ, 169, 563

Grevesse, N., & Sauval, A. J. 1998, Space Science Reviews, 85, 161

Hambaryan, V., Staude, A., Schwope, A. D., Scholz, R.-D., Kimeswenger, S., & Neuhäuser, R. 2004, A&A, 415, 265

Hambly, N. C., Davenhall, A. C., Irwin, M. J., & MacGillivray, H. T. 2001a, MNRAS, 326, 1315

Hambly, N. C., Henry, T. J., Subasavage, J. P., Brown, M. A., & Jao, W.-C. 2004, AJ, 128, 437

Hambly, N. C., Irwin, M. J., & MacGillivray, H. T. 2001b, MNRAS, 326, 1295

Hambly, N. C., MacGillivray, H. T., Read, M. A., Tritton, S. B., Thomson, E. B., Kelly, B. D., Morgan, D. H., Smith, R. E., Driver, S. P., Williamson, J., Parker, Q. A., Hawkins, M. R. S., Williams, P. M., & Lawrence, A. 2001c, MNRAS, 326,

1279

Hansen, B. M. S. 2003, ApJ, 582, 915

Hansen, B. M. S., Anderson, J., Brewer, J., Dotter, A., Fahlman, G. G., Hurley, J., King, I., Reitzel, D., Richer, H. B., Rich, R. M., Shara, M. M., & Stetson, P. B. 2007, ArXiv Astrophysics e-prints. `astro-ph/0701738`

Harris, H. C., Dahn, C. C., Vrba, F. J., Henden, A. A., Liebert, J., Schmidt, G. D., & Reid, I. N. 1999, ApJ, 524, 1000

Harris, H. C., Liebert, J., Kleinman, S. J., Nitta, A., Anderson, S. F., Knapp, G. R., Krzesiński, J., Schmidt, G., Strauss, M. A., Vanden Berk, D., Eisenstein, D., Hawley, S., Margon, B., Munn, J. A., Silvestri, N. M., Smith, J. A., Szkody, P., Collinge, M. J., Dahn, C. C., Fan, X., Hall, P. B., Schneider, D. P., Brinkmann, J., Burles, S., Gunn, J. E., Hennessy, G. S., Hindsley, R., Ivezić, Z., Kent, S., Lamb, D. Q., Lupton, R. H., Nichol, R. C., Pier, J. R., Schlegel, D. J., SubbaRao, M., Uomoto, A., Yanny, B., & York, D. G. 2003, AJ, 126, 1023

Henry, T. J., Backman, D. E., Blackwell, J., Okimura, T., & Jue, S. 2003, in Astrophysics and Space Science Library, edited by T. D. Oswalt, vol. 289, 111

Henry, T. J., Ianna, P. A., Kirkpatrick, J. D., & Jahreiss, H. 1997, AJ, 114, 388

Henry, T. J., Jao, W.-C., Subasavage, J. P., Beaulieu, T. D., Ianna, P. A., Costa, E., & Méndez, R. A. 2006, AJ, 132, 2360

Henry, T. J., Subasavage, J. P., Brown, M. A., Beaulieu, T. D., Jao, W.-C., & Hambly, N. C. 2004, AJ, 128, 2460

Henry, T. J., Walkowicz, L. M., Barto, T. C., & Golimowski, D. A. 2002, AJ, 123, 2002

Hertzsprung, E. 1922, Bull. Astron. Inst. Netherlands, 1, 91

Holberg, J. B., & Bergeron, P. 2006, AJ, 132, 1221

Holberg, J. B., Oswalt, T. D., & Sion, E. M. 2002, ApJ, 571, 512

Iben, I., & Renzini, A. 1984, Phys. Rep., 105, 329

Jao, W.-C., Henry, T. J., Subasavage, J. P., Brown, M. A., Ianna, P. A., Bartlett, J. L., Costa, E., & Méndez, R. A. 2005, AJ, 129, 1954

Kawka, A., & Vennes, S. 2006, ApJ, 643, 402

Kawka, A., Vennes, S., & Thorstensen, J. R. 2004, AJ, 127, 1702

Kilic, M., von Hippel, T., Leggett, S. K., & Winget, D. E. 2006, ApJ, 646, 474

Kilkenny, D., O'Donoghue, D., Koen, C., Stobie, R. S., & Chen, A. 1997, MNRAS, 287, 867

Kretz, W. C. 1900, Contributions from the Rutherford Observatory of Columbia University New York, 16, 1

Landolt, A. U. 1992, AJ, 104, 340

Lang, K. R., & Gingerich, O. 1979, A source book in astronomy and astrophysics, 1900-1975 (Cambridge, Mass.; Harvard University Press)

Lépine, S. 2005, AJ, 130, 1247

Lépine, S., Rich, R. M., Neill, J. D., Caulet, A., & Shara, M. M. 2002a, ApJ, 581, L47

Lépine, S., Rich, R. M., & Shara, M. M. 2003a, ApJ, 591, L49

— 2005, ApJ, 633, L121

Lépine, S., & Shara, M. M. 2005, AJ, 129, 1483

Lépine, S., Shara, M. M., & Rich, R. M. 2002b, AJ, 124, 1190

— 2003b, ApJ, 585, L69

— 2003c, AJ, 126, 921

— 2004, ApJ, 602, L125

Liebert, J., Bergeron, P., & Holberg, J. B. 2003, AJ, 125, 348

Lodieu, N., Scholz, R.-D., & McCaughrean, M. J. 2002, A&A, 389, L20

Luyten, W. J. 1922, PASP, 34, 365

— 1949, ApJ, 109, 528

— 1979a, LHS catalogue. A catalogue of stars with proper motions exceeding 0"5 annually (Minneapolis: University of Minnesota), 2nd ed.

— 1979b, New Luyten Catalogue of Stars with Proper Motions Larger than Two Tenths of an Arcsecond (Minneapolis: University of Minnesota Press)

Madau, P., Ferguson, H. C., Dickinson, M. E., Giavalisco, M., Steidel, C. C., & Fruchter, A. 1996, MNRAS, 283, 1388

Massey, P. 1997, A User's Guide to CCD Reductions with IRAF, (Tucson, Arizona: NOAO)

Massey, P., Valdes, F., & Barnes, J. 1992, A User's Guide to Reducing Slit Spectra with IRAF, (Tucson, Arizona: NOAO)

McCook, G. P., & Sion, E. M. 1999, ApJS, 121, 1

Mihalas, D., & Binney, J. 1981, Galactic astronomy: Structure and kinematics /2nd edition/ (San Francisco, CA,: W. H. Freeman and Co.)

Montagnier, G., Ségransan, D., Beuzit, J.-L., Forveille, T., Delorme, P., Delfosse, X., Perrier, C., Udry, S., Mayor, M., Chauvin, G., Lagrange, A.-M., Mouillet, D., Fusco, T., Gigan, P., & Stadler, E. 2006, A&A, 460, L19

Monteiro, H., Jao, W.-C., Henry, T., Subasavage, J., & Beaulieu, T. 2006, ApJ, 638, 446

Morgan, D. H. 1995, in IAU Colloq. 148: The Future Utilisation of Schmidt Telescopes, edited by J. Chapman, R. Cannon, S. Harrison, & B. Hidayat, vol. 84 of Astronomical Society of the Pacific Conference Series, 137

Oppenheimer, B. R., Golimowski, D. A., Kulkarni, S. R., Matthews, K., Nakajima, T., Creech-Eakman, M., & Durrance, S. T. 2001a, AJ, 121, 2189

Oppenheimer, B. R., Hambly, N. C., Digby, A. P., Hodgkin, S. T., & Saumon, D. 2001b, Science, 292, 698

Pauli, E.-M., Napiwotzki, R., Heber, U., Altmann, M., & Odenkirchen, M. 2006, A&A, 447, 173

Perryman, M. A. C., Lindegren, L., Kovalevsky, J., Hoeg, E., Bastian, U., Bernacca, P. L., Crézé, M., Donati, F., Grenon, M., van Leeuwen, F., van der Marel, H., Mignard, F., Murray, C. A., Le Poole, R. S., Schrijver, H., Turon, C., Arenou, F., Froeschlé, M., & Petersen, C. S. 1997, A&A, 323, L49

Philip, A. G. D., Devorkin, D. H., & Russell, H. N. 1977, Dudley Observatory Reports, 13

Pokorny, R. S., Jones, H. R. A., & Hambly, N. C. 2003, A&A, 397, 575

Pokorny, R. S., Jones, H. R. A., Hambly, N. C., & Pinfield, D. J. 2004, A&A, 421, 763

Press, W. H., Teukolsky, S. A., Vetterling, W. T., & Flannery, B. P. 1992, Numerical recipes in FORTRAN. The art of scientific computing (Cambridge: Cambridge University Press), 2nd ed.

Provencal, J. L., Shipman, H. L., Hog, E., & Thejll, P. 1998, ApJ, 494, 759

Provencal, J. L., Shipman, H. L., Koester, D., Wesemael, F., & Bergeron, P. 2002, ApJ, 568, 324

Putnam, W. L. 1994, The explorers of Mars Hill : a centennial history of Lowell Observatory, 1894-1994 (West Kennebunk, Me. : Published for Lowell Observatory by Phoenix Pub.)

Raghavan, D., Henry, T. J., Mason, B. D., Subasavage, J. P., Jao, W.-C., Beaulieu, T. D., & Hambly, N. C. 2006, ApJ, 646, 523

Reid, I. N. 2005, ARA&A, 43, 247

Reid, I. N., Kirkpatrick, J. D., Liebert, J., Gizis, J. E., Dahn, C. C., & Monet, D. G. 2002, AJ, 124, 519

Richer, H. B., Brewer, J., Fahlman, G. G., Gibson, B. K., Hansen, B. M., Ibata, R., Kalirai, J. S., Limongi, M., Rich, R. M., Saviane, I., Shara, M. M., & Stetson, P. B.

2002, ApJ, 574, L151

Riess, A. G., Filippenko, A. V., Challis, P., Clocchiatti, A., Diercks, A., Garnavich, P. M., Gilliland, R. L., Hogan, C. J., Jha, S., Kirshner, R. P., Leibundgut, B., Phillips, M. M., Reiss, D., Schmidt, B. P., Schommer, R. A., Smith, R. C., Spyromilio, J., Stubbs, C., Suntzeff, N. B., & Tonry, J. 1998, AJ, 116, 1009

Ruiz, M. T., & Maza, J. 1987, Revista Mexicana de Astronomia y Astrofisica, 14, 381

Ruiz, M. T., Maza, J., Wischnjewsky, M., & Gonzalez, L. E. 1986, ApJ, 304, L25

Ruiz, M. T., Takamiya, M. Y., Mendez, R., Maza, J., & Wishnjewsky, M. 1993, AJ, 106, 2575

Ruiz, M. T., Wischnjewsky, M., Rojo, P. M., & Gonzalez, L. E. 2001, ApJS, 133, 119

Russell, H. N. 1914, Nature, 93, 252

Schaeberle, J. M. 1896, AJ, 17, 37

Scholz, R.-D., Ibata, R., Irwin, M., Lehmann, I., Salvato, M., & Schweitzer, A. 2002a, MNRAS, 329, 109

Scholz, R.-D., Irwin, M., Ibata, R., Jahreiß, H., & Malkov, O. Y. 2000, A&A, 353, 958

Scholz, R.-D., Lehmann, I., Matute, I., & Zinnecker, H. 2004a, A&A, 425, 519

Scholz, R.-D., Lodieu, N., & McCaughrean, M. J. 2004b, A&A, 428, L25

Scholz, R.-D., & Meusinger, H. 2002, MNRAS, 336, L49

Scholz, R.-D., Szokoly, G. P., Andersen, M., Ibata, R., & Irwin, M. J. 2002b, ApJ, 565, 539

Schweizer, F. 1979, PASP, 91, 149

Skrutskie, M. F., Cutri, R. M., Stiening, R., Weinberg, M. D., Schneider, S., Carpenter, J. M., Beichman, C., Capps, R., Chester, T., Elias, J., Huchra, J., Liebert, J., Lonsdale, C., Monet, D. G., Price, S., Seitzer, P., Jarrett, T., Kirkpatrick, J. D., Gizis, J. E., Howard, E., Evans, T., Fowler, J., Fullmer, L., Hurt, R., Light, R., Kopan, E. L., Marsh, K. A., McCallon, H. L., Tam, R., Van Dyk, S., & Wheelock, S. 2006, AJ, 131, 1163

Stein, J. 1930, Catalogo Astrographigo (Sezione Vaticana) (Rome: Typografia Polyglotta Vaticana)

Struve, O. 1866, MNRAS, 26, 268

— 1873, MNRAS, 33, 430

Subasavage, J. P., Henry, T. J., Bergeron, P., Dufour, P., Hambly, N. C., & Beaulieu, T. D. 2007, AJ, 134, 252

Subasavage, J. P., Henry, T. J., Hambly, N. C., Brown, M. A., & Jao, W.-C. 2005a, AJ, 129, 413

Subasavage, J. P., Henry, T. J., Hambly, N. C., Brown, M. A., Jao, W.-C., & Finch, C. T. 2005b, AJ, 130, 1658

Teegarden, B. J., Pravdo, S. H., Hicks, M., Lawrence, K., Shaklan, S. B., Covey, K., Fraser, O., Hawley, S. L., McGlynn, T., & Reid, I. N. 2003, ApJ, 589, L51

Thompson, R. I., Eisenstein, D., Fan, X., Dickinson, M., Illingworth, G., & Kennicutt, R. C., Jr. 2006, ApJ, 647, 787

Tucker, R. H. 1905, Lick Observatory Bulletin, 4, 187

van Altena, W. F., Lee, J. T., & Hoffleit, E. D. 1995, The general catalogue of trigonometric [stellar] parallaxes (New Haven, CT: Yale University Observatory), 4th ed.

van Maanen, A. 1915, Contributions from the Mount Wilson Observatory / Carnegie Institution of Washington, 96, 1

Vilkki, E. U. 1978, AJ, 83, 978

Weis, E. W. 1996, AJ, 112, 2300

Wroblewski, H., & Costa, E. 1999, A&AS, 139, 25

— 2001, A&A, 367, 725

Wroblewski, H., & Torres, C. 1989, A&AS, 78, 231

— 1991, A&AS, 91, 129

— 1994, A&AS, 105, 179

— 1996, A&AS, 115, 481

— 1997, A&AS, 122, 447

Appendices

Appendix A

Astrometric Data for the Known 25 pc White Dwarfs

Coordinates are equinox J2000 and were adjusted to account for proper motion from the time of observation to epoch 2000. The proper motions compiled in this table were collected using the following priorities.

1. *Hipparcos* (Perryman et al. 1997)

2. LSPM-North (Lépine & Shara 2005)

3. SCR (this work)

4. NLTT (Luyten 1979b)

In a few cases, proper motion information was not available in any of these sources. For these, any published proper motion was used. The parallax weighted means for objects with more than one parallax were calculated using the formula,

$$\pi_{mean} = \frac{\displaystyle\sum_{i=1}^{n} \frac{\pi_i}{\sigma_{\pi_i}^2}}{\displaystyle\sum_{i=1}^{n} \frac{1}{\sigma_{\pi_i}^2}}, \tag{A.1}$$

$$\sigma_{\pi_{mean}} = \frac{1}{\sqrt{\displaystyle\sum_{i=1}^{n} \frac{1}{\sigma_{\pi_i}^2}}}. \tag{A.2}$$

Table. A.1: Astrometric Data for Known White Dwarfs within 25 pc.

WD Name (1)	R.A. (J2000) (2)	Decl. (3)	Ref. (4)	μ (arcsec) (5)	θ (deg) (6)	Ref. (7)	Parallax (mas) (8)	Ref. (9)	$V_{\tan}$ (km s^{-1}) (10)	Notes (11)
2359−434	00 02 10.73	−43 09 55.5	M	1.026	139.7	S	127.40± 6.80	Y	38.2	
0000−345	00 02 40.10	−34 13 39.5	M	0.788	169.4	S	75.70± 9.00	Y	49.3	
0009+501	00 12 14.74	+50 25 20.8	Le	0.708	219.3	Le	90.60± 3.70	Y	37.0	
0011−134	00 14 12.79	−13 11 01.0	M	0.927	216.1	S	51.30± 3.80	Y	85.7	
0029−021	00 32 09.85	−02 54 02.4	M	0.505	121.0	L	42.60± 1.00	Y	56.2	
0038+555	00 41 22.03	+55 50 08.3	Le	0.332	102.2	Le	43.40± 2.00	Y	36.3	
0038−226	00 41 26.03	−22 21 02.3	M	0.604	230.5	S	101.20±10.40	Y	28.3	
0046+051	00 49 09.90	+05 23 19.0	H	2.978	152.9	H	231.88± 1.79	Y,H	60.9	1
0101+048	01 03 49.93	+05 04 30.5	Le	0.394	51.5	Le	46.90± 3.80	Y	39.8	
0115+159	01 18 00.09	+16 10 20.6	Le	0.640	181.2	Le	64.90± 3.00	Y	46.7	
0135−052AB	01 37 59.39	−04 59 44.7	M	0.675	121.5	S	81.00± 2.80	Y	39.5	
0148+467	01 52 02.96	+47 00 06.7	H	0.124	0.6	H	63.08± 3.79	H	9.3	
0208+396	02 11 20.85	+39 55 21.5	Le	1.146	115.5	Le	59.80± 3.50	Y	90.8	
0213+427	02 16 56.53	+42 58 10.4	Le	1.010	125.2	Le	50.20± 4.10	Y	95.4	
0230−144	02 32 37.91	−14 11 51.9	M	0.728	174.1	S	64.00± 3.90	Y	53.9	
0243−026	02 46 30.81	−02 27 23.3	M	0.542	154.9	S	47.10± 5.00	Y	54.5	
0245+541	02 48 36.43	+54 23 22.4	Le	0.574	228.1	Le	96.60± 3.10	Y	28.2	
0310−688	03 10 31.02	−68 36 03.4	H	0.112	158.1	H	98.37± 1.45	Y,H	5.4	1
0322−019	03 25 11.05	−01 49 15.1	M	0.906	164.4	S	59.50± 3.20	T	72.2	
0326−273	03 28 48.80	−27 19 00.1	M	0.839	63.0	L	57.60±13.60	Y	69.0	
0341+182	03 44 34.86	+18 26 09.8	Le	1.194	160.0	Le	52.60± 3.00	Y	107.6	
0357+081	04 00 26.68	+08 14 06.9	Le	0.534	223.3	Le	56.10± 3.70	Y	45.1	
0413−077	04 15 16.32	−07 39 10.3	H	4.088	213.2	H	199.00± 0.77	Y,H	97.4	1,2
0423+120	04 25 53.72	+12 11 48.3	Le	0.247	205.1	Le	57.60± 2.50	T	20.3	
0426+588	04 31 11.52	+58 58 37.5	H	2.427	147.6	H	180.63± 0.78	Y,H	63.7	1
0433+270	04 36 44.89	+27 09 51.6	Le	0.264	122.3	Le	56.64± 1.12	Y,H	22.1	1
0435−088	04 37 47.41	−08 49 10.7	M	1.573	171.9	S	105.20± 2.60	Y	70.9	
0503−174	05 05 52.45	−17 22 43.4	M	0.682	13.9	S	45.60± 4.00	Y	70.9	
0548−001	05 51 19.48	+00 10 21.1	M	0.213	22.0	L	90.30± 2.80	Y	11.2	

Table. A.1: continued

WD Name (1)	R.A. (J2000) (2)	Decl. (3)	Ref. (4)	μ (arcsec) (5)	θ (deg) (6)	Ref. (7)	Parallax (mas) (8)	Ref. (9)	$V_{\rm tan}$ (km s^{-1}) (10)	Notes (11)
0552−041	05 55 09.53	−04 10 07.1	M	2.377	167.0	L	155.00± 2.10	Y	72.7	
0553+053	05 56 25.47	+05 21 48.4	Le	1.026	205.1	Le	125.00± 3.60	Y	38.9	
0618+067	06 20 47.75	+06 45 17.1	Le	0.532	91.2	Le	44.20± 4.20	Y	57.1	
0642−166	06 45 08.92	−16 42 58.0	H	1.339	204.1	H	380.02± 1.28	Y,H	16.7	1,2
0644+025	06 47 22.15	+02 31 08.9	Le	0.425	273.1	Le	54.20± 5.50	Y	37.2	
0644+375	06 47 37.99	+37 30 57.1	H	0.962	193.6	H	65.84± 1.78	Y,H	69.3	1
0657+320	07 00 51.67	+31 57 43.9	Le	0.687	149.8	Le	53.50± 0.90	Y	60.9	
0659−063	07 01 54.85	−06 27 46.2	M	0.870	181.6	S	81.00±24.20	Y	50.9	
0706+377	07 10 14.33	+37 40 19.5	Le	0.350	216.9	Le	41.20± 2.40	Y	40.3	
0727+482AB	07 30 47.33	+48 10 26.3	Le	1.279	190.2	Le	90.00± 1.00	Y	67.4	
0736+053	07 39 18.12	+05 13 30.0	H	1.259	214.7	H	286.05± 0.81	Y,H	20.9	1,2
0738−172	07 40 20.78	−17 24 49.2	M	1.252	116.0	L	112.40± 2.70	Y	52.8	
0743−336	07 45 38.43	−33 55 51.3	M	1.677	351.6	S	65.78± 0.56	Y,H	120.8	1
0747+073A	07 50 14.58	+07 11 48.8	Le	1.801	276.6	Le	54.70± 0.70	Y	156.1	
0747+073B	07 50 15.35	+07 11 37.1	Le	1.801	276.6	Le	54.70± 0.70	Y	156.1	
0752−676	07 53 08.16	−67 47 31.5	M	2.128	135.8	S	141.20± 8.40	Y	71.4	
0827+328	08 30 39.47	+32 41 47.3	Le	0.537	195.7	Le	44.90± 3.80	Y	56.7	
0839−327	08 41 32.42	−32 56 32.9	M	1.745	322.0	S	112.70± 9.70	Y	73.4	
0856+331	08 59 14.71	+32 57 12.1	Le	0.330	271.4	Le	48.80± 3.40	Y	32.1	
0912+536	09 15 56.10	+53 25 23.7	Le	1.559	224.2	Le	97.30± 1.90	Y	75.9	
0946+534	09 50 17.14	+53 15 15.0	Le	0.259	261.8	Le	43.50± 3.50	Y	28.2	
0955+247	09 57 48.36	+24 32 55.6	Le	0.415	223.3	Le	40.90± 4.50	Y	48.1	
1019+637	10 23 09.07	+63 27 41.6	Le	0.386	52.7	Le	61.20± 3.60	Y	29.9	
1043−188	10 45 40.25	−19 06 46.5	H	1.960	252.2	H	56.90± 6.50	Y	163.3	2
1055−072	10 57 35.13	−07 31 23.2	M	0.816	275.5	S	82.30± 3.50	Y	47.0	
1121+216	11 24 12.97	+21 21 35.6	Le	1.033	269.5	Le	74.40± 2.80	Y	65.8	
1132−325	11 34 29.49	−32 49 52.8	H	1.063	320.8	H	104.84± 0.81	Y,H	48.1	1,2
1134+300	11 37 05.11	+29 47 58.3	H	0.147	267.7	H	65.79± 3.43	Y,H	10.6	1
1142−645	11 45 42.92	−64 50 29.5	H	2.688	97.4	H	216.57± 2.01	Y,H	58.8	1
1208+576	12 11 29.27	+57 24 17.4	Le	0.550	131.6	Le	48.90± 4.60	Y	53.3	

Table. A.1: continued

WD Name (1)	R.A. (J2000) (2)	Decl. (3)	Ref. (4)	μ (arcsec) (5)	θ (deg) (6)	Ref. (7)	Parallax (mas) (8)	Ref. (9)	V_{tan} (km s^{-1}) (10)	Notes (11)
1214+032	12 16 51.85	+02 58 02.9	Le	0.689	292.4	Le	46.30± 3.40	Y	70.5	
1236−495	12 38 49.78	−49 48 00.2	M	0.553	260.9	S	61.00± 9.40	Y	43.0	
1257+037	13 00 09.06	+03 28 41.1	Le	0.958	205.9	Le	60.30± 3.80	Y	75.3	
1309+853	13 08 41.18	+85 02 28.2	Le	0.322	140.2	Le	55.40± 8.30	Y	27.6	
1310−472	13 12 56.47	−47 28 07.6	M	2.128	254.7	R	66.50± 2.40	Y	151.7	
1327−083	13 30 13.64	−08 34 29.5	H	1.205	246.8	H	60.91± 2.04	Y,H	93.8	1,3
1334+039	13 36 31.85	+03 40 46.1	Le	3.880	252.8	Le	121.40± 3.40	Y	151.5	
1344+106	13 47 24.37	+10 21 37.9	Le	0.893	261.0	Le	49.90± 3.60	Y	84.8	
1345+238	13 48 03.02	+23 34 46.3	Le	1.491	274.9	Le	82.90± 2.20	Y	85.3	
1444−174	14 47 25.34	−17 42 15.8	M	1.177	253.0	L	69.00± 4.00	Y	80.9	
1544−377	15 47 29.10	−37 54 58.7	H	0.468	242.8	H	65.65± 0.77	Y,H	33.8	1,2
1609+135	16 11 25.61	+13 22 17.8	Le	0.534	178.3	Le	54.50± 4.70	Y	46.4	
1620−391	16 23 33.84	−39 13 46.2	H	0.076	90.0	H	77.50± 0.80	Y,H	4.6	1,3,4
1625+093	16 27 53.48	+09 12 16.1	Le	0.480	192.2	Le	42.80± 3.70	Y	53.2	
1626+368	16 28 25.00	+36 46 15.8	Le	0.890	327.1	Le	62.70± 2.00	Y	67.3	
1633+572	16 34 21.56	+57 10 09.0	Le	1.636	317.5	Le	69.20± 2.50	Y	112.1	
1633+433	16 35 01.42	+43 17 36.4	Le	0.370	143.5	Le	66.20± 3.00	Y	26.5	
1639+537	16 40 57.14	+53 41 09.3	Le	0.233	212.4	Le	47.40± 3.50	Y	23.3	
1647+591	16 48 25.64	+59 03 22.7	H	0.324	154.5	H	89.25± 2.08	Y,H	17.2	1
1655+215	16 57 09.86	+21 26 48.7	Le	0.572	177.6	Le	43.00± 3.10	Y	63.1	
1705+030	17 08 07.96	+02 57 37.1	Le	0.391	180.6	Le	57.00± 5.40	Y	32.5	
1748+708	17 48 08.01	+70 52 36.0	Le	1.685	311.6	Le	164.70± 2.40	Y	48.5	
1756+827	17 49 50.16	+82 46 26.1	Le	3.590	336.5	Le	63.90± 2.90	Y	266.3	
1820+609	18 21 19.84	+61 01 07.5	Le	0.711	168.5	Le	78.20± 4.10	Y	43.1	
1829+547	18 30 20.28	+54 47 27.2	Le	0.401	317.4	Le	66.80± 5.60	Y	28.5	
1840+042	18 43 25.72	+04 20 22.8	M	0.145	302.1	U	40.20± 3.40	Y	17.1	
1900+705	19 00 10.26	+70 39 51.5	Le	0.508	10.4	Le	77.00± 2.30	Y	31.3	
1917+386	19 18 58.63	+38 43 21.5	Le	0.246	172.8	Le	85.50± 3.40	Y	13.6	
1917−077	19 20 34.93	−07 40 00.1	H	0.169	198.9	H	98.10± 2.36	Y,H	8.2	1
1919+145	19 21 40.42	+14 40 41.4	M	0.075	205.6	V	50.50± 5.50	Y	7.0	

Table. A.1: continued

WD Name (1)	R.A. (J2000) (2)	Decl. (3)	Ref. (4)	μ (arcsec) (5)	θ (deg) (6)	Ref. (7)	Parallax (mas) (8)	Ref. (9)	V_{tan} (km s^{-1}) (10)	Notes (11)
1935+276	19 37 13.75	+27 43 18.7	Le	0.437	87.0	Le	55.70± 2.90	Y	37.2	
1953−011	19 56 29.22	−01 02 32.6	M	0.836	212.0	S	87.80± 2.90	Y	45.1	
2002−110	20 05 34.88	−10 56 54.6	M	1.065	93.8	S	57.70± 0.80	Y	87.5	
2007−303	20 10 56.85	−30 13 06.6	H	0.427	234.1	H	65.06± 3.85	H	31.1	
2011+065	20 13 55.68	+06 42 44.9	Le	0.623	203.6	Le	44.70± 1.90	Y	66.1	
2032+248	20 34 21.88	+25 03 49.8	H	0.694	215.6	H	68.61± 1.76	Y,H	47.9	1
2039−202	20 42 34.75	−20 04 36.0	H	0.368	105.4	H	46.45± 3.64	Y,H	37.6	1
2048+263	20 50 20.65	+26 30 40.8	Le	0.511	235.5	Le	49.80± 3.40	Y	48.6	
2054−050	20 56 48.53	−04 50 49.1	H	0.817	105.6	H	59.65± 3.16	Y,H	64.9	1
2105−820	21 13 16.86	−81 49 12.8	M	0.370	167.0	L	58.60± 8.80	Y	29.9	
2117+539	21 18 56.27	+54 12 41.2	Le	0.223	338.7	Le	50.70± 7.40	Y	20.8	
2126+734	21 26 57.69	+73 38 44.5	Le	0.291	171.1	Le	47.10± 2.40	Y	29.3	
2140+207	21 42 41.00	+20 59 58.2	Le	0.677	199.8	Le	79.90± 3.20	Y	40.2	
2149+021	21 52 25.38	+02 23 19.6	H	0.304	175.7	H	40.57± 2.18	Y,H	35.5	1
2154−512	21 57 41.21	−51 00 22.2	H	0.375	184.7	H	62.04± 2.59	Y,H	28.7	1
2246+223	22 49 05.56	+22 36 31.9	Le	0.523	82.8	Le	52.50± 4.10	Y	47.2	
2248+293	22 51 23.03	+29 39 44.3	Le	1.256	83.4	Le	47.80± 4.20	Y	124.5	
2251−070	22 53 53.35	−06 46 54.4	M	2.586	105.2	S	123.70± 4.30	Y	99.1	
2326+049	23 28 47.62	+05 14 54.2	Le	0.493	237.5	Le	73.40± 4.00	Y	31.8	
2341+322	23 43 50.72	+32 32 46.7	H	0.229	252.1	H	56.88± 1.78	Y,H	19.1	1
2347+292	23 49 55.03	+29 34 04.0	Le	0.500	186.0	Le	46.50± 4.10	Y	51.0	

Notes.—Units of right ascension are hours, minutes, and seconds, and units of declination are degrees, arcminutes, and arcseconds.

(1) Parallax is a weighted mean of the independent measurements of the HIPPARCOS and the Yale Parallax catalogs.

(2) Coordinates, proper motion, and parallax are for the primary component. These quantities are not determined directly for the WD secondary because the angular separation is small.

(3) Parallax incorporates two independent measurements (one for the primary and one for the secondary) from the Yale Parallax catalog.

(4) Parallax incorporates two independent measurements (one for the primary and one for the secondary) from the HIPPARCOS catalog.

References.—(H) Perryman et al. 1997; (L) Luyten 1979a; (Le) Lépine & Shara 2005; (M) Skrutskie et al. 2006; (R) Ruiz et al. 1986; (S) SCR unpublished values; (U) Dahn et al. 1982; (V) Vilkki 1978; (Y) van Altena et al. 1995

Appendix B

Photometric Data for the Known 25 pc White Dwarfs

Magnitudes in the UBV-bands are on the Johnson system. Magnitudes in the RI-bands are on the Kron-Cousins system. Infrared JHK_S magnitudes are in the 2MASS system. For the cases in which the JHK_S magnitudes are weighted means from the 2MASS database (Skrutskie et al. 2006) and from Bergeron et al. (2001), the latter were transformed from the CIT system to the 2MASS system using the transformation equations of Carpenter (2001) prior to the weighted mean calculations. In general, the uncertainties for the optical and infrared photometry are quoted to be $\sim$3% and $\sim$5% respectively. In the cases where the data are marked by a ":", the uncertainties are $\sim$10%.

Table. B.1: Photometric Data for Known White Dwarfs within 25 pc.

WD (1)	U_J (2)	B_J (3)	V_J (4)	R_{KC} (5)	I_{KC} (6)	Ref. (7)	J (8)	H (9)	K_S (10)	Ref. (11)
2359−434.........	...	13.19	12.95	12.81	12.65	1	12.60	12.43	12.45	2
0000−345.........	...	15.46	15.02	14.72	14.45	3	14.12	14.02	13.97	2,3
0009+501.........	...	14.81	14.36	14.08	13.77	3	13.48	13.25	13.19	2,3
0011−134.........	...	16.52	15.89	15.56	15.22	3	14.82	14.59	14.53	2,3
0029−021.........	...	18.44	17.32	16.71	16.18	3	15.59	15.38	15.31	2,3
0038+555.........	...	14.10	14.05	14.01	13.93	3	14.07:	13.98:	13.97:	2
0038−226.........	...	15.20	14.50	14.08	13.71	3	13.34	13.48	13.74	2
0046+051.........	...	12.94	12.40	12.14	11.91	1	11.68	11.58	11.50	2,3
0101+048.........	...	14.26	14.00	13.83	13.66	3	13.50	13.40	13.42	2
0115+159.........	...	13.95	13.85	13.74	13.65	3	13.72	13.69	13.72	2,3
0135−052AB......	...	13.19J	12.86J	12.63J	12.38J	3	12.13J	11.95J	11.96J	2
0148+467.........	...	...	...	...	...	...	12.77	12.83	12.85	2
0208+396.........	...	14.84	14.51	14.26	14.04	3	13.82	13.67	13.60	2,3
0213+427.........	...	16.95	16.22	15.77	15.37	3	14.98	14.73:	14.52:	3
0230−144.........	...	16.46	15.77	15.34	14.93	3	14.47	14.22	14.11	2,3
0243−026.........	...	15.94	15.54	15.28	15.01	3	14.68	14.55	14.48	2,3
0245+541.........	...	16.28	15.36	14.84	14.36	3	13.87	13.59	13.51	2,3
0310−688.........	10.69	11.40	11.37	11.45	11.53	4	11.76	11.79	11.86	2
0322−019.........	...	16.94	16.12	15.66	15.24	5	14.76	14.44	14.38	2
0326−273.........	...	...	...	...	...	...	13.22	13.11	13.10	2
0341+182.........	...	15.52	15.19	14.91	14.65	3	14.56	14.31	14.22	2
0357+081.........	...	16.62	15.92	15.51	15.09	3	14.57	14.34	14.19	2,3
0413−077.........	...	...	...	...	...	...	9.85	9.99	9.86	2
0423+120.........	...	15.90	15.42	15.11	14.80	5	14.49	14.35	14.25	2
0426+588.........	...	12.73	12.43	12.17	11.86	3	11.81	11.74	11.66	3
0433+270.........	...	16.48	15.81	15.40	15.01	3	14.60	14.28	14.18	2,3
0435−088.........	...	14.08	13.75	13.43	13.18	3	13.01	12.91	12.76	2
0503−174.........	...	16.73	16.01	15.57	15.11	3	14.68	14.38	14.25	2,3
0548−001.........	...	15.08	14.56	14.22	13.95	3	13.44	13.67	13.66	2,3
0552−041.........	...	15.48	14.47	13.97	13.49	3	13.04	12.87	12.78	2,3

Table. B.1: continued

WD (1)	U_J (2)	B_J (3)	V_J (4)	R_{KC} (5)	I_{KC} (6)	Ref. (7)	J (8)	H (9)	K_S (10)	Ref. (11)
0553+053	...	14.78	14.16	13.78	13.41	3	12.93	12.73	12.65	2,3
0618+067	...	16.97	16.41	16.05	15.67	3	15.32	15.04	14.97	2,3
0642−166	...	...	...	...	...	...	...	...	...	...
0644+025	...	16.06	15.71	15.48	15.25	3	14.91	14.82	14.84	2,3
0644+375	...	...	...	...	...	...	12.66:	12.66	12.76	2
0657+320	...	17.64	16.62	16.09	15.61	3	15.01	14.72	14.67	2,3
0659−063	...	15.86	15.43	15.13	14.83	3	14.54	14.22	14.36	2
0706+377	...	15.94	15.64	15.38	15.16	3	15.02	14.83	14.81	2,3
0727+482AB	...	15.63J	14.65J	14.12J	13.63J	5	13.08J	12.84J	12.76J	2
0736+053	...	...	...	...	...	...	...	...	...	...
0738−172	...	13.25	13.01	12.86	12.71	1	12.65	12.61	12.55	2,3
0743−336	...	17.81	16.60	15.96	15.39	3	14.80	14.64	14.50	2,3
0747+073A	...	17.69	16.63	16.05	15.55	3	14.98	14.73	14.68	2,3
0747+073B	...	18.17	16.96	16.31	15.70	3	15.03	14.90	14.82	2,3
0752−676	...	14.60	13.95	13.58	13.20	3	12.73	12.49	12.37	2,3
0827+328	...	16.05	15.73	15.51	15.26	3	14.98	14.89	14.82	2,3
0839−327	...	12.06	11.85	11.75	11.63	1	11.58	11.54	11.55	2
0856+331	...	15.19	15.16	15.03	14.97	3	15.14	15.11	15.11	2,3
0912+536	...	14.19	13.84	13.64	13.51	3	13.29	13.20	13.12	2,3
0946+534	...	15.35	15.18	15.05	14.90	3	14.89	14.88	14.87	2,3
0955+247	...	15.30	15.06	14.94	14.74	3	14.65	14.62	14.64	2,3
1019+637	...	15.08	14.70	14.45	14.17	3	13.86	13.69	13.66	2,3
1043−188	...	16.09	15.52	15.03	...	3	14.62	14.41	14.36	3
1055−072	...	14.63	14.33	14.13	13.91	3	13.77	13.69	13.55	2,3
1121+216	...	14.52	14.21	14.01	13.76	3	13.57	13.42	13.39	2,3
1132−325	...	...	...	...	...	...	...	...	...	...
1134+300	...	...	...	...	...	...	...	...	...	...
1142−645	...	11.66	11.49	11.33	11.20	3	11.18	11.13	11.10	2,3
1208+576	...	16.35	15.78	15.41	15.04	3	14.66	14.38	14.33	2,3
1214+032	...	...	...	...	...	...	...	...	...	...
1236−495	...	13.98	13.80	13.82	13.83	3	13.82	13.84	13.94	2,3

Table. B.1: continued

WD (1)	U_J (2)	B_J (3)	V_J (4)	R_{KC} (5)	I_{KC} (6)	Ref. (7)	J (8)	H (9)	K_S (10)	Ref. (11)
1257+037	...	16.50	15.84	15.46	15.08	3	14.62	14.33	14.23	2,3
1309+853	...	...	...	...	...	...	...	...	...	...
1310−472	...	18.52	17.13	16.41	15.72	3	15.15	15.09	14.97	2,3
1327−083	...	...	...	...	...	...	...	...	...	...
1334+039	...	15.56	14.61	14.09	13.63	1	13.06	12.82	12.69	2,3
1344+106	...	15.50	15.12	14.90	14.64	3	14.39	14.17	14.19	2,3
1345+238	...	16.86	15.71	15.12	14.58	3	13.92	13.67	13.60	2,3
1444−174	...	17.47	16.44	15.95	15.43	3	14.94	14.71	14.67	2,3
1544−377	...	13.15:	12.97:	12.75:	12.37:	3	...	...	...	...
1609+135	...	15.31	15.11	15.01	14.87	3	14.82	14.77	14.75	2,3
1620−391	...	...	...	...	...	...	...	...	...	...
1625+093	...	16.48	16.14	15.87	15.62	3	15.29	15.14	15.04	2,3
1626+368	...	14.02	13.83	13.75	13.66	3	13.62	13.63	13.57	2,3
1633+572	...	15.49	14.99	14.68	14.38	3	14.09	14.04	14.03	2,3
1633+433	...	15.27	14.84	14.57	14.28	3	13.98	13.77	13.65	2,3
1639+537	...	15.34	15.05	14.84	14.66	3	14.50	14.47	14.39	2,3
1647+591	...	...	...	...	...	...	...	...	...	...
1655+215	...	14.34	14.13	14.03	13.92	3	13.88	13.81	13.85	2,3
1705+030	...	15.63	15.20	14.96	14.74	3	14.57	14.50	14.47	2,3
1748+708	...	14.59	14.12	13.64	13.28	6	12.71	12.56	12.50	2,3
1756+827	...	14.69	14.34	14.12	13.87	3	13.63	13.47	13.43	2
1820+609	...	16.67	15.69	15.15	14.64	3	14.04	13.79	13.71	2,3
1829+547	...	16.06	15.57	15.28	14.97	3	14.78	14.55	14.48	2,3
1840+042	...	15.01	14.79	14.66	14.52	3	14.44	14.37	14.65	2
1900+705	...	13.31	13.25	13.24	13.23	3	13.33	13.44	13.42	2
1917+386	...	15.06	14.61	14.31	14.04	3	13.77	13.68	13.53	2,3
1917−077	...	12.32	12.28	12.24	12.20	1	12.35	12.36	12.42	2
1919+145	...	...	...	...	...	...	...	...	...	...
1935+276	...	...	...	...	...	...	...	...	...	...
1953−011	...	14.01	13.72	13.53	13.32	1	13.07	13.03	13.01	2,3
2002−110	...	18.11	16.95	16.36	15.86	3	15.29	15.07	15.01	2,3

Table. B.1: continued

WD (1)	U_J (2)	B_J (3)	V_J (4)	R_{KC} (5)	I_{KC} (6)	Ref. (7)	J (8)	H (9)	K_S (10)	Ref. (11)
2007−303 · · · · · · · ·	11.58	12.27	12.21	12.29	12.35	4	12.58	12.64	12.70	2
2011+065 · · · · · · · ·	· · ·	16.16	15.78	15.51	15.25	3	14.97	14.80	14.73	3
2032+248 · · · · · · · ·	· · ·	· · ·	· · ·	· · ·	· · ·	· · ·	12.04	12.07	12.19	2
2039−202 · · · · · · · ·	· · ·	12.33	12.40	12.50	12.62	1	12.83	12.92	13.00	2
2048+263 · · · · · · · ·	· · ·	16.55	15.63	15.11	14.63	3	14.10	13.84	13.77	3
2054−050 · · · · · · · ·	· · ·	17.89	16.69	16.03	15.37	3	14.78	14.61	14.49	2,3
2105−820 · · · · · · · ·	· · ·	13.82	13.61	13.56	13.47	3	13.48	13.47	13.54	2,3
2117+539 · · · · · · · ·	11.78	12.41	12.36	· · ·	· · ·	7	12.68	12.79	12.85	2
2126+734 · · · · · · · ·	· · ·	· · ·	· · ·	· · ·	· · ·	· · ·	13.10	13.16	13.17	2
2140+207 · · · · · · · ·	· · ·	13.37	13.24	13.10	12.98	3	12.97	12.93	12.92	2,3
2149+021 · · · · · · · ·	11.94	12.73	12.74	12.84	12.93	4	13.20	13.29	13.40	2
2154−512 · · · · · · · ·	· · ·	14.93	14.74	14.30	14.13	3	13.85	13.81	13.56	2,3
2246+223 · · · · · · · ·	· · ·	14.56	14.39	14.34	14.25	3	14.32	14.32	14.35	2,3
2248+293 · · · · · · · ·	· · ·	16.20	15.54	15.14	14.75	3	14.32	13.98	13.94	2
2251−070 · · · · · · · ·	· · ·	17.55	15.71	15.10	14.56	3	13.98	13.67	13.49	2,3
2326+049 · · · · · · · ·	· · ·	· · ·	· · ·	· · ·	· · ·	· · ·	· · ·	· · ·	· · ·	· · ·
2341+322 · · · · · · · ·	· · ·	· · ·	· · ·	· · ·	· · ·	· · ·	· · ·	· · ·	· · ·	· · ·
2347+292 · · · · · · · ·	· · ·	16.35	15.76	15.41	15.04	3	14.57	14.35	14.20	2,3

NOTE.—J: joined (combined) photometry.

REFERENCES.—(1) Bessel 1990; (2) Skrutskie et al. 2006; (3) Bergeron et al. 2001; (4) Landolt 1992; (5) Bergeron et al. 1997; (6) Weis 1996; (7) Carney & Latham 1987.

Appendix C

New Proper Motion Discoveries that Overlap with Two Surveys

Upon compiling all of the new HPM discoveries with $\mu \geq 0.5'' \, \mathrm{yr}^{-1}$, several objects were found to be duplicates, although two surveys claimed the discovery. It is necessary to identify the duplicates so that the counts compiled in Table 5.4 are unique objects. I attempt to assign one of two causes for the discrepancy of each duplicate; (*a*) the second survey was completed several months to years after the first such that poor cross-referencing is likely, and (*b*) the two surveys were underway simultaneously and both discovered the object before any previously published discovery. For any object that was published at least six months before the second discovery publication, I assign the former cause. For those objects whose discovery publications are dated within six months of one another, I assign the latter cause.

Table. C.1: New Proper Motion Discoveries that Overlap with Two Surveys

Survey One Star Name	Ref.	Survey Two Star Name	Ref.	Original Discovery Survey	Note
ER 2	1	WT 392	2	Calan-ESO	a
LHS 1140	3	WT 1138	4	LHS	a
LHS 1147	3	WT 1147	4	LHS	a
LHS 1152	3	WT 1161	4	LHS	a
LHS 1160	3	WT 1170	4	LHS	a
LHS 3983	3	WT 1007	5	LHS	a
SCR 0308-8212	6	SIPS 0308-8212	7	SCR	b
SCR 0452-7321	6	SIPS 0452-7322	7	SCR	b
SCR 1240-8209	6	SIPS 1240-8209	7	SCR	b
SCR 2130-7710	6	SIPS 2130-7710	7	SCR	b
SIPS 0052-6201	7	PM J00522-6201	8	SIPS	b
SIPS 1039-3819	7	PM J10395-3820	8	SIPS	b
SIPS 1141-3624	7	PM J11413-3624	8	SIPS	b
SIPS 1231-4018	7	PM J12313-4018	8	SIPS	b
SIPS 1251-3846	7	PM J12515-3846	8	SIPS	b
SIPS 1337-4311	7	PM J13379-4311	8	SIPS	b
SIPS 1338-3752	7	PM J13384-3752	8	SIPS	b
SIPS 1342-3534	7	PM J13423-3534	8	SIPS	b
SIPS 1541-3609	7	PM J15413-3609	8	SIPS	b

Table. C.1: continued

Survey One Star Name	Ref.	Survey Two Star Name	Ref.	Original Discovery Survey	Note
SIPS 1910-4132C	7	PM J19105-4132	8	SIPS	b
SIPS 1910-4133A	7	PM J19105-4133	8	SIPS	b
SIPS 2053-5409	7	PM J20530-5409	8	SIPS	b
SCR 2235-7722	6	PM J22359-7722	8	SCR	a
PM J01253-4545	8	SCR 0125-4545	9	LSPM	b
PM J03007-4653	8	SCR 0300-4653	9	LSPM	b
PM J07401-4257	8	SCR 0740-4257	9	LSPM	b
PM J08152-3600	8	SCR 0815-3600	9	LSPM	b
PM J08186-3110	8	SCR 0818-3110	9	LSPM	b
PM J08276-3003	8	SCR 0827-3002	9	LSPM	b
PM J08458-3051	8	SCR 0845-3051	9	LSPM	b
PM J08471-3046	8	SCR 0847-3046	9	LSPM	b
PM J09047-3804	8	SCR 0904-3804	9	LSPM	b
PM J09271-4137	8	SCR 0927-4137	9	LSPM	b
PM J09566-4234	8	SCR 0956-4234	9	LSPM	b
PM J10050-4322	8	SCR 1005-4322	9	LSPM	b
PM J10538-3858	8	SCR 1053-3858	9	LSPM	b
PM J10587-3854	8	SCR 1058-3854	9	LSPM	b
PM J11104-3608	8	SCR 1110-3608	9	LSPM	b
PM J11256-3834	8	SCR 1125-3834	9	LSPM	b
PM J11329-4039	8	SCR 1132-4039	9	LSPM	b
PM J11495-4248	8	SCR 1149-4248	9	LSPM	b
PM J11511-4142	8	SCR 1151-4142	9	LSPM	b
PM J11596-4256	8	SCR 1159-4256	9	LSPM	b
PM J12042-4037	8	SCR 1204-4037	9	LSPM	b
PM J12146-4603	8	SCR 1214-4603	9	LSPM	b
PM J12201-4546	8	SCR 1220-4546	9	LSPM	b
PM J12277-4541	8	SCR 1227-4541	9	LSPM	b
PM J12300-3411	8	SCR 1230-3411	9	LSPM	b
PM J13276-3551	8	SCR 1327-3551	9	LSPM	b
PM J14005-3935	8	SCR 1400-3935	9	LSPM	b
PM J14123-3941	8	SCR 1412-3941	9	LSPM	b
PM J14373-4002	8	SCR 1437-4002	9	LSPM	b
PM J14558-3914	8	SCR 1455-3914	9	LSPM	b
PM J14570-4705	8	SCR 1457-4705	9	LSPM	b
PM J15054-4620	8	SCR 1505-4620	9	LSPM	b
PM J15116-3403	8	SCR 1511-3403	9	LSPM	b
PM J15334-3634	8	SCR 1533-3634	9	LSPM	b
PM J16019-3421	8	SCR 1601-3421	9	LSPM	b
PM J16087-4442	8	SCR 1608-4442	9	LSPM	b
PM J16138-3040	8	SCR 1613-3040	9	LSPM	b
PM J19167-3638	8	SCR 1916-3638	9	LSPM	b
PM J19184-4554	8	SCR 1918-4554	9	LSPM	b
PM J19248-3356	8	SCR 1924-3356	9	LSPM	b
PM J19403-3944	8	SCR 1940-3944	9	LSPM	b
PM J21324-3922	8	SCR 2132-3922	9	LSPM	b
PM J22040-3347	8	SCR 2204-3347	9	LSPM	b

NOTES.—(a) Duplicate is likely because of poor cross-referencing. (b) Duplicate is because both discovery surveys were underway simultaneously and each discovered the object before any previously published discovery.

REFERENCES.—(1) Ruiz & Maza 1987; (2) Wroblewski & Torres 1991; (3) Luyten 1979a; (4) Wroblewski & Torres 1996; (5) Wroblewski & Torres 1994; (6) Subasavage et al. 2005a; (7) Deacon et al. 2005a; (8) Lépine 2005; (9) Subasavage et al. 2005b

Appendix D

Red Subdwarf Candidates Among the New SCR Discoveries

As outlined in Section 5.3.2.1, subdwarf candidates are identified by having $R_{59F} - J$ > 1.0 and having RPM (H_R) within 4.0 mag of the somewhat arbitrary dashed line separating the WDs from the subdwarfs in the RPM diagram. Subsequent follow-up spectroscopy has revealed that several are in fact subdwarfs. Confirmed subdwarfs are noted in column (5) of the following table.

Table. D.1: Red Subdwarf Candidates Among the New SCR Discoveries

Name (1)	R_{59F} (2)	$R_{59F} - J$ (3)	$H_{R_{59F}}$ (4)	Confirmed (5)
SCR0242-5935	15.02	1.46	18.36	Y
SCR0255-7242	15.44	1.70	18.65	N
SCR0406-6735	14.98	1.45	18.90	Y
SCR0433-7740	15.86	1.81	19.41	Y
SCR0529-3950	14.40	1.94	17.44	Y
SCR0629-6938	16.23	2.56	19.60	Y
SCR0654-7358	16.24	2.25	19.58	Y
SCR0658-0655	14.68	2.36	18.47	N
SCR0701-0655	15.75	2.02	19.58	Y
SCR0708-4709	12.48	1.04	15.50	Y
SCR0709-4648	13.49	1.30	16.57	Y
SCR0740-0540	16.04	2.54	19.39	N
SCR0754-2338	14.80	1.45	18.21	N
SCR0804-1256	15.66	2.08	19.07	N
SCR0816-7727	14.43	1.81	18.58	N
SCR0837-4639	13.89	1.70	17.14	N
SCR0913-1049	15.19	1.82	19.32	N
SCR1001-2257	15.88	1.60	19.02	N
SCR1107-4135	14.72	2.53	20.09	Y
SCR1149-4248	13.09	1.43	17.98	N
SCR1220-4546	14.59	1.89	18.98	N
SCR1227-4541	14.19	1.44	19.77	N
SCR1241-4717	14.38	1.61	17.54	N
SCR1320-7542	15.82	1.89	19.01	N
SCR1338-5622	14.90	1.76	18.59	N
SCR1342-3544	16.02	2.71	19.46	N
SCR1400-3935	15.44	1.98	18.97	N
SCR1433-3847	16.40	2.03	19.74	Y
SCR1442-4810	14.33	1.35	17.86	N
SCR1455-3914	14.52	2.02	19.03	Y
SCR1457-4705	15.23	1.70	18.79	N
SCR1457-3904	15.86	2.17	18.99	Y
SCR1559-4442	14.81	2.03	18.00	N
SCR1608-4229	15.81	2.24	18.86	N
SCR1613-3040	15.41	2.26	19.00	Y
SCR1621-2810	16.01	2.21	19.34	N
SCR1627-7337	13.89	1.23	17.10	N

Table. D.1: continued

Name (1)	R_{59F} (2)	$R_{59F} - J$ (3)	$H_{R_{59F}}$ (4)	Confirmed (5)
SCR1735-7020	16.14	3.32	21.06	N
SCR1739-8222	15.04	2.14	18.37	Y
SCR1740-5646	15.90	2.07	19.16	Y
SCR1756-5927	15.73	2.29	19.38	Y
SCR1817-5318	13.27	1.34	17.22	N
SCR1822-4542	15.13	1.48	18.33	Y
SCR1832-4217	13.64	1.45	16.98	N
SCR1835-8754	16.02	1.92	20.05	N
SCR1843-7849	15.70	2.43	20.06	Y
SCR1913-1001	14.81	2.10	18.61	Y
SCR1916-3638	15.88	2.22	21.46	Y
SCR1924-3356	13.77	1.33	17.47	N
SCR1926-5218	15.22	1.68	18.69	N
SCR1946-4945	15.39	1.88	19.22	N
SCR1958-5609	15.55	2.25	19.02	Y
SCR2018-6606	15.76	2.08	19.08	Y
SCR2101-5437	14.59	1.80	18.71	Y
SCR2104-5229	15.42	1.98	18.43	Y
SCR2109-5226	15.97	2.22	20.46	Y
SCR2151-8604	14.48	1.74	17.77	N
SCR2200-0240	15.30	2.79	19.45	N
SCR2204-3347	14.29	1.97	19.29	Y
SCR2235-7722	16.36	2.19	20.29	N
SCR2249-6324	16.28	1.58	19.56	N
SCR2305-7729	15.73	1.91	18.89	N
SCR2317-5140	15.02	2.19	18.26	N
SCR2329-8758	14.48	1.77	17.64	N
SCR2335-5020	15.17	2.03	19.27	N

Appendix E

Finders for the New SCR Discoveries

SCR 0000-5029
1996.62

SCR 0005-6103
1999.63

SCR 0006-6617
1993.64

SCR 0038-5038
1993.70

SCR 0051-8441
1995.52

SCR 0111-4908
1990.80

SCR 0122-6400
1993.85

SCR 0125-4545
1999.79

SCR 0128-7104
1999.87

SCR 0130-0532
1997.75

SCR 0133-7200
1999.87

SCR 0135-5943
1997.90

SCR 0138-6029
1999.63

SCR 0142-3133
1999.77

SCR 0149-8038
1991.63

SCR 0210-6252
1989.73

Figure. E.1: Finder charts for the new SCR systems in the R_{59F} filter, $5'$ on a side. North is up; east is to the left. The observation epoch for each frame is given.

| SCR 0210-6622 | SCR 0223-0558 | SCR 0224-6433 | SCR 0234-8204 |
| 1989.73 | 1999.79 | 1989.73 | 1989.89 |

| SCR 0242-5934 | SCR 0247-6627 | SCR 0252-7038 | SCR 0252-7522 |
| 1991.79 | 1996.87 | 1987.72 | 1994.01 |

| SCR 0255-7242 | SCR 0300-4653 | SCR 0303-7210 | SCR 0308-8212 |
| 1994.01 | 1990.73 | 1994.01 | 1989.89 |

| SCR 0311-6215 | SCR 0331-4404 | SCR 0331-8251 | SCR 0342-6407 |
| 1991.91 | 1991.79 | 1994.99 | 1989.89 |

Figure. E.1: *Continued*

SCR 0406-6735 1992.99 SCR 0411-8654 1994.99 SCR 0420-7006 1992.99 SCR 0424-7243 1993.05

SCR 0433-7740 1989.89 SCR 0452-7322 1993.05 SCR 0525-7425 1988.15 SCR 0529-3950 1992.02

SCR 0533-3908 1992.02 SCR 0537-5612 1991.12 SCR 0615-1812 1996.13 SCR 0615-5807 1995.07

SCR 0618-6704 1996.14 SCR 0623-6701 1996.14 SCR 0629-6938 1991.11 SCR 0630-7643AB 1990.00

Figure. E.1: *Continued*

Figure. E.1: *Continued*

SCR 0727-1404
1986.20

SCR 0727-1421
1986.20

SCR 0730-5707
1994.95

SCR 0730-7527
1989.99

SCR 0731-0954
1985.96

SCR 0736-3024
1992.19

SCR 0740-0540
1985.96

SCR 0740-4257
1992.18

SCR 0740-7212
1996.14

SCR 0742-3012
1992.19

SCR 0744-6941
1996.14

SCR 0745-0725
1985.96

SCR 0753-2524
1995.09

SCR 0754-2338
1995.09

SCR 0754-3809
1991.21

SCR 0756-5434
1994.95

Figure. E.1: *Continued*

Figure. E.1: *Continued*

Figure. E.1: *Continued*

SCR 0913-1049 SCR 0913-8311 SCR 0914-4134 SCR 0917-3849
1991.43   1996.20   1996.20   1996.20

SCR 0927-4137 SCR 0942-6428 SCR 0956-4234 SCR 0956-8518
1991.43   1991.12   1992.03   1996.20

SCR 1001-2257 SCR 1005-4322 SCR 1011-8106 SCR 1014-4428
1995.10   1992.25   1991.28   1992.25

SCR 1053-3858 SCR 1054-5159 SCR 1057-5103 SCR 1058-3854
1993.47   1995.31   1995.31   1993.47

Figure. E.1: *Continued*

218

SCR 1104-8352
1993.25

SCR 1107-4135
1990.10

SCR 1109-4631
1995.11

SCR 1110-3608
1992.32

SCR 1117-3202
1991.20

SCR 1125-3834
1990.10

SCR 1132-4039
1996.22

SCR 1132-8446
1993.25

SCR 1138-7721
1991.21

SCR 1143-7047
1991.27

SCR 1149-4248
1996.22

SCR 1151-4142
1996.22

SCR 1151-4624
1991.34

SCR 1155-7904
1991.29

SCR 1157-0149
1988.31

SCR 1158-5103
1991.12

Figure. E.1: *Continued*

SCR 1159-4256
1993.08

SCR 1204-4037
1995.40

SCR 1206-3500
1991.28

SCR 1208-3723
1991.28

SCR 1211-6849
1994.10

SCR 1213-4820
1991.12

SCR 1214-4603
1993.08

SCR 1220-4546
1993.08

SCR 1223-3654
1991.35

SCR 1227-4541
1991.42

SCR 1230-3411
1991.35

SCR 1235-4527
1991.42

SCR 1239-4759
1994.42

SCR 1240-8116
1991.29

SCR 1240-8209
1991.29

SCR 1241-4717
1991.42

Figure. E.1: *Continued*

SCR 1245-5506
1991.12

SCR 1246-1236
1993.24

SCR 1247-0525
1992.41

SCR 1251-1232
1993.24

SCR 1256-1316
1997.42

SCR 1257-5554AB
1991.12

SCR 1320-7542
1996.45

SCR 1321-3629
1992.25

SCR 1322-7254
1996.45

SCR 1327-3551
1991.21

SCR 1328-7253
1996.45

SCR 1331-5138
1997.28

SCR 1338-5622
1994.19

SCR 1340-4427
1991.23

SCR 1342-3544
1991.21

SCR 1345-5101
1997.28

Figure. E.1: *Continued*

SCR 1400-3935   SCR 1409-5337   SCR 1412-3941   SCR 1412-4954
1989.18   1994.42   1995.48   1990.46

SCR 1420-5106   SCR 1429-4808   SCR 1433-3846   SCR 1437-4002
1993.47   1993.47   1995.48   1991.23

SCR 1442-4810   SCR 1443-5502   SCR 1444-3426   SCR 1445-5046
1993.47   1993.54   1991.21   1993.47

SCR 1450-3742   SCR 1455-3914   SCR 1457-3904   SCR 1457-4705
1991.21   1991.23   1991.23   1994.61
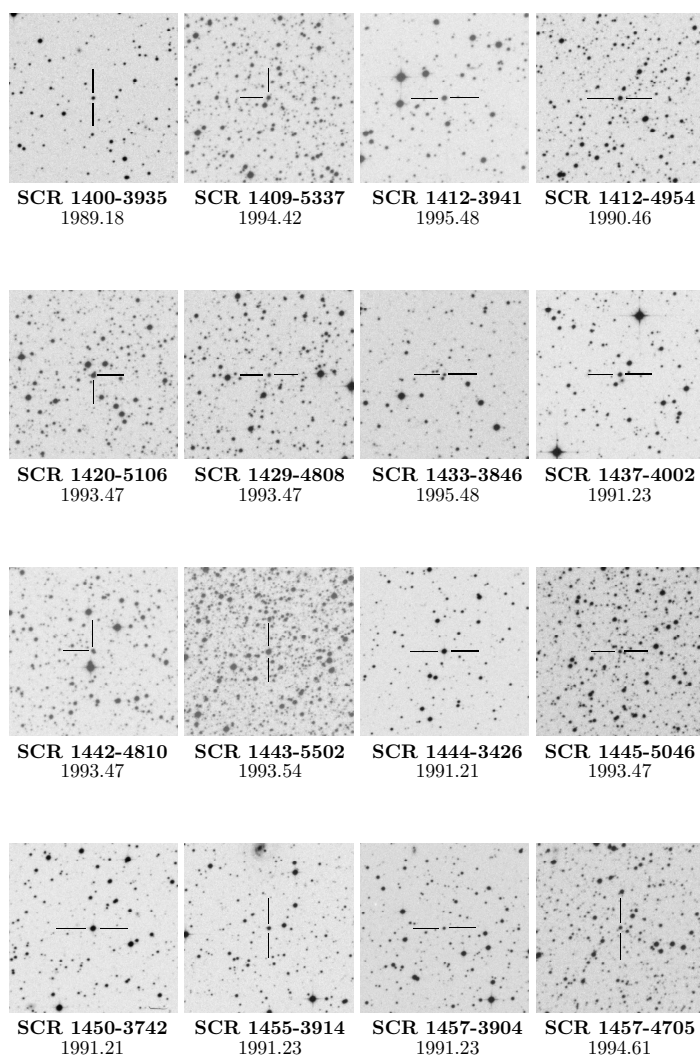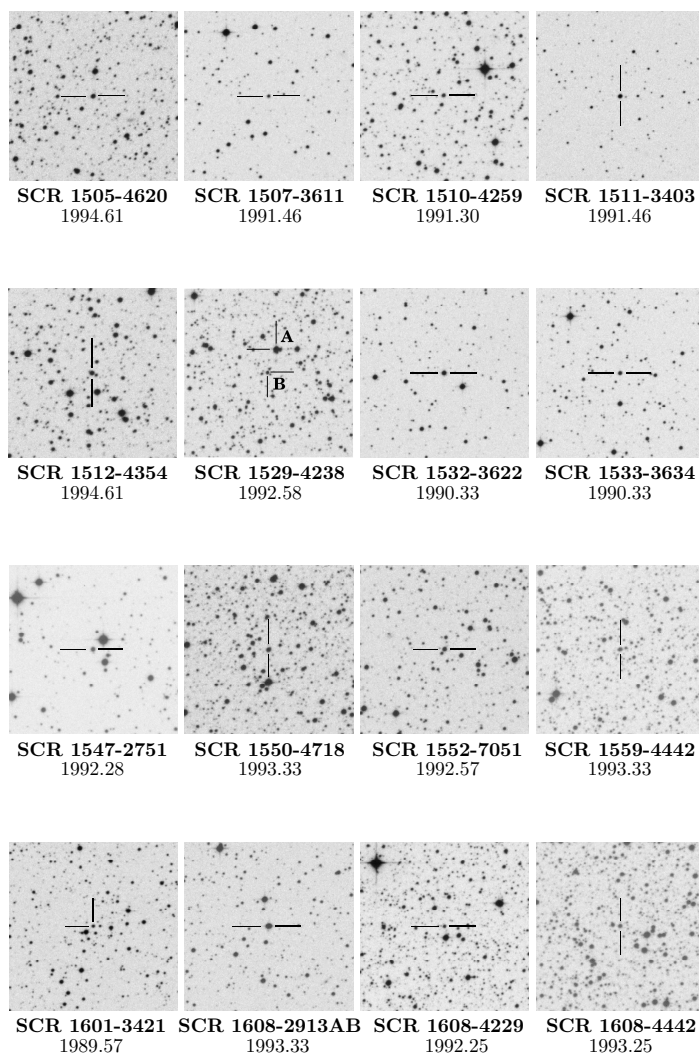
Figure. E.1: *Continued*

Figure. E.1: *Continued*

SCR 1613-3040
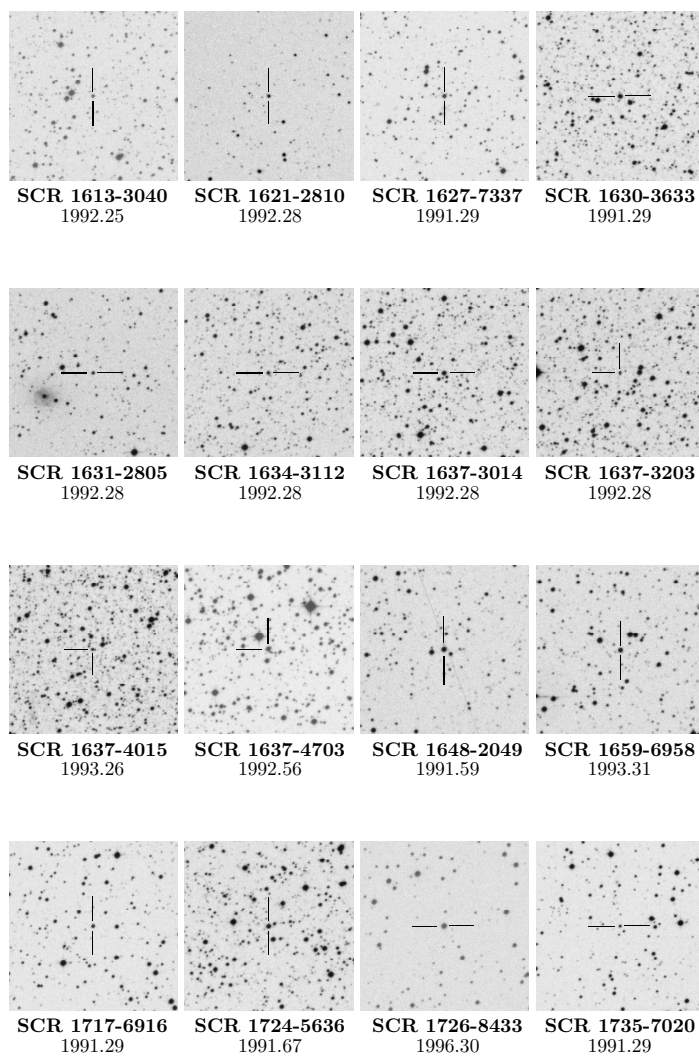1992.25

SCR 1621-2810
1992.28

SCR 1627-7337
1991.29

SCR 1630-3633
1991.29

SCR 1631-2805
1992.28

SCR 1634-3112
1992.28

SCR 1637-3014
1992.28

SCR 1637-3203
1992.28

SCR 1637-4015
1993.26

SCR 1637-4703
1992.56

SCR 1648-2049
1991.59

SCR 1659-6958
1993.31

SCR 1717-6916
1991.29

SCR 1724-5636
1991.67

SCR 1726-8433
1996.30

SCR 1735-7020
1991.29

Figure. E.1: *Continued*

224

Figure. E.1: *Continued*

SCR 1835-8754
1997.93

SCR 1841-4347
1991.67

SCR 1843-7848
1994.30

SCR 1845-6357
1993.62

SCR 1847-1922
1991.59

SCR 1848-6855
1992.66

SCR 1855-6914
1992.66

SCR 1856-1951
1991.59

SCR 1857-4309
1991.67

SCR 1902-5043
1993.62

SCR 1910-4338
1993.32

SCR 1912-5034
1993.62

SCR 1913-1001
1988.45

SCR 1913-2312
1991.62

SCR 1916-3638
1992.57

SCR 1918-3323
1992.57

Figure. E.1: *Continued*

SCR 1918-4554
1993.32

SCR 1924-3356
1992.57

SCR 1926-5218
1991.60

SCR 1928-3634
1993.31

SCR 1931-0306
1986.45

SCR 1931-5840
1993.46

SCR 1940-3944
1989.59

SCR 1946-4945
1991.60

SCR 1948-5914
1993.46

SCR 1954-7356
1991.75

SCR 1958-5609
1991.66

SCR 1959-3631
1990.72

SCR 1959-5549
1991.66

SCR 2001-4239
1995.42

SCR 2007-1915
1992.36

SCR 2007-3551
1990.72

Figure. E.1: *Continued*
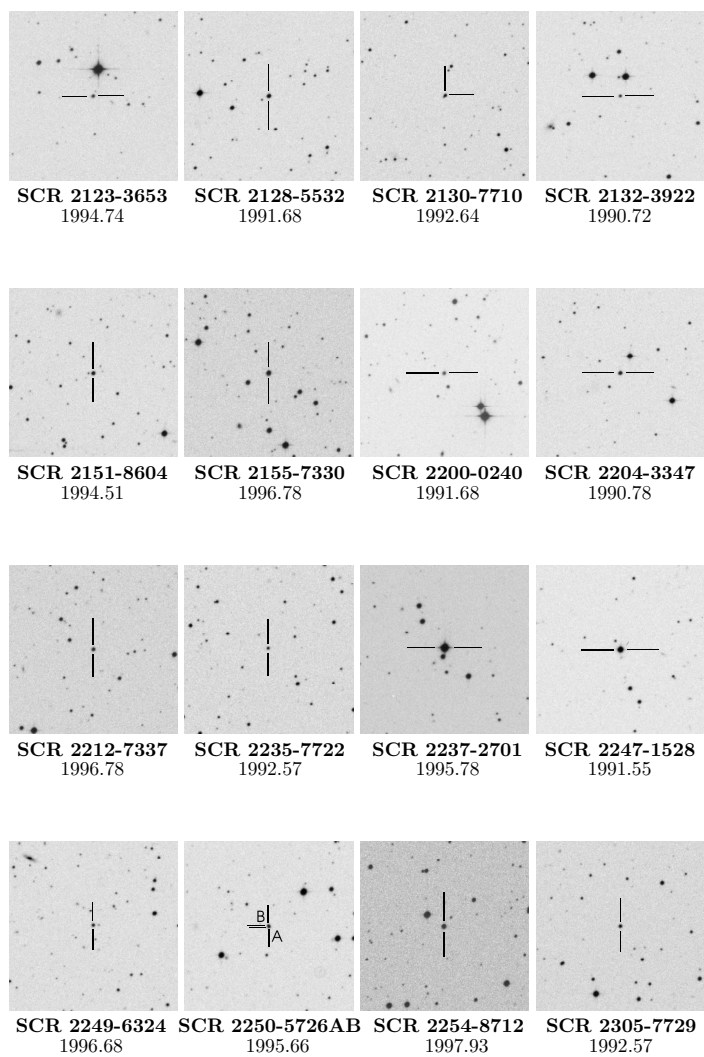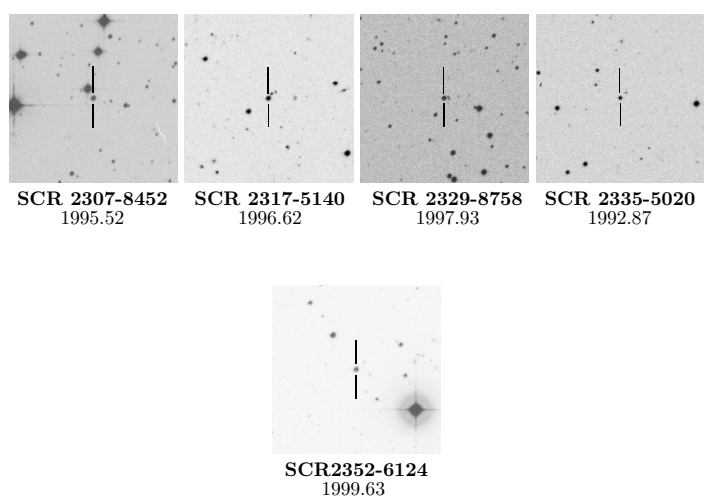
Figure. E.1: *Continued*

Figure. E.1: *Continued*

SCR 2307-8452   **SCR 2317-5140**   **SCR 2329-8758**   **SCR 2335-5020**
1995.52   1996.62   1997.93   1992.87

SCR2352-6124
1999.63

Figure. E.1: *Continued*